THE EFFECT OF MANUFACTURING AND ASSEMBLING TOLERANCES ON THE PERFORMANCE OF 1-18 GHZ DOUBLE RIDGED GUIDE HORN ANTENNAS

by

Benjamin Jacobs

Submitted in partial fulfilment of the requirements for the degree

Master of Engineering (Electronic Engineering)

in the

Department of Electrical, Electronic and Computer Engineering
Faculty of Engineering, the Built Environment and Information Technology

UNIVERSITY OF PRETORIA

August 2010

SUMMARY

THE EFFECT OF MANUFACTURING AND ASSEMBLING TOLERANCES ON THE PERFORMANCE OF 1-18 GHZ DOUBLE RIDGED GUIDE HORN ANTENNAS

Author: Benjamin Jacobs
Supervisor: Professor J. W. Odendaal
Co-Supervisor: Professor J. Joubert
Department: Electrical, Electronic and Computer Engineering
Faculty: Engineering, Built Environment and Information Technology
University: University of Pretoria
Degree: Masters degree of Engineering (Electronic)
Keywords: Double Ridge Guide Horn antenna, gaps, manufacturing tolerances, method of moments, numerical model, performance deviation, sensitivity.

It is known that the 1-18 GHz Double Ridge Guide Horn (DRGH) antenna is highly sensitive to tolerances in manufacturing. Since a typical DRGH antenna is constructed from a number of individual parts, tolerances in the machining, even when numerically controlled, and errors in the assembly can easily lead to gaps between subsections. Performance deviations, most notably resonances in the boresight gain and VSWR was observed in a number of manufactured 1-18 GHz DRGH antennas. The exact cause of the performance deviations had to be determined in order to identify which sections of the antenna need to be redesigned in such a way that the effects of the manufacturing and assembling tolerances on the performance of typical mass produced DRGH antennas are reduced or eliminated. It was hypothesised that gaps most notable in the waveguide launcher section and especially the coaxial feeding section is the cause of the sharp resonance effects. This hypothesis was confirmed during the study. A highly accurate Method of Moments (MoM) numerical model of the 1-18 GHz DRGH antenna was developed, gaps were then implemented in between various parts of the model and the results observed. Based on these results a new improved 1-18 GHz DRGH antenna was designed with reduced sensitivity to manufacturing tolerances and improved performance.

OPSOMMING

DIE DIE IMPAK VAN VERVAARDIGING EN MONTERINGS TOLERANSIES OP DIE WERKVERRIGTING VAN 1-18 GHZ DUBBEL RIF GOLFLEIER HORING ANTENNA'S

Outeur: Benjamin Jacobs
Promotor: Professor J. W. Odendaal
Mede Promotor: Professor J. Joubert
Departement: Elektriese, Elektroniese en Rekenaar Ingenieurswese
Fakulteit: Ingenieurswese, Bou-Omgewing en Inligtings Tegnologie
Universiteit: Universiteit van Pretoria
Graad: Meestersgraad in Ingenieurswese (Elektronies)
Keywords: Dubbel Rif Golfleier Horing antenna, spasies, vervaardigings toleransies, metode van momente, numeriese model, verswakte werkverrigting, sensitiwiteit.

Dit is alombekend dat die 1-18 GHz Dubbel Rif Golfleier Horing (DRGH) antenna baie sensitief is vir vervaardigings toleransies. 'n Tipiese DRGH antenna bestaan uit verskeie individuele onderdele. Toleransies in vervaardiging, selfs al word die proses numeries beheer, kan dus lei tot spasies tussen verskillende dele. Die waarneming van verswakte werkverrigting, meer spesifiek resonansies in die wins en Spannings Staande Golf Verhouding (SSGV) by 'n aantal vervaardigde 1-18 GHz DRGH antennes het gelei tot verdere studie. Om die 1-18 GHz ontwerp minder sensitief te maak ten opsigte van toleransies, moes die presiese oorsaak van die verswakte werkverrigting bepaal word. Aan die begin van die studie was die vermoede dat spasies in veral die golfleierlanseerder en meer spesifiek die koaksiale voer seksie, die oorsaak is van die resonansies. Die hipotese is in die daaropvolgende ondersoek bevestig. 'n Hoogs akkurate Metode van Momente (MvM) numeriese model is vir die 1-18 GHz DRGH antenna ontwikkel. Spasies is tussen verskeie parte van die model ge-inkorporeer en die resultate is ondersoek. 'n Nuwe verbeterde 1-18 GHz DRGH antenna op die ondersoek gebaseer, is ontwikkel. Die antenna het verminderde sensitiwiteit ten opsigte van vervaardigings toleransies sowel as verbeterde werkverrigting.

ACKNOWLEDGEMENTS

I would like to acknowledge the support of SAAB Electronic Defence Systems, particularly the Antennas group and more specifically Riaan Booysen, Dirk Baker and Johan du Toit.

I'm further greatly indebted and thankful for the help and support of the following people:

My supervisors, Professor J. W. Odendaal and Professor J. Joubert for creating a number of opportunities for me.

My family, mother, brother and especially my father, whose guidance and example inspire me.

Marie Jacobs, who during the course of this study first became my friend, girlfriend, fiance and subsequently my wife. With you by my side difficult times seemed like a breeze.

My Saviour, Jesus Christ, who has been amazingly generous to me and provided me with the abilities and strength to complete this work.

TABLE OF CONTENTS

CHAPTER 1 INTRODUCTION

1.1. Introduction

In this chapter an introduction to the study is provided. The background and motivation for the study are discussed in Section 1.2. Section 1.3 outlines the scope and objectives of the study. A short summary is presented on the original contributions made by the study in Section 1.4. The layout of the dissertation is briefly summarised in Section 1.5.

1.2. Background and motivation

Horn antennas have been in widespread use since the late 1950s. This type of antenna has a number of desirable characteristics such as high directive gain, low sidelobes, efficient power handling and easy excitation [1 - 3]. Applications include ElectroMagnetic Compatibility (EMC) testing, as gain standards and source antennas in measurement facilities and as part of Electronic Warfare (EW), radar and communications systems. In the 1970s ridges were incorporated into the design of the basic pyramidal horn [4] to reduce the cut-off frequency of the fundamental mode and thus increase the Maximum Usable Bandwidth (MUB) to typically 12:1.

Originally Radio Frequency (RF) network theory was used to design the Double Ridge Guide Horn (DRGH) antenna. Methods such as the transverse resonance [4 - 7] and Mode Matching (MM) method [8 - 11] are based on circuit and waveguide theory and are semi-analytical methods that require a number of simplifying assumptions. The design of the coaxial waveguide launcher had to be done by experimentation [4, 12]. Even the profile of the ridges was determined more effectively through experimentation. Since then the increase in computational power has made it possible to use numerical methods such as Method of Moments (MoM), Finite Element Method (FEM) and Finite Difference Time Domain (FDTD) techniques to analyse and design DRGH antennas over a broad band [1, 2, 13].

The traditional 1-18 GHz DRGH antenna was adapted from designs by Kerr for a 1-12 GHz horn [12]. The 1-18 GHz DRGH antenna is used extensively in antenna and ElectroMagnetic Interference/Electromagnetic Compatibility (EMI/EMC) measurement.

MIL-STD-461F specifies this antenna for emissions and immunity testing in the 1-18 GHz frequency range [14]. A well-behaved antenna pattern is an absolute necessity for antenna measurement as well as EMI/EMC testing. Using numerical methods it was recently shown that the pattern of this antenna deteriorates in the frequency band above 12 GHz, [1, 2, 15] due to the presence of higher order modes. The main beam splits into four large side lobes and the boresight gain is reduced by approximately 6 dB at 18 GHz.

A number of studies followed to further analyse and address the pattern deterioration problem [16 - 18]. Subsequently a new improved design that produces a single main beam across the band was developed [3, 16, 18]. The waveguide adaptor section was redesigned and mode suppression fins included. The dielectric sidewalls were removed. The E-plane flares' outline was changed to reduce edge diffractions. The ridges were redesigned to provide a better aperture match. The antenna was also scaled to be slightly smaller, in order to shift the appearance of higher order modes to higher out of band frequencies. These design improvements were also implemented for the 200 MHz-2 GHz and 18-40 GHz DRGH antennas [19, 20].

Sensitivity studies were also performed as part of the redesign and analysis effort [16, 17]. The effects of ridge separation at the launching section of the traditional 1-18 GHz DRGH, the position of the feeding probe and the radius of the probe are presented in [16]. In [17] the effects of probe position, cavity height, probe diameter and ridge curvature was investigated for a 1-14 GHz DRGH antenna. The studies mentioned above all made use of commercial numerical solvers such as FEKO, CST and HFSS.

Tolerances in fabrication and assembly of wideband DRGH antennas were problematic issues right from the start. In 1964 Walton and Sundberg writes one of the most influential papers on design of DRGH antennas, and mention that unless extreme care is taken in the fabrication process, results can be disappointing [4]. Since a typical DRGH antenna is constructed from a number of individual parts, tolerances in the machining, even when numerically controlled, and errors in the assembly can easily lead to gaps between subsections. In the same studies that first revealed the pattern deterioration, it was mentioned that the inclusion of gaps in the bottom of the cavity as well as the flaps of the numerical model gave more accurate results at certain frequencies [1, 2, 15]. How the gaps

were implemented was not described nor was the effect of the gaps completely characterised. In the study that first introduced the new improved 1-18 GHz DRGH antenna, it is assumed that gaps in the assembly led to discrepancies between measured and simulated boresight gain values [18]. No further investigations were done to confirm this hypothesis.

These effects were found to be especially pronounced during the production of a number of DRGH antennas where a high degree of repeatability is necessary. Performance deviations, most notably resonances in the boresight gain, were observed in a number of manufactured 1-18 GHz DRGH antennas. Performance deterioration was also observed in the VSWR whereas the known pattern deterioration problem above 12 GHz typically seen in this type of antenna is only observed in the patterns and boresight gain. Some of the antennas were disassembled and reassembled a number of times. In the process the gain dips would shift in frequency or disappear, the cause being unknown. With a lot of effort a number of antennas could be produced that had no deep resonances. The performance was still far from desirable with a fair amount of gain variation between production antennas, especially in the vicinity of 14 GHz.

The observations made during the manufacture of 1-18 GHz DRGH antennas prompted further research and investigation into which parts of the antenna need to be tightly controlled in order to achieve the desired results. Simply machining all the antenna parts to the tightest tolerance of 0.05 mm is costly and still does not ensure adequate performance. The antenna needs to be designed and assembled in such a way as to minimise manufacturing tolerances and improve repeatability. This is true for both the traditional and new 1-18 GHz DRGH antenna designs. It was found during construction that the cavity and feeding section is especially sensitive. Loosening of the grub screws holding the coaxial feeding section in place or replacement of the feeding section affected the performance of the on-axis gain dramatically. In order to further investigate and characterise the effect of gaps on antenna performance, a highly detailed broadband model of the horn antenna had to be implemented in a numerical software package. Since the gaps are of the order magnitude 0.5 - 0.05 mm, the model had to be very accurate.

1.3. Scope and objectives

As mentioned in the previous section, performance deviations, most notably resonances in the boresight gain and VSWR were observed in a number of manufactured 1-18 GHz DRGH antennas. The exact cause of the performance deviations had to be determined in order to identify which sections of the antenna need to be redesigned in such a way that the effects of the manufacturing and assembling tolerances on the performance of typical mass produced DRGH antennas are reduced and or eliminated. To this end the following detailed objectives is defined below:

Development of numerical model: A highly accurate, fully parametric numerical model of the 1-18 GHz DRGH antenna had to be developed. Due to small tolerances and known sensitivity an investigation that only relied on experimentation would not be able to determine the exact cause and effect of specific mechanical defects. It was for instance observed that measured performance results varied significantly just by reassembling the antenna. In a numerical model gaps or mechanical defects are created in one location only and thus a cause-effect relationship could be established.

Implementation of gaps in numerical model: Gaps were implemented in the electromagnetic model in the following sections: the waveguide launcher/adapter, flared waveguide and most notably the feeding section. In practice the gaps formed when the antenna is incorrectly assembled or assembled from parts with excessive tolerances, would not be as precise and perfect as with the gaps implemented in a numerical model. The effect of the gaps can, however, still be characterised and compared to typical measured data.

Identification of sensitive areas: The electromagnetic interactions inside the DRGH antenna are very complicated and it is assumed that there is interaction between various mechanical defects. The goal of this study was, however, not to provide a complete characterisation of these interaction effects, but rather to localise the most sensitive areas of the DRGH antenna. Therefore each type of gap was only evaluated on its own and not in the presence of other types of gaps. Based on observed results it was hypothesised that the main source of performance deviations, most notably resonances in gain and VSWR, is the

coaxial feeding section and this section's interface with the ridges. This hypothesis was confirmed during the study.

New improved design: Using the knowledge gained in this study a redesigned 1-18 DRGH antenna was designed. The goal was to provide a design that would reduce the possibility of gaps by having fewer parts and redesigning parts were necessary. A secondary goal was to improve performance from the current state-of-the-art design without pattern breakup.

1.4. Original contributions

Improved numerical model with dielectric material: As part of this study a highly accurate, fully parametric numerical model of the 1-18 GHz antenna that includes a coaxial feed and connector was developed. The dimensions for the electromagnetic model were obtained from a Solid Works model of the antenna. The electromagnetic model includes dielectric materials for the N-type connector. The effect of dielectric sidewalls on the performance of the antenna was also simulated. Previous simulations did not include dielectric materials for the connector and no results were presented for simulations with and without dielectric sidewalls. With this model it is shown how accuracy can be improved by including dielectric materials. The model also uses a waveguide feed, which is an improvement on other models that used less accurate feeding methods. Comparison with measured data shows excellent agreement with the numerical model.

Comprehensive investigation of manufacturing tolerances, specifically gaps: A number of sensitivity studies have been done on the 1-18 GHz DRGH antenna [1, 2, 15 - 17]. It is important to note that most of these studies focussed on the sensitivity of the antenna with regard to slight variations in the dimensions of the various parts. The focus of the present study is on performance deterioration due to gaps formed between parts, because of manufacturing tolerances. In the same studies that revealed the pattern deterioration problem of the traditional 1-18 GHz DRGH antenna, it was also mentioned that the inclusion of gaps in the order of 0.5 - 0.05 mm in the bottom of the cavity as well as the flaps of the numerical model gave more accurate results [1, 2, 15]. It is mentioned that increased accuracy was only obtained for certain frequencies and not across the entire

band when including the gaps. How the gaps were implemented was not described nor was the effect of the gaps completely characterised. This dissertation provides a comprehensive investigation on the effects of gaps on the performance of the 1-18 GHz DRGH antenna.

Causal relationship between gaps and resonance effects: The exact cause of the performance deviations, most notably resonances in gain and VSWR, of mass produced DRGH antennas was unknown. This study clearly shows how gaps due to manufacturing tolerances can cause performance variations. The most important cause-effect relationship established is that gaps between the coaxial feeding section and this section's interface with the ridges causes resonances in gain and VSWR.

Knowledge for design and fault finding: Using the results in this study design engineers will be able to design 1-18 GHz DRGH antennas that are easier to manufacture with improved repeatability. Furthermore, in the event that an antenna does have reduced performance, the information provided can be used to identify the problem and replace only the defective part or assembly causing the variance.

New improved design: Using the knowledge gained in this study a redesigned 1-18 DRGH antenna is presented with improved performance, easier construction and reduced sensitivity to manufacturing tolerances. This antenna's low and high band gain performance as well as VSWR is also improved from the current state of the art 1-18 GHz DRGH antennas.

1.5. Overview of the dissertation

The structure of the dissertation is as follows:

Chapter 2: In this chapter a literature study presents the development of the DRGH in detail. The focus is specifically on the current state of the art for the design and manufacture of DRGH antennas and specifically the 1-18 GHz DRGH antenna. The development of the antenna is firstly discussed with regard to the design tools used to design and analyse these antennas. Then every section of the antenna is defined and described so as to provide the required background and insight needed to evaluate the rest

of the dissertation. The performance deviations and pattern deterioration of the traditional 1-18 GHz DRGH antenna design is evaluated. Then the design improvements made in the current state of the art 1-18 GHz DRGH antenna is summarised. Finally studies related to the sensitivity of the 1-18 GHz DRGH antenna are discussed.

Chapter 3: The development of the 1-18 GHz DRGH antenna numerical model, used in this dissertation, is described in this chapter. This model was implemented in FEKO and contains a number of improvements over current models. A comparison between measured and simulated results show excellent agreement after the improvements in the model was implemented.

Chapter 4: A detailed description of the mechanical defects implemented in the basic numerical model is presented in this chapter. The typical defects observed in the manufacture of this antenna type are discussed as well as possible origins of the defects. The simulated results for the numerical model with the implemented mechanical defects are then presented and the effects of the defects on the performance of the antenna characterised. These results are compared to typical measured results and a number of observations are made with regard to which areas are the most sensitive to tolerances.

Chapter 5: In this chapter a number of design improvements in the manufacture and assembly procedures are suggested to improve accuracy and repeatability of the manufacturing process. The results of the characterisation can also be used for fault finding procedures when an antenna does not meet the required performance criteria. A method to correct performance loss due to mechanical defects of already manufactured DRGH antennas is discussed. A redesigned 1-18 DRGH antenna is presented with improved performance, easier construction and reduced sensitivity to manufacturing tolerances.

Chapter 6: The dissertation is concluded in this chapter. A summary of the contribution made by this dissertation is given as well as suggestions for future work.

CHAPTER 2 BACKGROUND OF DRGH ANTENNA DEVELOPMENT

2.1. Introduction

This chapter presents detailed background information on the development of the Double Ridge Guide Horn (DRGH) antenna. A short introduction to the background of the DRGH antenna is given in Section 2.2. The development of DRGH antennas is then discussed with regard to the tools used to design and analyse these antennas in Section 2.3. The limitations of these tools with regard to time, accuracy and computational resources are discussed. The basic horn antenna can be divided into two subsections; the coax to waveguide launcher/adapter and the flared waveguide section. These sections are described in detail along with the subsections they comprise of in Section 2.4. In Section 2.5 the typical performance as well as problems with regard to the performance of these antennas are presented. Section 2.6 present a summary of the problems related to the construction, assembly and sensitivity of the antenna. This section forms the background for the rest of the dissertation. The focus being on understanding what parts of the antenna is sensitive to errors in the assembly and or design of the practical implemented antenna. Finally, in Section 2.7, the chapter is summarised.

2.2. Background of the DRGH antenna

Typical types of horns include standard horns (which could be sectoral or pyramidal horns), conical horns, corrugated, quad [21, 22] and DRGH antennas. The focus of this dissertation is on DRGH horns and specifically the 1-18 GHz implementation. However, the results can be extended to other types of DRGH antennas.

The DRGH antenna has developed over a number of years from the standard rectangular pyramidal horn antenna (see Figure 2.1). The DRGH antenna has a number of characteristics such as high directive gain, low sidelobes, efficient power handling and easy excitation that has led to widespread use. Applications include ElectroMagnetic Compatibility (EMC) testing, as gain standards and source antennas in measurement facilities and as part of Electronic Warfare (EW), radar and communications systems.

Various types of DRGH antennas are in use today, depending on performance and especially bandwidth. For emissions and immunity testing the 200 MHz - 2 GHz DRGH antenna is specified by MIL-STD-461F for the 200 MHz - 1 GHz range and the 1-18 GHz DRGH antenna for the 1-18 GHz range [14].

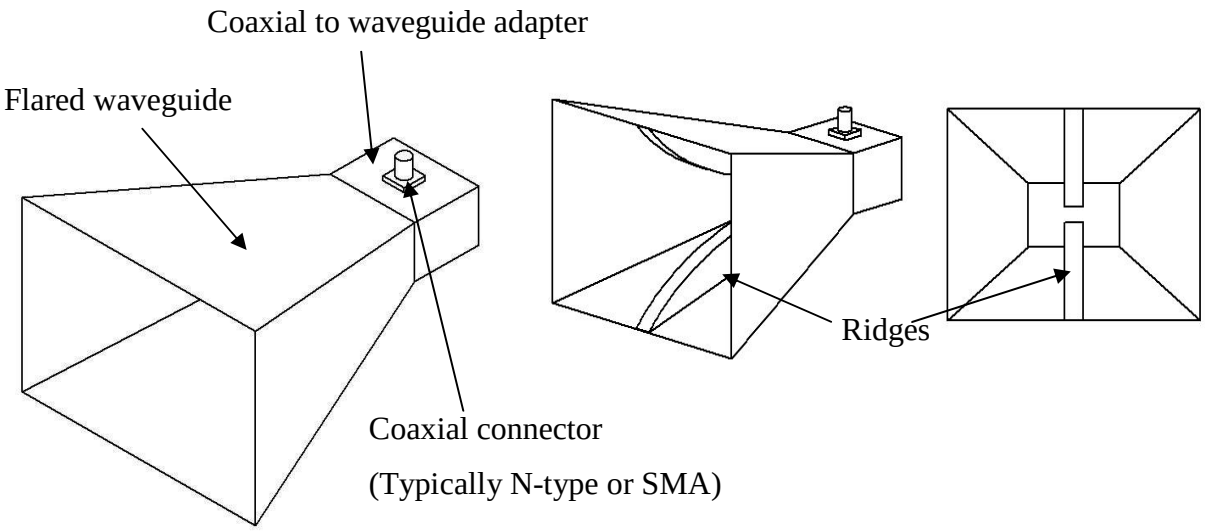

Figure 2.1. Standard rectangular pyramidal horn antenna (left), DRGH antenna (right).

Figure 2.2 shows the traditional 1-18 GHz DRGH antenna based on the Kerr design. This antenna is especially popular since its broad bandwidth allows measurement over a large frequency range without adjustment to the measurement setup.

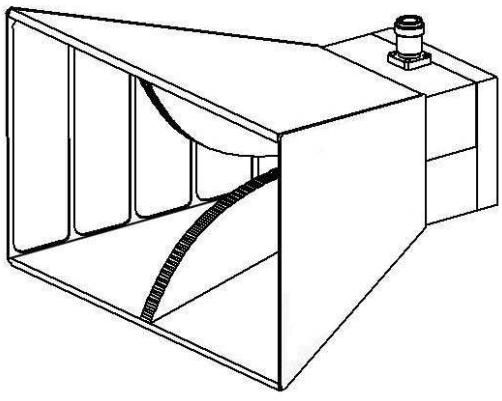

Figure 2.2. Traditional 1-18 GHz DRGH antenna based on Kerr design and specified by MIL-STD-461F for the 1-18 GHz measurement range [14].

2.3. Methods of design and analysis

Historically the basic design of horn antennas was done using analytical and semi-analytical methods such as the aperture, transverse resonance [4 - 7] and mode matching [8 - 11] methods. Due to the limitations of these methods the DRGH antenna mostly had to be designed by experimentation [4, 12]. More recently with the advent of computers the design and analysis of this type of antenna is done almost exclusively with numerical approximations to Maxwell's equations. Initial implementations were limited to very simple problems using methods such as the UTD (Uniform Theory of Diffraction) [23] and 2D formulations of the MoM (Method of Moments) [24]. The astonishing increase in computational power and improvement in the numerical techniques have led to the development of powerful commercially available electromagnetic software packages such as FEKO, CST and HFSS. In the following sections the design of horn antennas with these various methods is discussed. This gives detailed background information related to the current model implementation of the traditional 1-18 GHz DRGH antenna.

2.3.1. Analytical and semi-analytical methods

Maxwell's equations describe the interaction and behaviour of electromagnetic fields. The solution to these equations is, however, quite complex and exact analytic solutions exist for only a small number of simple problems. Before the advent of computers, complex antenna problems had to be reduced to problems that could be analysed with analytical or semi-analytical methods. Thus, although the method used to analyse the problem might be exact (or nearly exact), usually the problem is simplified.

2.3.1.1 Transverse resonance method

As was discussed previously ridges can be used in rectangular waveguide to lower the cutoff frequency of the fundamental mode and increase the Maximum Usable Bandwidth (MUB). A single, double or quad ridge can be used. If dual polarisation is required with one antenna, quad ridges are used. For single polarised horn antennas the double ridge geometry is used. The transverse resonance method is a semi-analytical method used to

calculate the cutoff frequency of the modes, the impedance and attenuation in double ridged waveguide [5 - 7]. This method approximates the double ridged structure with a circuit model that includes capacitative susceptances for the effect of the fringing field from the step discontinuity formed by the ridge edges and for the capacitative effect of the gap between the ridges and the gap between the waveguide next to the ridges. Figure 2.3 shows the double ridged waveguide cross section geometry and the equivalent circuit model.

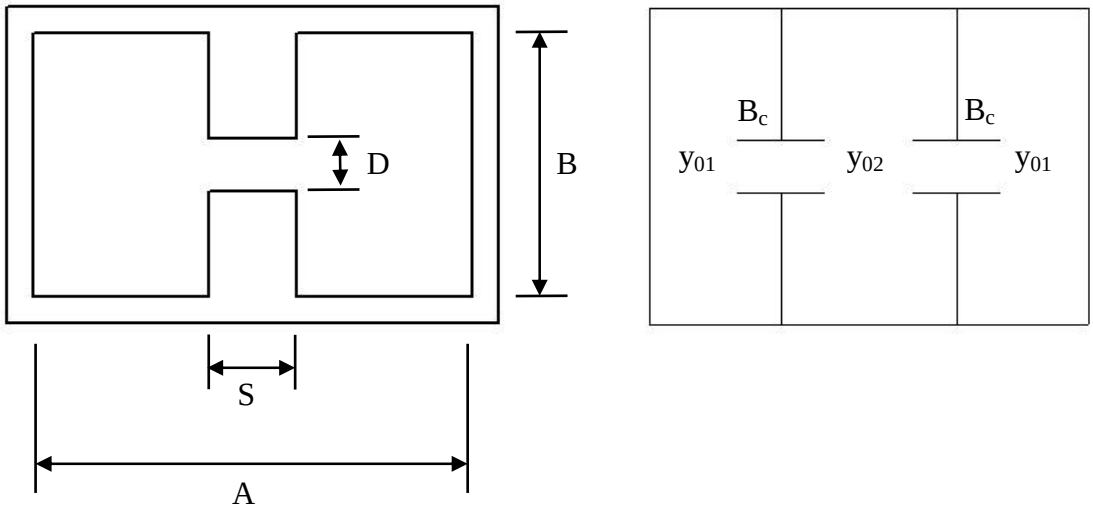

Figure 2.3. Ridged waveguide and equivalent circuit.

Equations were given in [5] and [6] for the cutoff frequency of various TE_{no} modes as well as the characteristic impedance of the double ridged waveguide at a specific frequency. The equations for the cutoff (λ_c) wavelength of the TE_{no} modes can be seen below [1 - 4]:

$$\frac{B}{D}\tan\theta_2 - \cot\theta_1 + \frac{B_c}{y_{01}} = 0 \qquad (1)$$

$$\frac{B}{D}\cot\theta_2 + \cot\theta_1 - \frac{B_c}{y_{01}} = 0 \qquad (2)$$

$$\theta_1 = \frac{360}{\lambda_c}\left(\frac{A-S}{2}\right) \quad \text{degrees} \qquad (3)$$

$$\theta_2 = \frac{360}{\lambda_c}\left(\frac{S}{2}\right) \quad \text{degrees} \qquad (4)$$

The notation as used in [4] was followed with A - the waveguide width, B - the waveguide height, D - the ridge gap and S - the ridge width. The waveguide dimensions used in equations (1)-(4) are shown in Figure 2.3. Equation (1) is used for the odd TE_{no} modes and equation (2) for the even modes. The $\frac{B_c}{y_{01}}$ term models the step discontinuity on both sides of the ridges and approximations for this term can be found in [25, 26]. The approximation for double ridged waveguide is given in [7, 25] as:

$$\frac{B_c}{y_{01}} \approx 2\left(\frac{B}{A}\right)\left(\frac{A}{\lambda_c}\right)\ln\left[\operatorname{cosec}\left(\frac{\pi D}{2B}\right)\right] \qquad (5)$$

These proximity effects have to be taken into account where the sidewalls and ridges are close together [6, 26].

Walton and Sundberg implemented equations (1)-(4) and the approximation of the fringing capacitance as given in [26] on a PC and calculated a number of curves that can be used to design the ridges of the coaxial to waveguide launcher section of the antenna [4]. The characteristic impedance (Z_0) of the ridged waveguide at a required frequency (F) was also calculated using equations (6) – (8) given in [6] with F_c the cutoff frequency:

$$Z_{0\infty} = 1/y_{0\infty} \qquad (6)$$

$$y_{0\infty} = 2\sqrt{\frac{\varepsilon_0}{\mu_0}}\frac{\lambda_c}{2\pi D}\left\{\frac{2D}{\lambda c}\cos^2\left(\frac{\pi S}{\lambda_c}\right)\ln\left[\operatorname{cosec}\left(\frac{\pi D}{2B}\right)\right]+\frac{\pi S}{2\lambda_c}+\frac{1}{4}\sin\left(\frac{2\pi S}{\lambda_c}\right)+\frac{D\cos^2\left(\frac{\pi S}{\lambda_c}\right)}{B\sin^2\left(\frac{\pi}{\lambda_c}(A-S)\right)}\left[\frac{\pi(A-S)}{2\lambda_c}-\frac{1}{4}\sin\left(\frac{2\pi(A-S)}{\lambda_c}\right)\right]\right\} \qquad (7)$$

$$Z_0 = Z_{0\infty}/\sqrt{1-\left(\frac{F_c}{F}\right)^2} \qquad (8)$$

The same approach was also used by [17] to design the ridged waveguide launcher of a 1-14 GHz DRGH antenna.

Implementation of the transverse resonance method on a PC today requires minimal resources and allows calculation of the modes that will propagate in a matter of seconds. This method is not an exact method, but approximates the double ridged structure with a circuit. Furthermore its use is limited to the design of the ridged waveguide launcher section and the geometry of double ridged waveguide. It cannot be used to design complicated launchers with cross sections that vary along the axial dimension of the horn antenna, as is typically used for the 1-18 GHz DRGH antennas. The method can also not be used to design the dimensions of the ridged waveguide in the flared waveguide section where the waveguide acts more like a two conductor transmission line (formed by the ridges) than a waveguide [27].

2.3.2. Numerical solvers

The analysis of more complex geometries requires the use of numerical approximations. A number of Computational ElectroMagnetic (CEM) techniques, numerical approximations to Maxwell's equations are discussed in this section. Each technique has certain drawbacks and advantages, it is necessary to choose the best technique based on the problem at hand. Numerical techniques can be divided into asymptotic and full wave techniques respectively. Asymptotic techniques assume certain physical approximations to Maxwell's equations which becomes more accurate and valid with an asymptotic increase in frequency. Full wave methods on the other hand do not make any initial approximations, but rather approximate Maxwell's equations numerically. The three prominent full wave techniques namely Method of Moments (MoM), Finite Difference Time Domain (FDTD) and Finite Element Method (FEM) will be discussed in the following sections. These methods are implemented in the commercial electromagnetic software packages FEKO, CST and HFSS [28]. Detail with regard to the methods and implementation of the methods are beyond the scope of this dissertation, see [29] for a complete treatment of this topic. It is important to discuss the methods in terms of advantages and disadvantages in order to provide the required background to motivate the choice of the method used in this study. It should be noted that the 1-18 GHz DRGH antenna itself has been implemented in all three the previously mentioned software packages.

2.3.2.1 Method of Moments

The MoM is a full wave frequency domain CEM technique that uses the integral formulation of Maxwell's equations. FEKO is an example of a commercial available software package that implements this method. The radiating or scattering surface of a structure is replaced by equivalent currents and the desired performance parameters calculated from the equivalent currents. For example the radiation integral can be used to determine the radiation pattern once the current distribution is known. As a first step towards calculating the currents, the surface of the structure is discretized. A wire is discretized with segments and a surface with triangles.

The approximation to Maxwell's equations comes in this step where a certain current dependency is assumed across a single element with an applicable basis function (numerous types of basis functions exist). The effect of each element on each other element is then calculated using the appropriate Green's function. Application of boundary conditions on each element produces a set of linear equations that can be solved for each element to yield the required current distribution.

It is important to note that the matrix produced is dense[1] and thus the solution of the matrix requires significant memory resources. According to the FEKO user manual [30] the memory scales to the power of two for each basis function and the Central Processing Unit (CPU) time to the power of three for each basis function in the case of models consisting of wires. According to [29] the memory cost scale for models with surfaces to the power of 4 and the run time to the power of 6. This means that to double the frequency of operation will lead to a runtime increase by a factor between 16 and 64 and a memory increase by a factor of 16 [29].

2.3.2.2 Finite Difference Time Domain method

The FDTD method is a full wave time domain CEM technique. Classic FDTD uses the differential formulation of Maxwell's equations. The commercial software package CST

[1] Nearly all of the matrix elements is non-zero

uses a version of this method[2]. FDTD discretise the electromagnetic problem with a 3D staggered grid. Various types of grids are used. The equations (differential or integral) that relates the field quantities (for FDTD, $\vec{E}$ and $\vec{H}$) is then sampled at the grid points or nodes in space and time. Classic FDTD approximates the partial differential equations by finite difference equations. By applying boundary and initial conditions, the finite difference equations are then solved.

2.3.2.3 Finite Element Method

The FEM is a full wave frequency domain technique that uses the differential formulation of Maxwell's equations. The commercial software package HFSS is an example of a program that uses this method. The FEM method was historically firstly applied to structural mechanics and thermodynamics. In FEM the problem region is discretised with triangles for surfaces and tetrahedrons for volumes. Other types of higher order elements are also available. The $\vec{E}$ field on each element is calculated from Maxwell's partial differential equations by application of boundary conditions and initial values. According to [29] this calculation can be done either by variational analysis or weighted residuals (basis functions similar to MoM). A set of linear equations are thus formed and can be solved with standard matrix algebra. It is important to note that this matrix is sparse, unlike that produced by MoM, [29].

2.3.3. Advantages and disadvantages of the main numerical methods

2.3.3.1 Method of Moments

The main advantages of the MoM can be summarised as follows:

The MoM code is a source method, only surfaces are discretised and not the volumes between structures. This method is therefore extremely efficient for models containing mostly conducting surfaces (Perfectly Electrical Conducting (PEC)). The MoM is well

[2] Instead of the differential formulation of Maxwell's equations CST uses the integral equations. This is known as the Finite Integration Technique (FIT) [28].

suited for radiating or scattering structures since it already incorporates the radiation condition. Homogeneous dielectric structures can be included in the MoM with the Surface Equivalences (SEP) and Volume Equivalence Principles (VEP).

The main disadvantages of the MoM can be summarised as follows:

As mentioned previously, MoM has costly scaling with an increase in model size or operating frequency and computational constraints can quickly be reached with large models and wideband simulations. Furthermore, for the Volume Equivalence Principles (VEP), that is used for inhomogeneous structures the memory and runtime scales to the power of 9, which is very costly [29]. Therefore the MoM has limited application for structures that include inhomogeneous dielectric meshes. The MoM is a frequency domain method and thus needs to recalculate the solution for each frequency point. It can be used for wideband simulations depending on the runtime requirement and model size.

2.3.3.2 Finite Difference Time Domain

The main advantages of the FDTD can be summarised as follows:

Firstly, due to the fact that FDTD is a time domain method, the wideband response can be computed with a single simulation whereas MoM has to recompute the solution for each frequency. The runtime of FDTD scales to the power of 5.5 for each unkown [29], this is slightly better than that of MoM. For wideband systems this means that MoM will be slower than FDTD by at least the factor of the number of frequencies. FDTD is also well suited to problems that include inhomogeneous dielectrics.

The main disadvantages of the FDTD can be summarised as follows:

The FDTD method discretise the electromagnetic problem with a 3D staggered grid, therefore curved metallic surfaces (for example the exponential ridge profile) will be approximated with a staircase type of mesh which leads to inaccuracies [31]. To deal with this problem a number of approaches has been proposed using nonorthogonal FDTD grids and locally conformal grids [32, 33]. Although FDTD scales better than MoM, this can be

offset by the dispersion effect which requires finer discretisation for larger electromagnetic problems [29]. This means that FDTD requires large amounts of memory for larger problems. This increase is especially due to the discretisation of FDTD in three dimensions while MoM only discretises surfaces. This also means that FDTD is not as efficient as MoM when the problem only consists of PEC structures. In the case of radiation and scattering problems MoM is also better suited than FDTD since the FDTD problem space must be surrounded by absorbing layers like the PML (Perfectly Matched Layer) to simulate unbounded regions, while MoM already includes the radiation condition.

2.3.3.3 Finite Element Method

The main advantages of the FEM can be summarised as follows:

The FEM is very good for smaller, complex, closed region structures that may contain inhomogeneous materials. The method is well suited for materials that have frequency and or direction dependant properties (dispersive and anisotropic). According to [29] the runtime scales to the power of between 5.5 and 6 for each unknown, which is slightly better than MoM for PEC structures and a lot better than the SEP or VEP used in MoM to model homogeneous dielectrics. Some new software packages can calculate coupled solutions between, for example, the ElectroMagnetic (EM) solution and a thermal or structural analysis. This is useful, for example, in high power applications [29].

The main disadvantages of the FEM can be summarised as follows:

Although FEM scales slightly better than MoM, this can be offset by the larger number of mesh elements required to model the problem in three dimensions (volume meshing versus surface meshing). In the case of large three dimensional problems the meshing becomes complex and time consuming [29]. In EM, FEM is therefore limited to smaller geometries that contain more complex features and materials such as microwave devices. As with the FDTD method, the radiation condition is also not part of the FEM formulation and therefore absorbing boundary conditions is used to calculated radiation and scattering.

2.4. DRGH antenna design development

The DRGH antenna can be viewed as consisting of a waveguide launcher/adaptor and flared rectangular waveguide section that serves as a transition between the waveguide and free space.

2.4.1. Coax to waveguide launcher

The MUB of standard pyramidal type horns is limited to typically 2:1 [10]. To increase the MUB of the antenna, ridges were introduced in both the adapter and flared sections. Ridges reduce the cutoff frequency of the fundamental mode. The MUB increases significantly when the gap between the ridges is small [4], this is because the next higher order mode is insensitive to changes in the gap width while the fundamental mode is very sensitive.

The following method is typically used to couple the power into the ridged adaptor; the outer conductor of the coaxial feed line is implemented using a bush that passes through a hole in the ridge and is connected to the top ridge and outer of the connector. The bottom ridge contains another bush, with a hole into which the inner conductor fits. The inner conductor consists of a pin passing through the bush and is connected to the bottom ridge at the bottom bush.

According to [4] the height of the waveguide launcher section must be less than λ at the highest operating frequency to prevent propagation of the TE_{02} mode. The design of ridges in ridged waveguide depends on the MUB desired. The various methods to design ridged waveguide were discussed in the previous section. Typically the transverse resonance method was used to design the ridged waveguide dimensions in the coax to waveguide launcher. The design of the rest of the launcher was done through experimentation and it was found that the launcher design plays a critical role in the antenna's performance [4, 12]. In [4] it was found that a critical dimension is the distance from the inner conductor centre to the back shorting plate which must be less than $\lambda/2$ at the highest operating frequency. If the inner conductor is located in the centre of the waveguide (thus in the centre of the ridges) and a short straight section of waveguide/ridge is used between the

probe and the flared waveguide section, the TE_{20} mode cannot be excited and the first higher order mode is the TE_{30} mode [4].

The launcher of the short axial length 1-12 GHz DRGH antenna developed in [12] had to be redesigned to ensure broadband operation. Specifically the launcher dimensions were made smaller to ensure operation at the high frequency end. The launcher dimensions also tapers out from the feedpoint to the launcher – horn interface [12]. The coaxial inserts' (coaxial feed line, called bushes in this dissertation) dimensions were reduced and the input connector changed from N-type to SMA. This improved high frequency VSWR at the expense of low frequency VSWR. Furthermore metal pins were included in the launcher to improve the high frequency VSWR. These rods were connected between the back of the ridge and the backshort [12]. The traditional 1-18 GHz DRGH and the new design incorporate these rods as part of the ridge profile.

Complete redesign of the launcher section of the traditional 1-18 GHz DRGH removed unwanted modes that caused performance deviations [18]. The new 1-18 GHz DRGH antenna design will, however, be discussed in more detail in Section 2.5.

2.4.2. Flared waveguide section

For pyramidal horns the aperture method calculation is used to determine the dimensions of the flared section to achieve the desired gain and beamwidth characteristics [34, 35]. Figure 2.4 shows the aperture dimensions of a pyramidal horn antenna. The introduction of ridges in the flared waveguide section complicates the aperture distribution and therefore this method cannot be used to design wideband DRGH antennas.

It is important to note that the aperture size of the traditional 1-18 GHz DRGH antenna is defined in MIL-STD-461-F [14]. The new 1-18 GHz DRGH antenna has a smaller aperture and does not include the E-plane sidewalls [36].

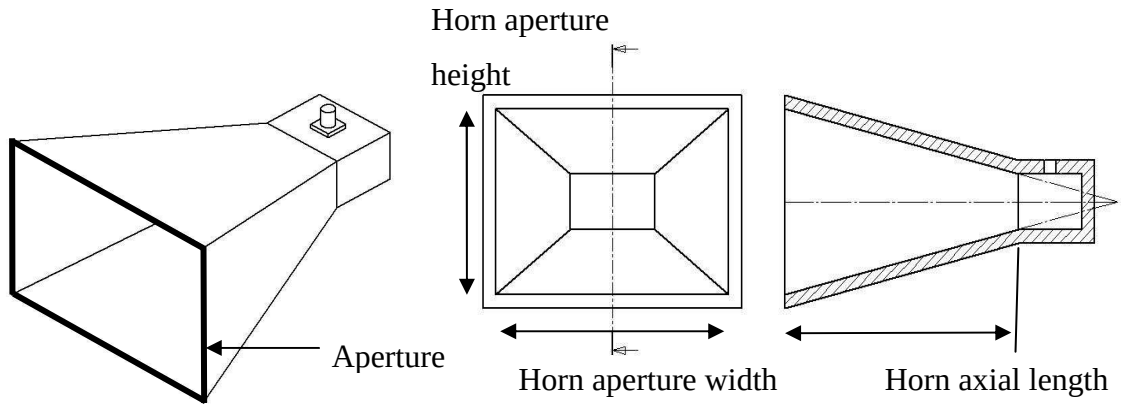

Figure 2.4. Flared waveguide section of the pyramidal horn antenna.

As mentioned in the previous section, ridges were introduced in both the adapter and flared sections to increase the MUB. The ridges of the waveguide adaptor were extended into the flared section to allow the TE_{10} mode to propagate. To allow the ridges to be terminated in the waveguide section, the H-plane aperture of the horn at the point of ridge termination must be at least $\lambda/2$ at the lowest operating frequency [4]. This ensures that the horn operates above cutoff for the TE_{10} mode.

The profile of the ridges is designed in order to provide a smooth impedance transition from the ridged waveguide at the coax launcher to that of free space (377 Ω), [4, 12]. In [4] it is suggested that the flared section should be reasonably long, at least $\lambda/2$ at the lowest operating frequency to ensure a smooth impedance taper. According to [4] ridges of horns with reduced axial length might cause undesirable radiation characteristics and reduced gain especially when a constant ridge width is used. In [12], however, the axial length reduction led to an increase in bandwidth, albeit with a small increase in VSWR in the low band. The launcher had to be redesigned since the initial short models (for a 1-12 GHz horn) experienced pattern degradation above 10 GHz. The best profiles were found through experimentation to be exponential profiles with a linear section at the start of the profile [4, 12], (to prevent excitation of TE_{20} mode, see previous section). In [4] it was found that as the MUB of the DRGH antenna is increased, VSWR peaks appear in the low band and increases in height and number. No explanation for this result could be found in [4]. It was found that a linear taper superimposed on the logarithmic curve improved the VSWR in the first octave of the frequency band for the 1-12 GHz DRGH designed in [12]. No explanation for this effect could be found either. The ridge shape can also be used to

improve the aperture match of the antenna [3, 16, 18, 27]. In [27] results were presented for a 2-11 GHz antenna derived from a DRGH. This antenna used cylinders at the end of the ridge profile as well as microwave absorbing material for aperture matching. This antenna had no E or H-plane sidewalls and thus operated more like a two conductor balanced transmission line [27].

Ridges were mostly implemented with constant width due to ease of fabrication. The width of the ridges can be used to ensure single mode propagation in the flared section of the waveguide [4]. The ridges affect the phase error of the E and H-plane differently and this must also be taken into account when designing the ridges [4].

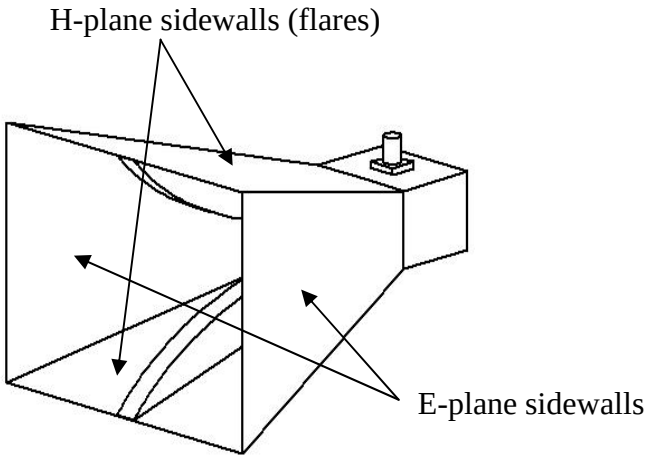

Figure 2.5. DRGH showing indicating H-plane and E-plane sidewalls.

Figure 2.5 clearly shows the location of the sidewalls. Initially the sidewalls of the flared section were of all metal construction. Later the E-plane sidewalls of DRGH antennas were implemented as a grid type construction, while the H-plane flares was solid metal. This was done, since it was shown in [12] that the E-plane sidewalls increase the low frequency gain, but has no significant effect above 3.5 GHz. It was found that the ridges control the radiation in the upper frequency band of operation (see [12] and [27]). Therefore these sidewalls could be substituted with a grid construction. The spacing of the grid elements is a tenth of a wavelength at the low end of the band in order to simulate a solid metal wall at these frequencies [12]. Grids etched on a dielectric substrate ([12] used glass-reinforced Teflon) reduced the weight of the antenna and makes the antenna easier to weatherproof and not as fragile when compared to using a grid only. For the new 1-18 GHz DRGH

antenna design, the E-plane sidewalls was completely removed since it was found that the dielectric substrate of these sidewalls is one of the factors that causes pattern deterioration above 12 GHz [18]. The new 1-18 GHz DRGH antenna design will be discussed in more detail in Section 2.5.

2.5. Typical performance and pattern deterioration

The initial 1-12 GHz DRGH design of [12] experienced pattern degradation at 10 GHz, which could be alleviated by redesign of the launcher section. It is stated that this 1-12 GHz DRGH antenna still experienced serious pattern degradation at 18 GHz. With the use of numerical methods it was shown recently that the pattern of the traditional 1-18 GHz DRGH antenna deteriorates in the frequency band above 12 GHz [1, 2, 15]. This was expected since the traditional 1-18 GHz DRGH antenna was just an adaption of the 1-12 GHz design in [12]. The main beam splits into four large side lobes and the boresight gain is reduced by approximately 6 dB at 18 GHz (see Figure 2.6). This makes the use of these antennas for EMC, measurement and reflector applications less desirable. These applications require a pattern that creates uniform fields across a wide frequency band [18]. The software package FEKO was used to investigate the pattern deterioration problem using a broadband numerical model that included the coaxial feeding section. The advantage of a numerical model is that it is easy and inexpensive to calculate full 3D radiation patterns. This is not the case when performing measurements. The pattern deterioration effect was much better observed with the 3D pattern data of the numerical model. DRGH antennas are usually only measured in the E and H-planes. In [1, 2, 15] after observations made with the simulation model, a pattern was also measured through the 45° plane of the DRGH. This pattern gave a better indication of the pattern deterioration. Using the broadband numerical model, calculation of the near fields in the aperture of the DRGH antenna revealed that the field patterns become more complex above 12 GHz, an indication of higher order mode propagation [1]. Therefore it was found that the traditional 1-18 GHz DRGH antenna experiences pattern deterioration due to the propagation of higher order modes [1, 2, 15]. It was speculated that a redesigned feeding section, dielectric inserts in the flared part of the horn or a dielectric lens would solve the problem [1, 2, 15].

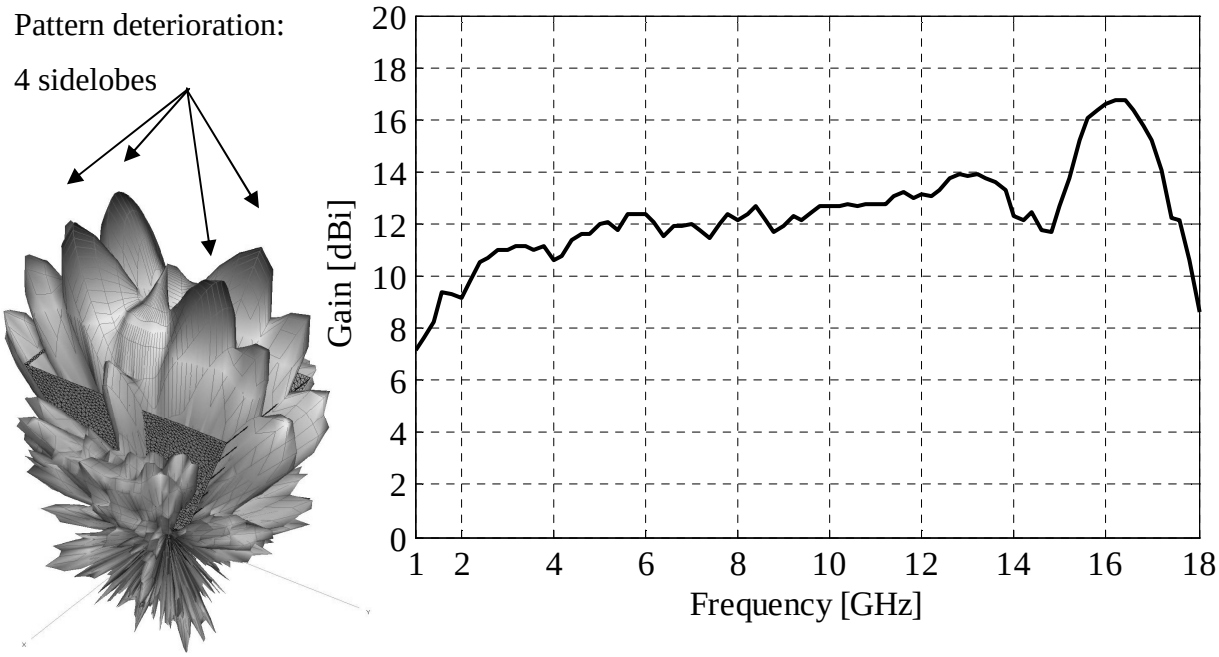

Figure 2.6. Pattern deterioration of traditional 1-18 GHz DRGH antenna.

A number of studies followed to further analyse and address the pattern deterioration problem [16 - 18]. Subsequently a new design that produces a single main beam across the band was developed [3, 16, 18]. A number of improvements were made and are summarised below:

Redesigned waveguide adaptor and mode suppression fins: The waveguide adaptor section was redesigned and mode suppression fins included. This was done in order to suppress the higher order modes that led to the pattern deterioration. Just behind the mode suppression fins, a cavity was included to reduce VSWR [36].

Antenna scaled: The antenna was scaled to be slightly smaller in order to shift the pattern deterioration problem to higher frequencies.

Removed dielectric sidewalls: In [1] it was found that the sidewalls of the wideband DRGH antenna do not influence the antenna's patterns at frequencies above 4 GHz. The broadband simulation model used in [1] for the traditional 1-18 GHz DRGH antenna did not include the dielectric material for the grid sidewalls and could therefore not recognise the effect that the sidewalls has on the high frequency performance. It was subsequently found that the sidewalls play an important part in the deterioration of the patterns at

frequencies above 12 GHz [18]. It was found that it is not the metallic strips itself, but rather the dielectric that causes an on-axis gain drop at 18 GHz [18]. Therefore the dielectric sidewalls were removed in the new design [18]. In this dissertation it was confirmed that the dielectric sidewalls increase the pattern breakup, especially at 18 GHz (see Section 3.3.4). The removal of the E-plane sidewalls has come at the expense of low-frequency gain and a corresponding increase in the low-frequency radiation pattern beamwidths [18].

Changed H-plane flares: The H-plane flares' outline was changed to reduce edge diffractions since sharp corners were formed at the edges of the H-plane flares due to the removal of the E-plane flares [3]. Coupled with the ridged profile that thus extend beyond the upper and lower H-plane flares, this improves the aperture match [36].

Redesigned ridges: The ridges were redesigned to provide a better aperture match. The new ridge curvature was found by using a linear section near the feed point, an intermediate exponential section and a circular section near the aperture [3]. It is interesting to observe that the ridge curvature as shown in Figure 20 of [36] was included into the patent, but the use of a cylindrical ridge section incorporated onto an exponential section was presented previously in 1982 [27].

In this new design the main radiation lobe is now directed towards boresight, the pattern is more constant with frequency and does not deteriorate anywhere in the operational bandwidth. This makes the new design suitable for EMC, measurement and use in reflectors. These design improvements were also extended to the 200 MHz-2 GHz and 18-40 GHz DRGH antennas [19, 20].

2.6. Sensitivity and tolerance problems

The earliest finding with regard to the sensitivity of DRGH antennas can be found in [4], it is stated that extreme care must be taken in the fabrication and assembly process of the antenna or the results can be disappointing. More recently a number of tolerance studies were performed on the traditional 1-18 GHz DRGH antenna [16, 17]. These studies used commercial numerical solvers such as FEKO, CST and HFSS. The effects of ridge

separation at the launching section of the traditional 1-18 GHz DRGH, the position of the feeding probe and the radius of the probe are presented in [16]. In [17] the effects of probe position, cavity height, probe diameter and ridge curvature were investigated for a 1-14 GHz DRGH antenna. The previous studies showed that this antenna is extremely sensitive to variations in tolerances. No tolerance or sensitivity study could be found with regard to gaps or mechanical imperfections formed by manufacturing tolerances and incorrect assembly. Since the antenna consists of a number of parts, tolerances in the machining, even when numerically controlled, and errors in the assembly could easily lead to gaps between subsections and incorrect dimensions.

In the same studies that revealed the pattern deterioration problem of the traditional 1-18 GHz DRGH antenna, it was also mentioned that the inclusion of gaps in the order of 0.5 - 0.05 mm in the bottom of the cavity as well as the flaps of the numerical model gave more accurate results [1, 2, 15]. It is mentioned that increased accuracy was only obtained for certain frequencies and not across the entire band when including the gaps. How the gaps were implemented was not described nor was the effect of the gaps completely characterised. Based on these observations, a precision manufactured 1-18 GHz DRGH antenna was used in the investigations of [1, 2, 15] to exclude the effect of mechanical imperfections. It is also important to note that this precision DRGH antenna made use of a precision N-type connector that is mode free up to 20 GHz. In [18] a good correlation between measured and simulated results was observed for the new design of the 1-18 GHz DRGH antenna. Discrepancies in gain were observed, but it was hypothesised that this is due to losses in the aluminium body, insufficient amount of unknowns in the simulation and interestingly the effects due to gaps between parts of the antenna. No further investigations were, however, done to confirm this hypothesis. A very limited sensitivity analysis on the new 1-18 GHz DRGH was performed in [3]. Only the variation in VSWR was investigated for two controlling parameters of the ridge profile.

2.7. Summary

The background of DRGH antennas was briefly discussed in this section. The design of this type of antenna was presented with regard to the design methods used such as the transverse resonance method, MoM, FDTD and FEM. The advantages and disadvantages

were evaluated for each method. The historical development of the 1-18 GHz DRGH antenna design to its current state was discussed by dividing the antenna design into two sections, the waveguide launcher and flared waveguide sections. The performance deviations and pattern deterioration of the traditional 1-18 GHz DRGH antenna design was then evaluated followed by the design improvements made in the new 1-18 GHz DRGH antenna were summarised. The radiation pattern of this design does not deteriorate in the upper band as with the traditional design. Finally, studies related to the sensitivity of the 1-18 GHz DRGH antenna were discussed. This antenna is very sensitive to manufacturing tolerances. Although a number of studies address the slight variation or tolerance of various parts of the antenna, no studies could be found that specifically focus on the effect of gaps formed by manufacturing tolerances in assembly.

CHAPTER 3 DEVELOPMENT OF THE SIMULATION MODEL

3.1. Introduction

As mentioned in Chapter 1, the main objective of this dissertation is to investigate and completely characterise the effect of manufacturing tolerances that can occur in the construction of 1-18 GHz Double Ridge Guide Horn (DRGH) antennas. An investigation that only relied on experimentation would not be able to determine the exact cause and effect of specific mechanical defects. It was observed that measured performance results varied significantly just by reassembling the antenna. Taking into account the accuracy with which parts can be machined, it would be very difficult to purposefully create parts with specified gaps. Even if these parts could be created accurately enough, the experiment would be influenced by virtue of the fact that the antenna would have to be disassembled and reassembled a number of times. Therefore a highly accurate, fully parametric numerical model of the 1-18 GHz antenna had to be developed. In a numerical model gaps/mechanical defects are created in one location only and thus a cause-effect relationship could be established and comparisons could be drawn between individual simulations.

Section 3.2 will shortly discuss the selection of the numerical method and the numerical software package used in this dissertation. In Section 3.3 the development of the 1-18 GHz DRGH antenna numerical model used in this dissertation is presented. Section 3.4 discusses the parameters and implementation related to the meshing of the 1-18 GHz DRGH antenna model. In Section 3.5 the model is validated using measured results of a carefully constructed DRGH antenna. Finally the chapter is concluded with a short summary in Section 3.6.

3.2. Selection of the numerical method and software

It is very important to choose the correct type of numerical approximation technique depending on the problem at hand. The first consideration when starting to implement an electromagnetic model is to choose the software package and therefore the corresponding

numerical method that will be used. Sections 2.3.2 and 2.3.3 outlined the various typical methods used namely Method of Moments (MoM), Finite Difference Time Domain (FDTD) and Finite Element Method (FEM) [28]. These methods are implemented in the most widely known commercial software packages namely FEKO, CST and HFSS. It was decided that for this study the MoM code as implemented in FEKO would be the best numerical approximation method.

The main advantage in connection with this study is that the MoM code (which FEKO uses) is a source method, only surfaces are discretised and not the volumes between structures. This has two advantages. Firstly the goal of this study was to implement very small gaps between subsections of the antenna. MoM only has to mesh the surface of the parts around the gaps while the other methods would have to mesh the air volume between the parts as well. Since these features would be very small (0.5 - 0.05 mm) this would mean mesh elements with small sizes near the gap and therefore a large number of extra unknowns with volume meshing. Secondly this model contains mostly conducting surfaces, for which the source method is ideally suited. The 1-18 GHz DRGH antenna is electrically very large at 18 GHz with a large volume of free space inside the horn. MoM only needs to model the conducting surfaces and not the large volume of air inside the antenna. Therefore the MoM will have much less unknowns to solve than the other methods. Since this antenna has a wide operational bandwidth, methods such as FDTD would normally be better, since the response is calculated in a single run. However, due to the fact that the MoM solution would have far less unknowns for this specific problem and therefore would require far less memory, computation of the wideband response would be comparable to the other methods.

FEKO also has the advantage of modelling the few homogeneous dielectric areas that the model contains with the Surface Equivalence Principle (SEP) method which would not add excessively more unknowns. Furthermore the MoM is well suited for radiating or scattering structures since it already incorporates the radiation condition and the main parameter used for comparison purposes was the boresight swept frequency gain of the antenna. This parameter was used since the resonance effects can be most easily observed in the boresight gain and a large amount of measured data was available for this parameter.

3.3. Development of the numerical model in FEKO

A Solid Works model of the mass produced 1-18 GHz DRGH antenna was used to obtain the dimensions for the various parts. The numerical model is fully parametric and can be adjusted as required for a tolerance/sensitivity study. The next section will show how each of the mechanical parts and sections was implemented as an electromagnetic model in FEKO.

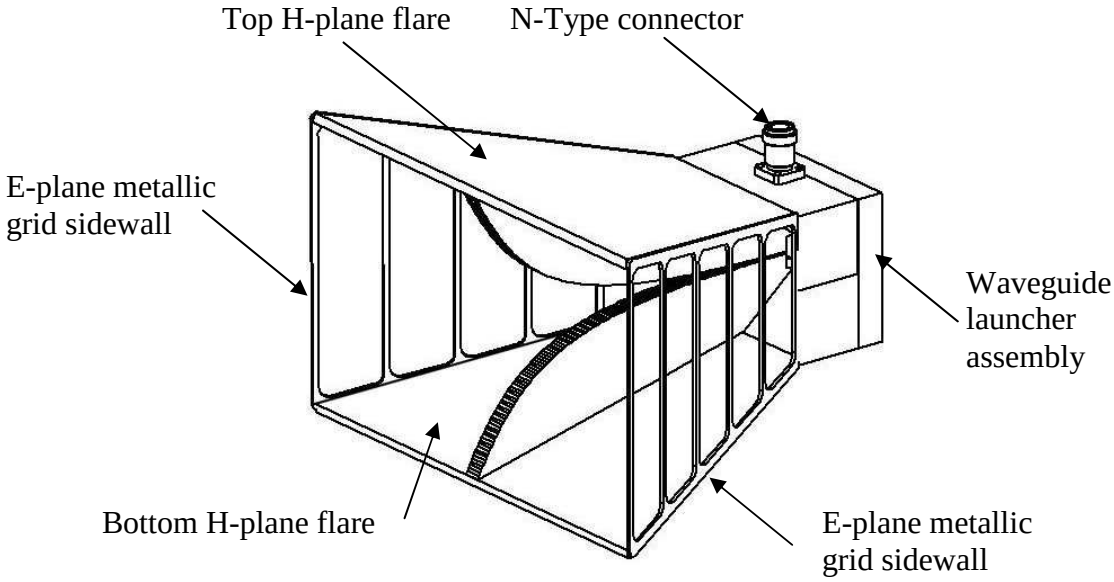

Figure 3.1. The 1-18 GHz DRGH antenna Solid Works model.

Figure 3.1 shows a typical 1-18 GHz DRGH antenna. The basic antenna can be divided into two sections, the waveguide launcher and flared waveguide sections. The waveguide launcher section consists of the waveguide launcher assembly and coaxial feeding section including the N-type connector. The flared waveguide consists of the E- and H-plane sidewalls and ridges.

Figure 3.2 shows the various parts (to the left) and assembly of the waveguide launcher section and ridges (to the right) with the top and bottom H-plane flares and the E-plane sidewalls removed for clarity. The parts from top to bottom are the backshort, launcher flares, launcher wedges and ridges.

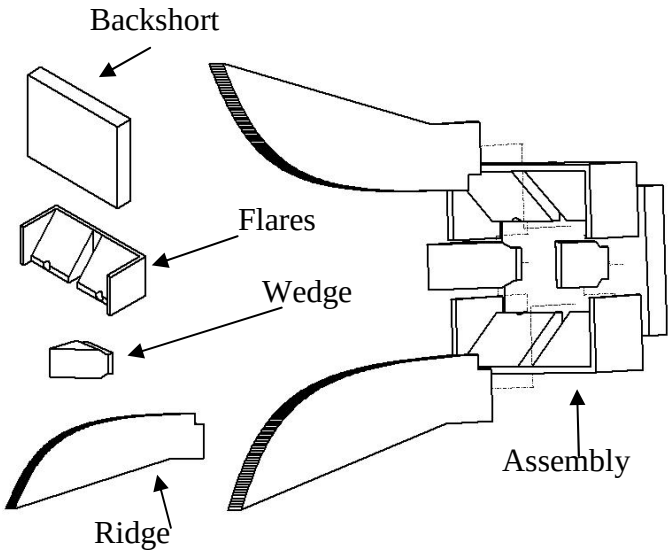

Figure 3.2. Ridges and waveguide launcher assembly with components.

Figure 3.3 shows the coaxial feeding section of the horn antenna. This section consists firstly of a connector (typically N-type). The outer conductor of the coaxial feed line is implemented using a bush that passes through a hole in the ridge and is connected to the top ridge and outer of the connector. The bottom ridge contains another bush, with a hole that is toleranced in order for a custom collet with spring fingers to be held with a press fit. The inner conductor consists of a pin passing through the bush and is connected to the bottom ridge using a collet-bush combination. This assembly allows for identical ridges to be manufactured for both the top and bottom ridges of the DRGH antenna.

In the next sections it will be shown how each of the assemblies and parts were modelled individually in FEKO and then combined to form the complete model.

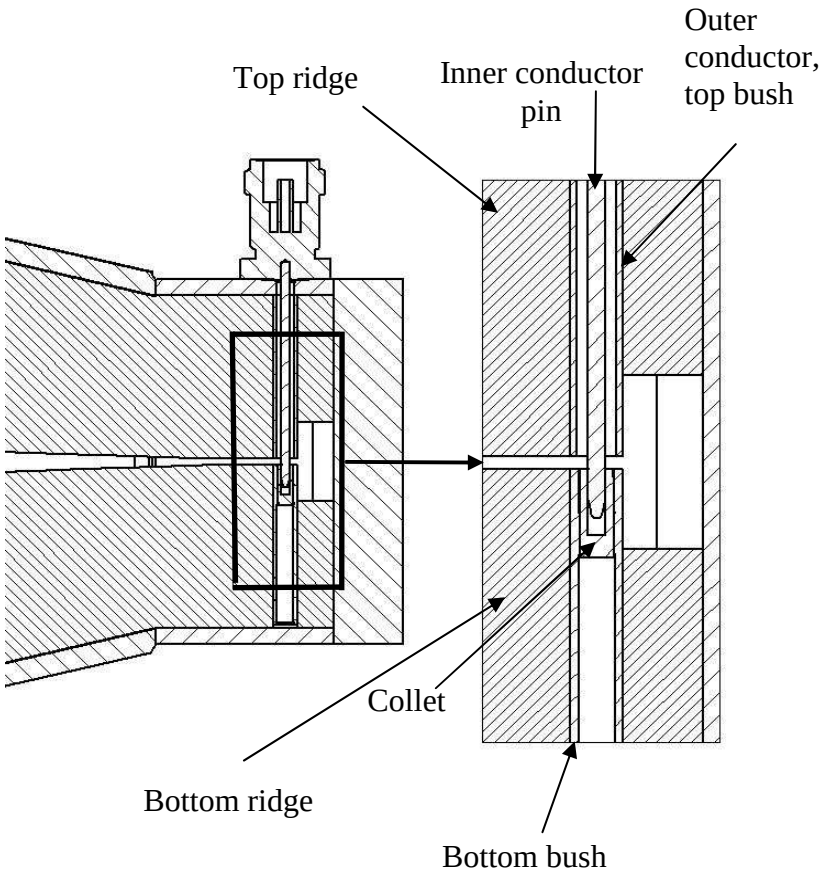

Figure 3.3. Cross sectional cut showing coaxial assembly.

3.3.1. Waveguide Launcher section of the DRGH

This section shows how the launcher assembly was modelled in FEKO. The waveguide launcher section includes the backshort, launcher flares, wedges and cavity part of the ridge.

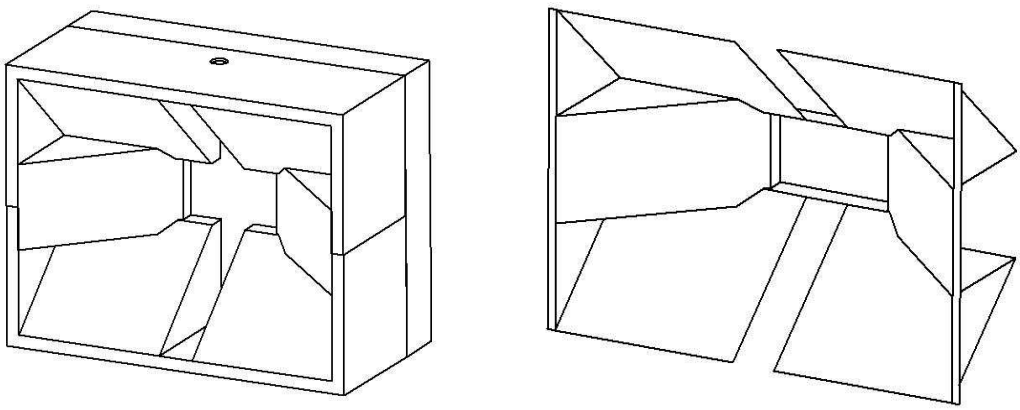

Figure 3.4. Model of waveguide launcher assembly (left), FEKO implementation (right).

Figure 3.4 shows the Solid Works model that was used to model the waveguide launcher section on the left and the FEKO implementation on the right. The dimensions were verified by overlaying the parasolid file from Solid Works with the FEKO file. The outside structure of the waveguide launcher section has little effect on the radiation characteristics of the DRGH antenna. In order to reduce the amount of unknowns in the final model, these plates were not included in the model.

3.3.2. Ridges

The profile of the ridge is typically exponential with a linear taper and a linear section that starts at the back of the feed point. Figure 3.5 shows the FEKO model of the ridges.

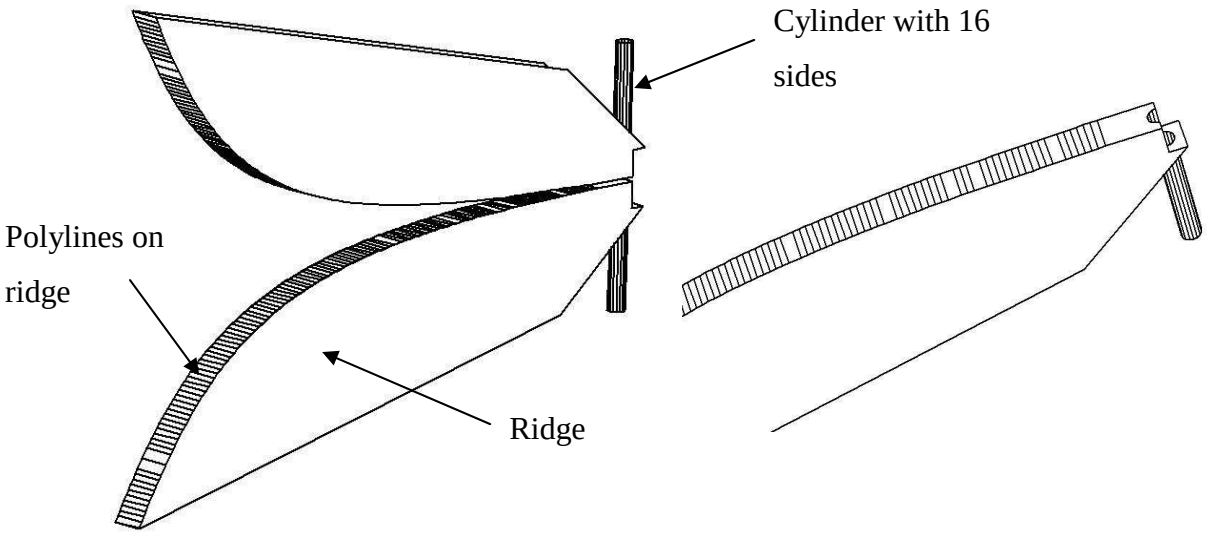

Figure 3.5. FEKO model of ridges.

A single polyline was created using imported points from a text file that contained the ridge profile. These points were obtained from the Solid Works model of the manufactured 1-18 GHz DRGH antenna. This curve was then swept to create a ridge with the correct width. The lines created by this sweep ensured that the ridge is meshed much finer and therefore the ridge profile would be modelled more accurately. Finer meshing on the ridges is also needed since most of the fields and currents are confined between the ridges. Sides were added to the ridge with polygons. The cylindrical section into which the feeding section was to be modelled was approximated by a cylinder with 16 sides. The cylinder was created by sweeping a 16 sided polyline along its axis. Perfectly round cylinders can

be modelled easily in FEKO. The lines and flat faces on the cylinder with 16 sides, however, force the mesher to mesh a much more homogeneous, symmetrical and ultimately better approximation to a round cylinder.

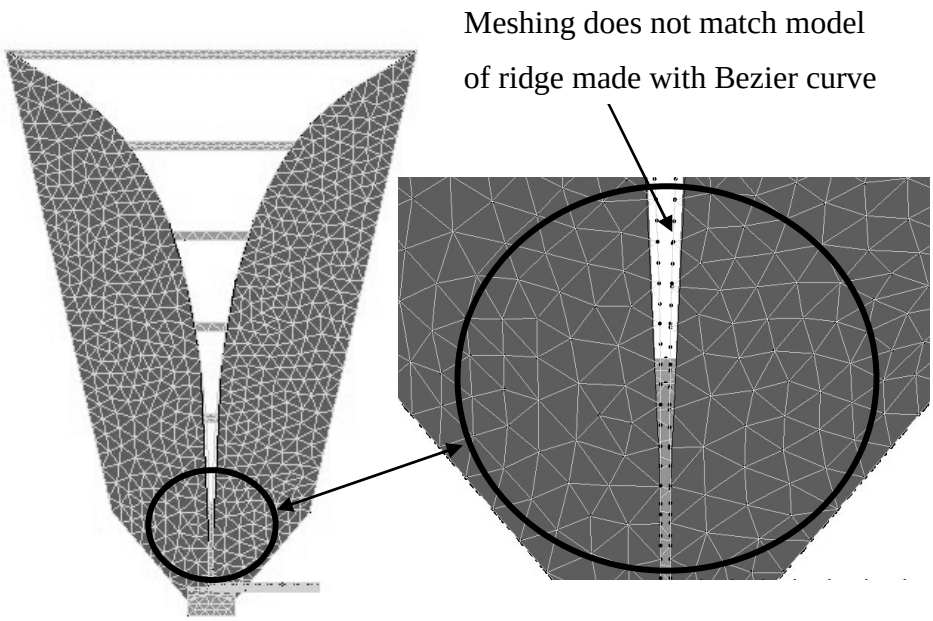

Figure 3.6. Inaccurate meshing when using Bezier curves for ridge profile.

It is important to note that initially Bezier spline curves were used to model the exponential profile of the ridges. Inaccurate VSWR results led to an investigation and closer study of the mesh revealed that the mesh did not follow the Bezier curve exactly as is shown in Figure 3.6. It might be possible that this is only a viewing error, however, after the ridges were created with polylines using the exact points from the Solid Works model the VSWR results became more accurate. The latest version of FEKO has an analytical curve model that would be ideal for ridges. Since the simulation model produced accurate results and the research was already nearly finished it was decided not to implement the analytical curve at such a late stage.

Figure 3.7 below shows how the ridges were unioned with the waveguide launcher assembly.

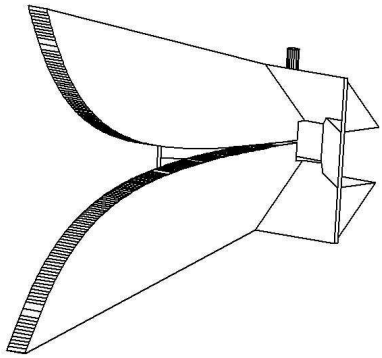

Figure 3.7. Ridges unioned with waveguide launcher assembly.

3.3.3. Coaxial feeding section of the DRGH

Historically the whole coaxial feeding section of DRGH antennas was modelled by connecting a wire between the ridges and placing a source on the wire. The model used in [1, 2, 15] modelled the complete coaxial feeding section in order to improve accuracy. This unfortunately means that the horn now only has 1 symmetry plane instead of two. The coaxial line in [1, 2, 15] was modelled with eight radially directed, equally spaced co-phasal voltage sources between the inner and outer conductor as shown in Figure 3.8 (a) in order to create a TEM mode on the coaxial line. The inner and outer conductors comprised two eight sided cylinders.

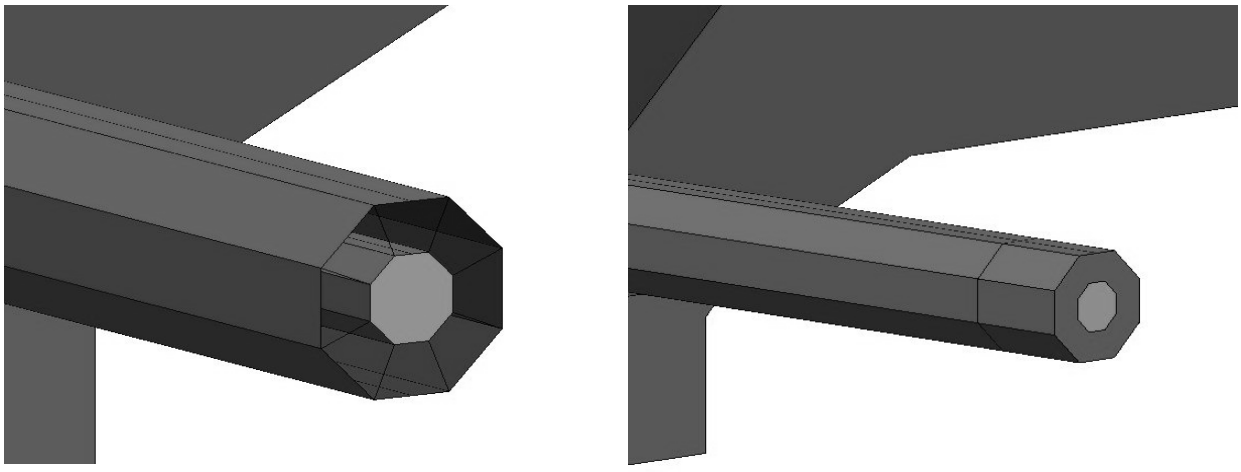

(a) (b)

Figure 3.8. Coaxial excitation with wires and sources (a) and with waveguide feed (b).

Currently FEKO includes a waveguide feed excitation for coaxial lines that produces a much more accurate TEM mode on the coaxial line. The excitation can also be forced to only excite the fundamental mode. The improved model with the waveguide feed can be seen in Figure 3.8 (b).

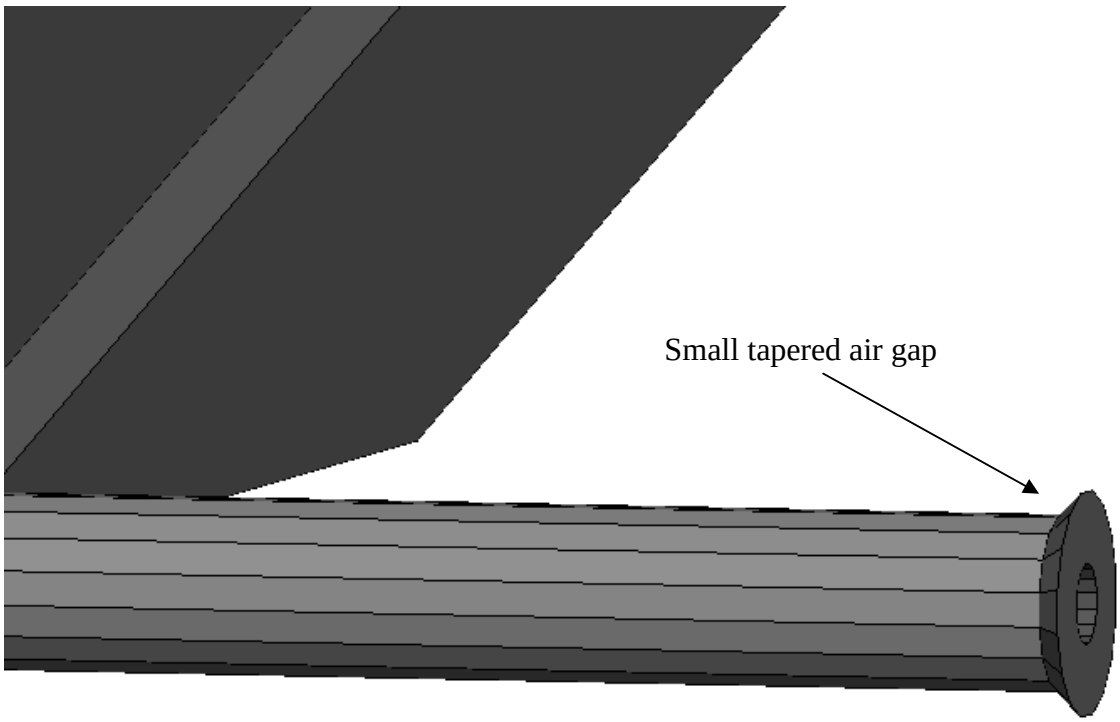

Figure 3.9. Small compensating air gap with a taper.

The N-type connector has a dielectric core while the coaxial line is filled with air. The discontinuity between the connector and the air filled coax line is compensated for by a small tapered air gap as shown in Figure 3.9. The waveguide excitation was applied inside the N-type connector on the face between the inner and outer conductor. The feed was forced to propagate only along the coaxial line towards the ridges and only the fundamental mode is excited at the feed point.

It is further important to notice that the meshing on the coaxial model of the inner and outer conductor was improved (enforced to be finer) by using a 16 sided cylinder instead of an 8 sided one as in [1, 2, 15]. The model of the N-type connector that includes the dielectric core is shown in Figure 3.10. The dielectric material was given the electrical properties of Teflon and evaluated with the SEP method.

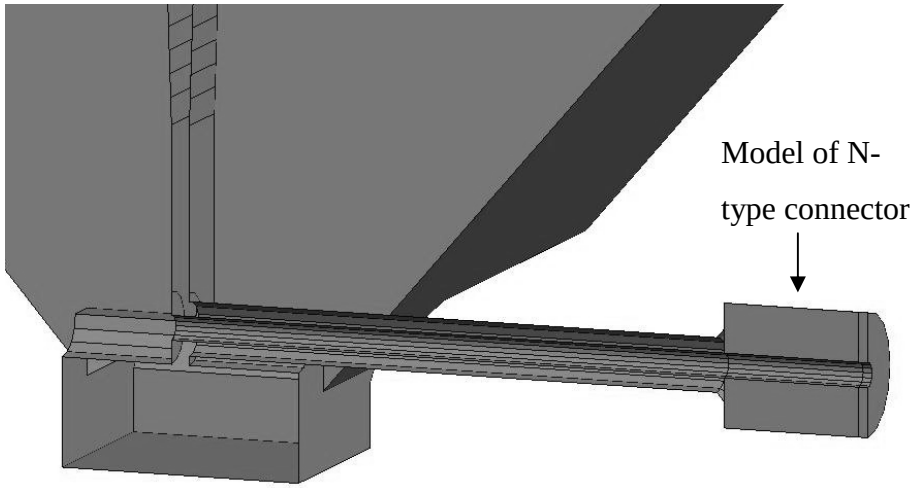

Figure 3.10. Model of N-type connector that includes dielectric core.

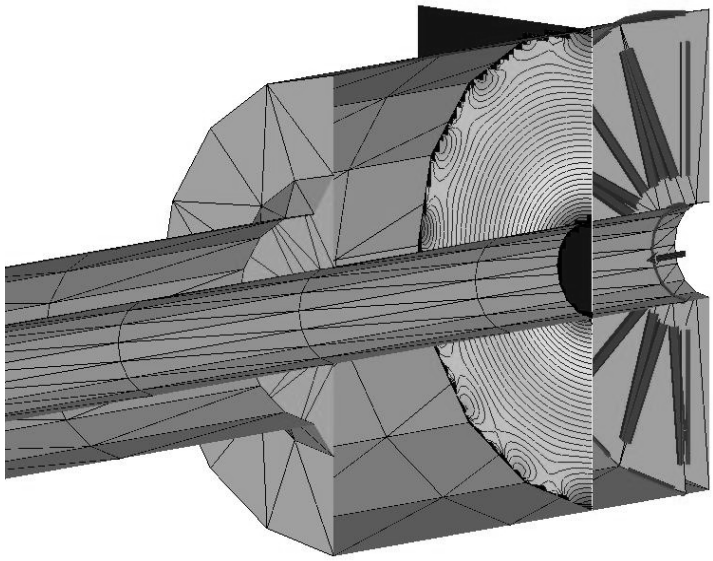

Figure 3.11. TEM mode in N-type connector.

A near field cut through the final N-type connector model, just below the waveguide port shows that a very accurate TEM mode has been excited in the coaxial feed line (Figure 3.11). Figures 3.12 and 3.13 show the TEM mode as it propagates along the coaxial line.

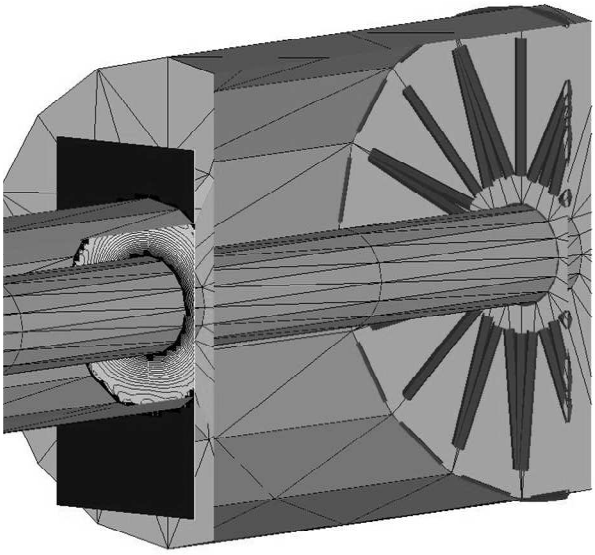

Figure 3.12. TEM mode inside coaxial line just after N-type connector.

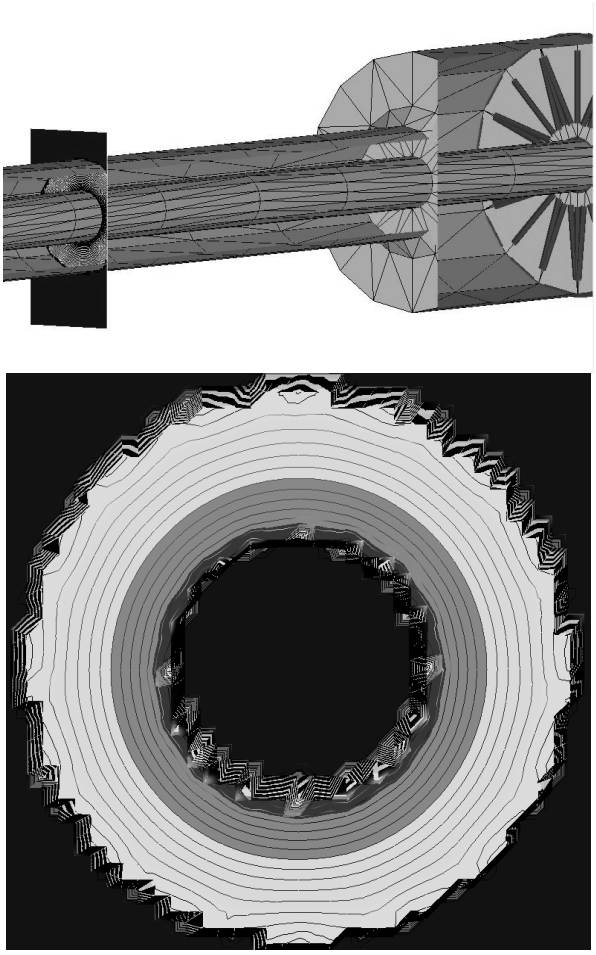

Figure 3.13. TEM mode in coaxial feed line.

3.3.4. Flared Waveguide section of the DRGH

The flared waveguide consists of three parts, the E- and H-plane sidewalls and the ridges. Figure 3.14 shows how the flared waveguide was implemented in FEKO. This figure shows how all the non-essential geometry features were removed, for example the finite thicknesses of the sidewalls. Spaces were left in the H-plane sides where the ridges were modelled (see Figure 3.14 below).

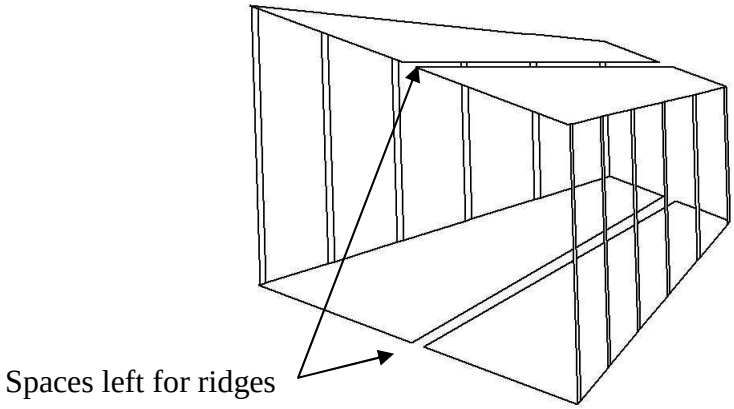

Figure 3.14. Flared waveguide E- and H-plane sidewalls.

The flared waveguide and the waveguide launcher FEKO models were combined to form the complete model. Figure 3.15 shows the final complete unmeshed FEKO model.

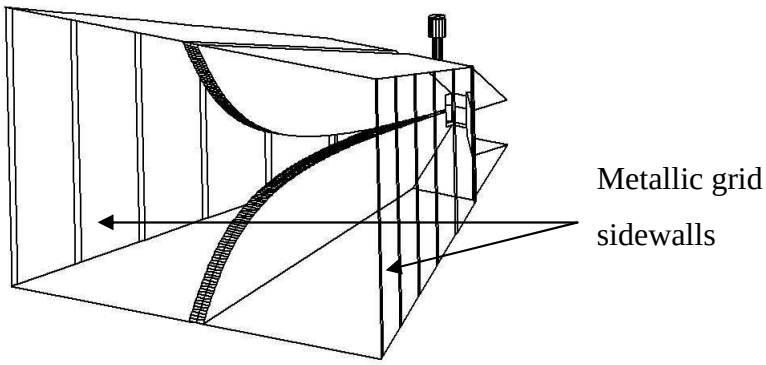

Figure 3.15. Final unmeshed FEKO model.

The traditional horn antenna suffers from pattern deterioration at frequencies above 12 GHz which can be reduced by removing the E-plane dielectric sidewalls [18]. It was found that it is not the metallic strips itself, but rather the dielectric on which the strip is printed that causes pattern breakup and an on-axis gain drop at 18 GHz [18]. Thus sidewalls of the grid type were implemented in the model to retain the low frequency performance of the DRGH. Removing the dielectric improved on axis gain performance from 8 dBi to 12 dBi at 18 GHz. The antenna still suffers from pattern breakup, but less pronounced.

Metallic grids on dielectric sidewalls

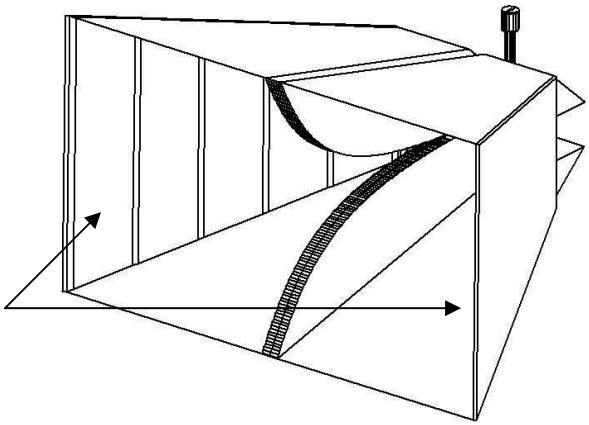

Figure 3.16. FEKO model with printed dielectric sidewalls.

Although the grid type sidewalls without dielectric materials were implemented, but it was decided to test if the same observation can be made in simulation with regard to performance deterioration as was previously proved experimentally [18]. Dielectric sidewalls with metallic grids were included for the model (see Figure 3.16) and the boresight gain results compared with that of the model with no dielectric sides. The results for the boresight gain can be seen in Figure 3.17. Exactly the same observation can be made from these simulation results as was found in [18], namely that the dielectric material is one of the causal factors in the pattern breakup at 18 GHz as can be observed by the increased boresight gain drop at 18 GHz.

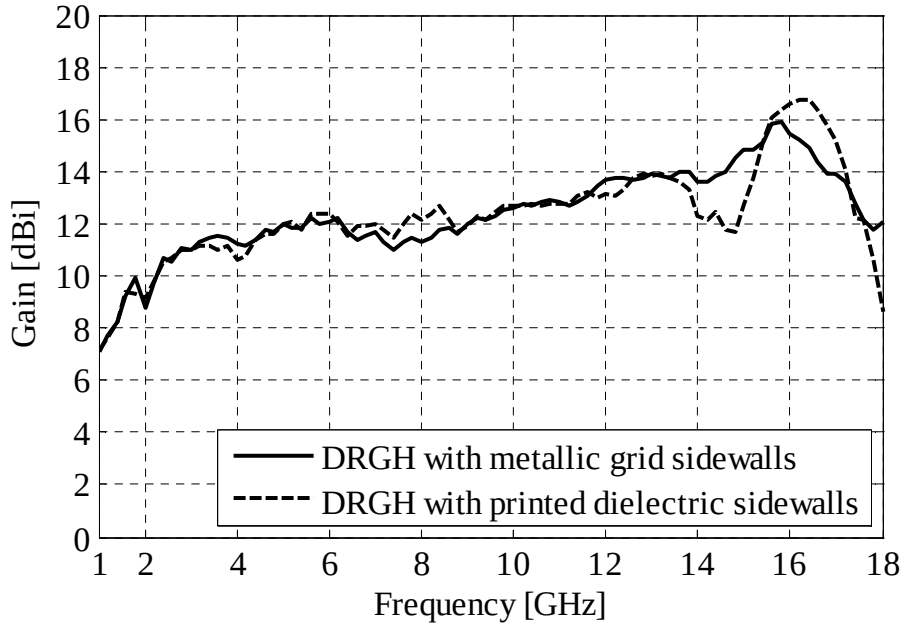

Figure 3.17. Pattern deterioration due to E-plane dielectric sidewalls as observed in boresight gain.

3.4. Meshing the DRGH model for simulation

The accuracy, memory requirement and runtime of an electromagnetic model are determined by the meshing. A too fine mesh might lead to very long runtimes or even impossible memory requirements, while a very coarse mesh might lead to inaccurate results. Typical guidelines for mesh element sizes are given in the FEKO user manual [30]. The recommended edge element size is given as λ/(5-6) with a preferred size of λ/(8-10).

The horn antenna model was discretised using perfectly electrically conducting (PEC) metallic triangles. The model was meshed with various mesh sizes to find the best trade-off between accuracy and physical constraints. It was found that an overall final maximum edge length size of λ/3 at 18 GHz provided accurate results as well as acceptable simulation times. FEKO does not allow the user to specify different mesh sizes for different frequencies; therefore the same mesh element size was used at all the other frequencies (5.56 mm). This means that the meshing improves as the frequency decreases. At 10.8 GHz the meshing is at the recommended size of λ/5 and this improves further for the lower frequencies. The basic model meshed at a mesh element size of λ/5 and λ/7 at 18

GHz was evaluated, but the results did not vary significantly (see Figure 3.18). The only variation was right at 18 GHz (difference approximately of 1 dB).

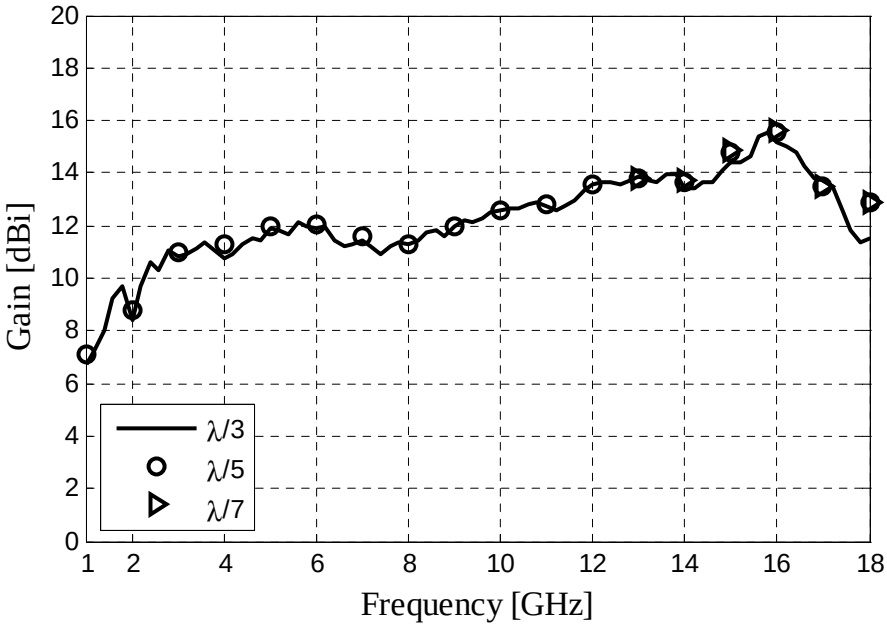

Figure 3.18. Boresight gain of simulated antenna with various mesh sizes.

Seeing that the result for the basic model (with a λ/3 mesh at 18 GHz) compared well to measured results i.e. was verified it was felt that it was not necessary to decrease the mesh element size (see Section 3.5). The slight increase in accuracy at 18 GHz did not justify the large amount of extra resources required when using smaller mesh elements (42 141 unknowns for λ/5 and 76 284 unknowns for λ/7 compared to 17 260 unknowns for λ/3). See Table 3.1 for more detail with regard to the computational requirements.

The final mesh was a non-uniform mesh (in FEKO referred to as non-homogeneous) with smaller and somewhat distorted mesh elements near the coaxial section and between the ridges. FEKO's mesher forces the mesh to be flat to flat surfaces/faces and to make connections at edge points. See Figures 3.19 and 3.20 below for a comparison between a coaxial line with flat faces and curved surfaces. Thus I could utilise the geometrical construction to force smaller mesh sizes in areas I expected to be more critical and to obtain a better representation of the geometry. According to [1, 2, 15] different geometry discretisations can lead to electromagnetic artefacts and since the meshing of certain areas was forced smaller and somewhat distorted, the mesh was not homogeneous. No strange effects due to a non-homogeneous mesh sizes were observed.

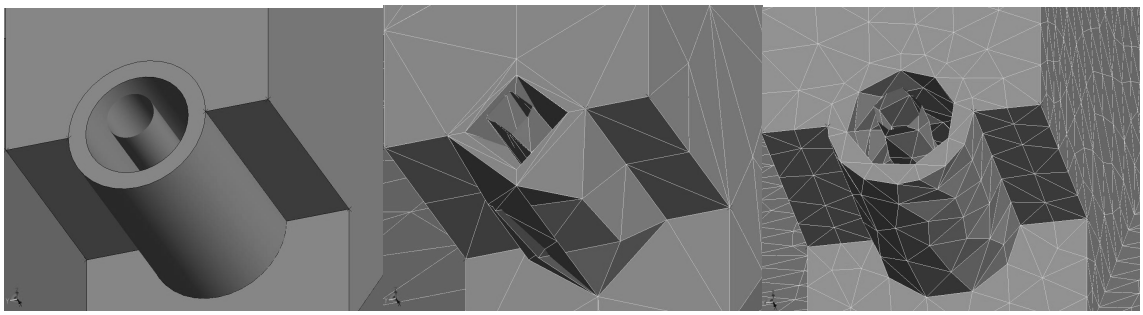

Figure 3.19. FEKO CAD model of cylindrical feed (left), Meshed cylindrical feed, λ/3 at 18 GHz (centre), Meshed cylindrical feed, λ/10 at 18 GHz (right).

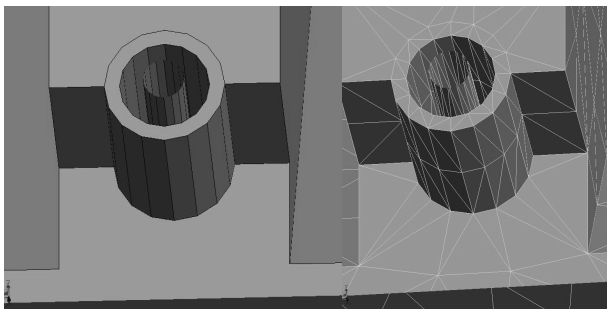

Figure 3.20. FEKO CAD model of polygonal feed (left), Meshed polygonal feed, λ/3 at 18 GHz.

To test the accuracy of the non-uniform mesh, the mesh was refined using FEKO's built in mesh refinement tool to obtain a more uniform mesh (the suggested mesh refinement tolerance was used). The simulation subsequently did not give any warnings of a non-homogenous mesh. A comparison for the boresight gain of the basic antenna model with uniform and non-uniform mesh can be seen in Figure 3.21. The simulation results for uniform and non-uniform meshes correspond very well with the spot frequencies at 5.5 and 18 GHz differing by approximately 1 dB. As mentioned previously the non-uniform mesh had 17 260 unknowns for λ/3 meshing. The uniform mesh has 19 287 unknowns. This is a very slight increase in the number of unknowns, but a 25% increase in the memory requirement and a 164% increase in simulation time (found to be slightly more than N^2 for memory and N^6 for processing time). The mesh could be refined even further to improve the uniformity of the mesh (i.e. less distorted mesh elements and overall uniform mesh size) with a substantial increase in computational resources required.

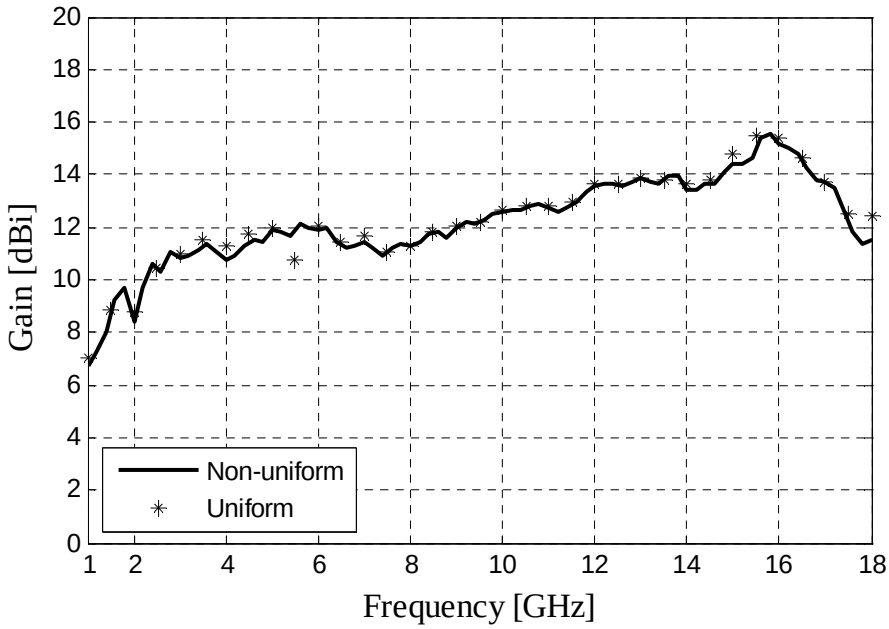

Figure 3.21. Boresight gain of basic simulated model with uniform and non-uniform meshing.

Table 3.1 gives an indication of the computational requirements for the various meshing schemes. The simulations were run on a 2.5 GHz quad core processor with a Windows XP professional operating system and 8 GB RAM. For the λ/7 mesh the RAM was insufficient and the simulation had to use hard drive disk space.

Table 3.1. Computational requirements for various meshing schemes.

Mesh (18 GHz)	Unknowns	Peak Memory (GB)	% Increase from case 1	Overall runtime per frequency point (h)	% Increase from case 1
λ/3 non-uniform	17260	1.117	-	0.198	-
λ/3 uniform	19159	1.397	25.07	0.523	164.43
λ/5 non-uniform	42141	3.32	197.22	3.394	1616.91
λ/7 non-uniform	76284	10.737	861.24	15.596	7789.57

What is important to note is that measured results were available before the numerical model of the antenna was developed. Therefore the accuracy of the model could be assessed as the model was developed. Since it was found that the model with non-uniform

mesh provided accurate results it was decided to continue with the non-uniform mesh (see Section 3.5).

The final meshed model is shown in Figure 3.22. The final mesh included the following number of elements:

- 11 126 metallic elements in free space
- 32 metallic elements in a dielectric
- 256 metallic elements on the surface of a dielectric
- 32 triangles for the surface of a dielectric

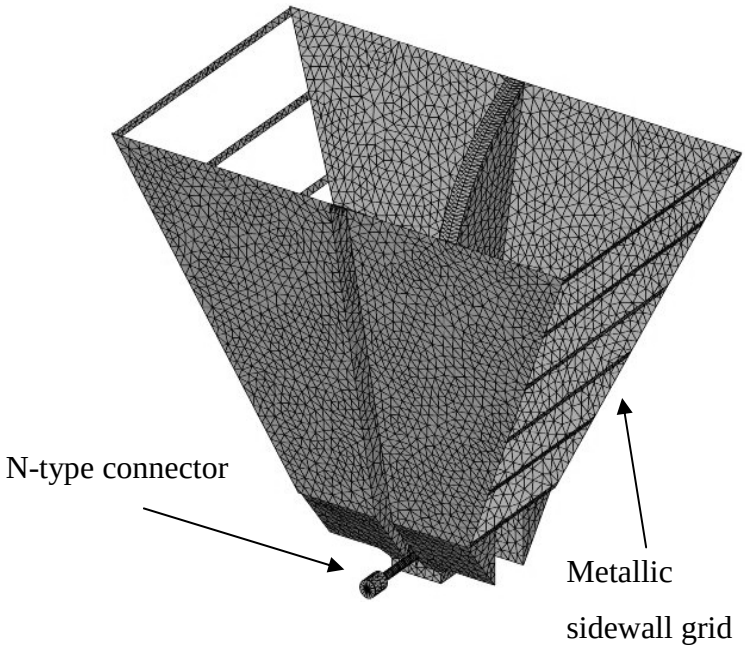

Figure 3.22. Final meshed FEKO model.

3.5. Experimental validation of the FEKO model

This model with the accurate coaxial feed has a single symmetry plane. A magnetic symmetry plane was implemented in order to reduce CPU time and memory without the loss of accuracy as was done in [1, 2, 15, 18]. The electric field integral equation was used. The combined field can be used to improve accuracy, but this will increase simulation time significantly. For the calculations performed by FEKO, single precision was used. FEKO

gives warnings when single precision is inadequate and double precision should be used, especially when the MoM matrices are nearly singular. No such warnings were found during simulation and therefore it was decided that single precision calculation would be adequate. The three dimensional far-field patterns were calculated as well as the reflection coefficient at the waveguide port at 86 linearly spaced frequency points between 1 and 18 GHz.

The final numerical model was validated using measured data of a carefully constructed DRGH antenna. The antenna measured was assembled with care to reduce any effects from manufacturing or assembly tolerances. Comparisons between measured and numerical boresight gain and VSWR for this DRGH antenna are presented in Figures 3.23 and 3.24, respectively. The maximum gain difference is 1.5 dB and the maximum VSWR difference is 0.4.

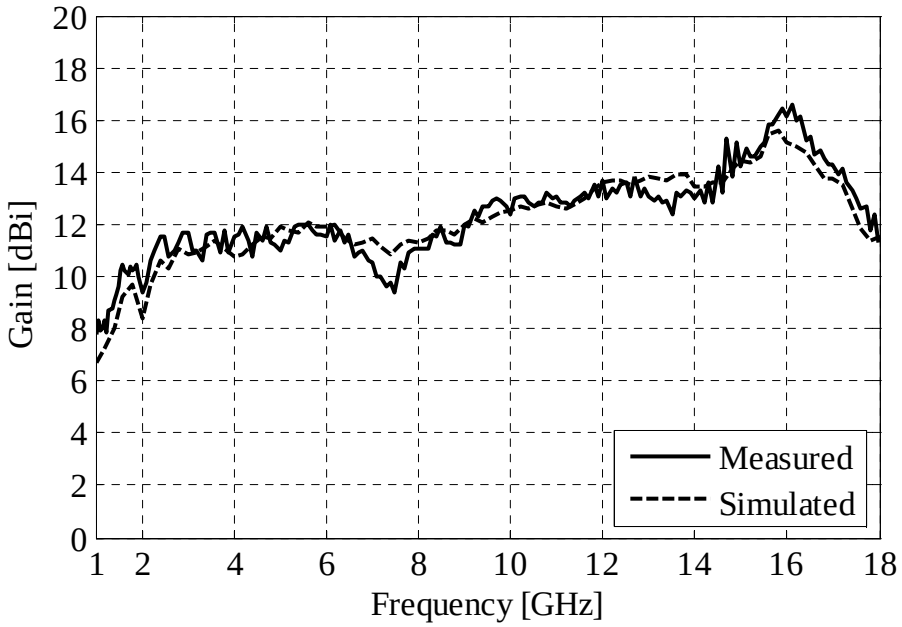

Figure 3.23. Comparison between FEKO model and measured results for boresight gain.

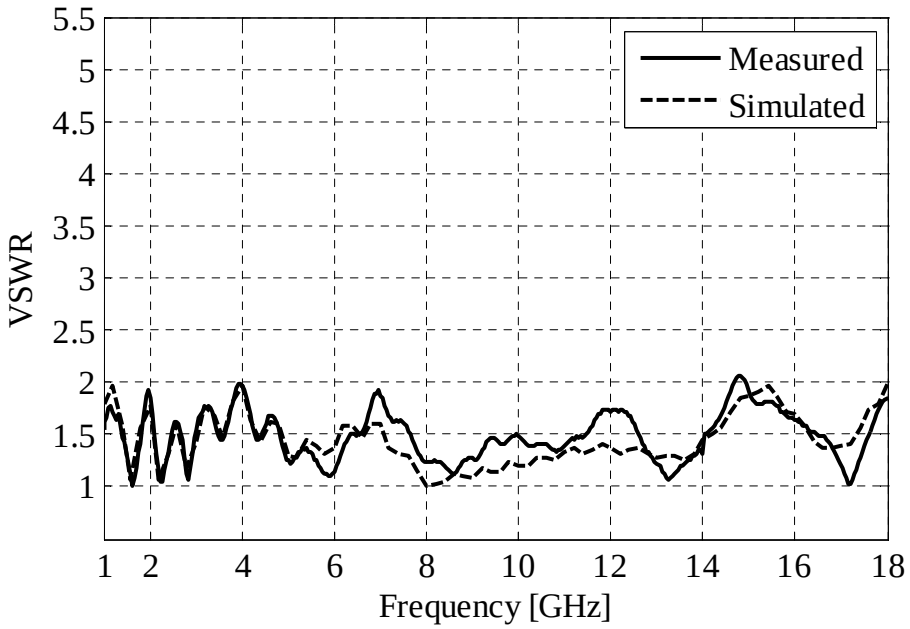

Figure 3.24. Comparison between FEKO model and measured results for VSWR.

Various differences between the simulated and measured models in [1, 2, 15] were explained by differences in the measurement setup versus perfect space in which the numerical model is placed, as well as discretisation at the feed not being fine enough. In [18] the differences are explained by losses in the aluminium body (which the simulation model does not have since PEC material is used), of the antenna as well as small gaps between the parts of the antenna.

The model developed in this dissertation is more accurate when compared to above-mentioned models. The most plausible explanation to the very small differences (for example the small ripples in the measured patterns) is tolerances in the machining and assembly process. Furthermore it must be remembered that typically the gain of the antenna can only be measured to within 0.5 dB. From the results above it was decided that the developed 1-18 GHz DRGH antenna numerical model is adequately accurate to conduct the present study.

3.6. Summary

At the beginning of this chapter the selection of the numerical method and corresponding software package were discussed. The MoM as implemented in FEKO was chosen as the best method for the present study.

The development of the numerical model of a typical 1-18 GHz DRGH antenna in FEKO was then presented in detail. The dimensions for the electromagnetic model were obtained from a Solid Works model of the antenna. The electromagnetic model includes dielectric materials for the N-type connector. The effect of dielectric sidewalls on the performance of the antenna was also investigated in simulation. The model uses a waveguide feed, which is an improvement over other models that used less accurate feeding methods.

Development of an accurate mesh from the CAD (Computer Aided Design) model is a very important step in development of an accurate numerical model. Important parameters such as the mesh sizes, homogeneity and precision were subsequently investigated in this chapter.

Finally comparison with measured data showed excellent agreement with the numerical model and therefore the model has been validated.

CHAPTER 4 MODELING OF MECHANICAL DEFECTS AND SIMULATION RESULTS

4.1. Introduction

A detailed description of the mechanical defects implemented in the basic numerical model is presented in this chapter. The typical defects observed in the manufacture of this antenna type are discussed as well as possible origins of the defects. The simulated results for the numerical model with the implemented mechanical defects are then presented and the effects of the defects on the performance of the antenna characterised. These results are compared to typical measured results and a number of observations are made with regard to which areas exhibit the highest sensitivity to tolerances.

In Section 4.2 a short discussion is given on the investigation into the cause of resonant behaviour in the 1-18 GHz Double Ridge Guide Horn (DRGH) antenna. Section 4.3 presents representative measured results of 1-18 GHz DRGH antennas with severe resonance problems in the boresight gain and VSWR. Results are also presented for the variation in boresight gain for a number of production antennas.

In Section 4.4 the implementation of gaps typically encountered during the mass production and assembly of DRGH antennas are presented. These gaps were incorporated into the very detailed FEKO model presented in the previous chapter. It is important to note that all the gaps included in the numerical model are ideal in the sense that they have constant dimensions and are symmetrical (in order to exploit symmetry and reduce computation time). In practice the gaps would not necessary be symmetrical and most certainly not ideal. After the implementation of each gap is presented, the simulation results are also given. The effects of the defects on the performance of the antenna are evaluated and discussed. These results are compared to typical measured results and a number of observations are made with regard to which areas are the most sensitive to tolerances.

Finally the chapter is concluded in Section 4.5 with a summary of the most important observations made in this chapter.

4.2. Investigation into the cause of resonant behaviour

It is hypothesised that tolerances in machining and misalignment in assembly leads to significant performance deterioration and more specific resonant behaviour. Manufacturing tolerances can lead to small variations in the dimensions of the parts. For example the ridge width might be larger than desired by 0.1 mm. Since the numerical model was made completely parametric it is easy to study the effects of small variations on the dimensions of the parts itself. In this dissertation the focus was on how gaps that are formed in the assembly of various parts with slight tolerances, lead to performance deterioration and not a sensitivity investigation on the parts itself. This type of study necessitated the addition of geometrical features depending on the type of gap considered. The features were implemented to be parametric for a complete sensitivity analysis.

A number of sections where gaps could be formed were identified. The antenna was divided into two main sections, namely the flared waveguide section and the waveguide launcher section for the purpose of the parametric study on the effect of manufacturing and assembly tolerances on the performance of a DRGH antenna. Various gaps were implemented in the flared waveguide section. These included gaps at the interfaces between the waveguide flares and sidewalls with the waveguide launcher section and ridges. It will be shown in this chapter that these gaps produced no significant effect on the VSWR and gain performance of the 1-18 GHz DRGH antenna. Gaps in the coaxial feed and waveguide launcher section were found to have the most pronounced effect on the performance of the antenna. Since dimensionally most of the gaps implemented are very small (0.5-0.05 mm) when compared to the rest of the model, it is very difficult to show how the gap is formed. Therefore pictures that indicate oversized gaps will be shown for clarity.

4.3. Measured results

Typical measured deterioration in the performance for mass produced DRGH antennas are illustrated in Figure 4.1 and 4.2. The measured gain data for two different 1-18 GHz DRGH antennas are shown in Figure 4.1 with severe resonances occurring in the vicinity

of 7 and 14 GHz. This figure shows that one of the antennas in fact has two resonances. Typical VSWR traces are shown in Figure 4.2.

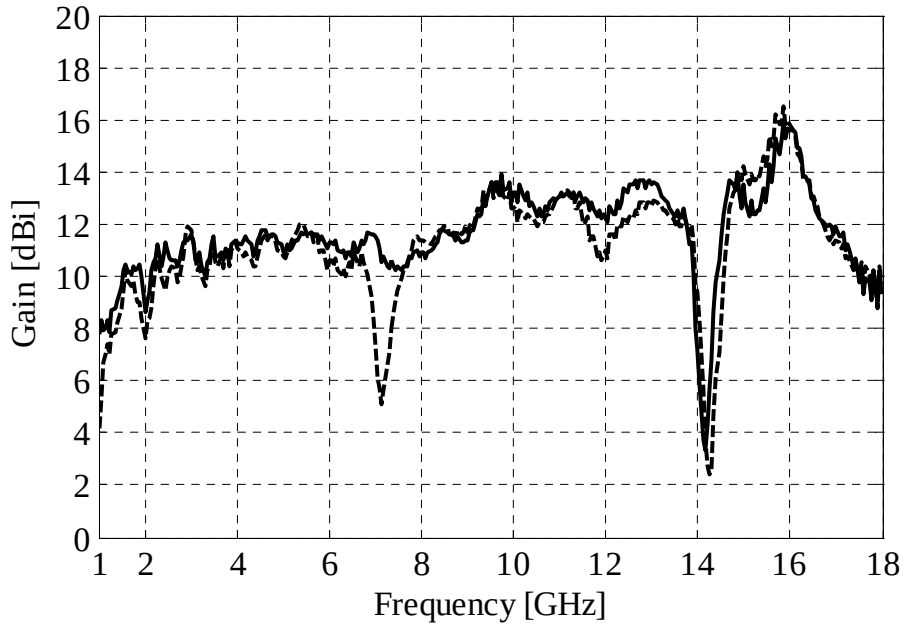

Figure 4.1. Typically measured gain results of production antennas with severe performance deviations (resonance effects).

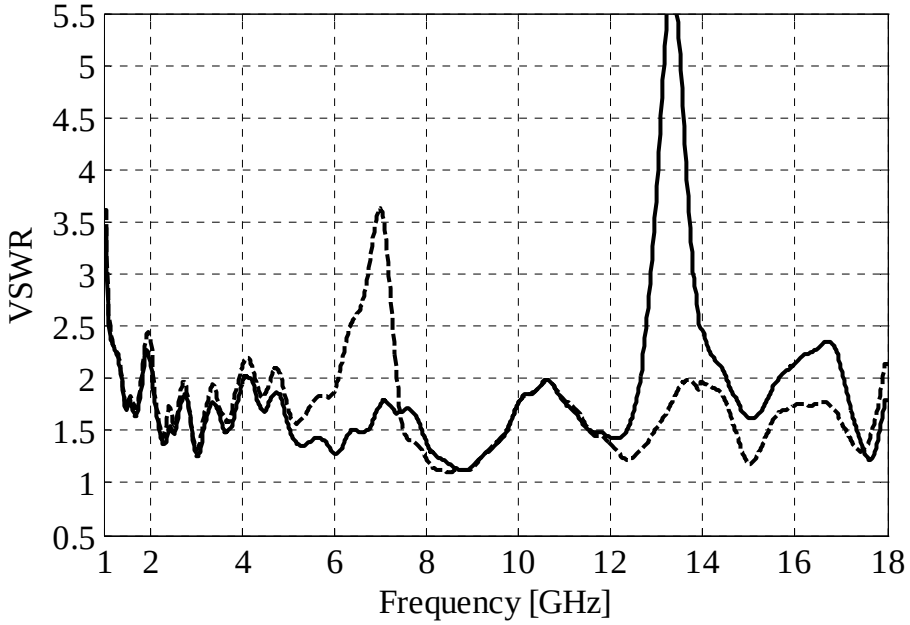

Figure 4.2. Typically measured VSWR results of production antennas with severe performance deviations (resonance effects).

It should be noted that the VSWR and gain traces of Figures 4.1 and 4.2 are not for the same antennas. It is also evident that the resonances are not at exactly the same

frequencies. Representative data was chosen from the measured data available to illustrate the problem. Some of these antennas were disassembled and reassembled a number of times. In the process the resonances would shift in frequency or disappear, the cause being unknown. Figures 4.3 to 4.7 show the the typical measured results between experiments for 5 production antennas.

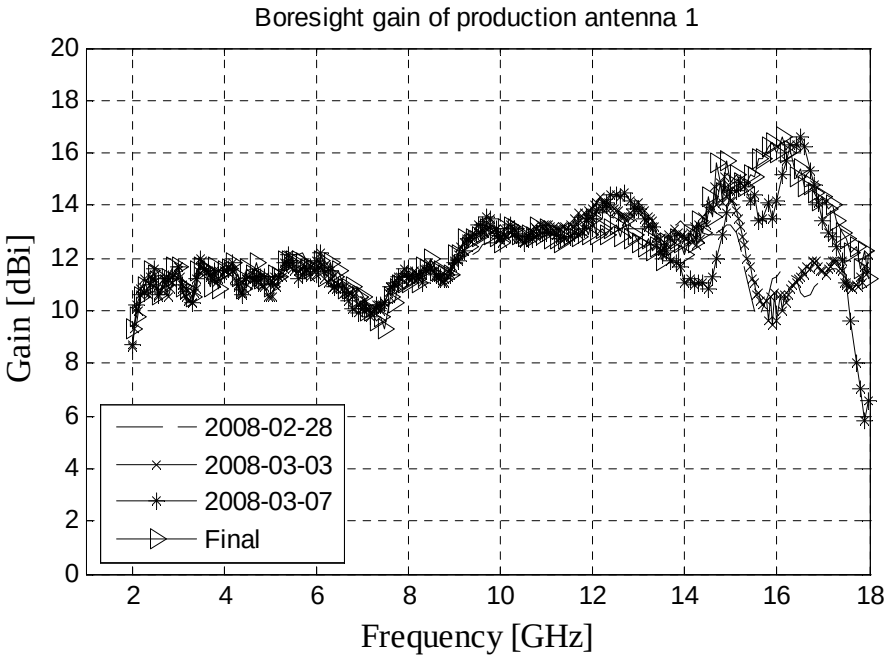

Figure 4.3. Typically measured gain results of production antenna 1.

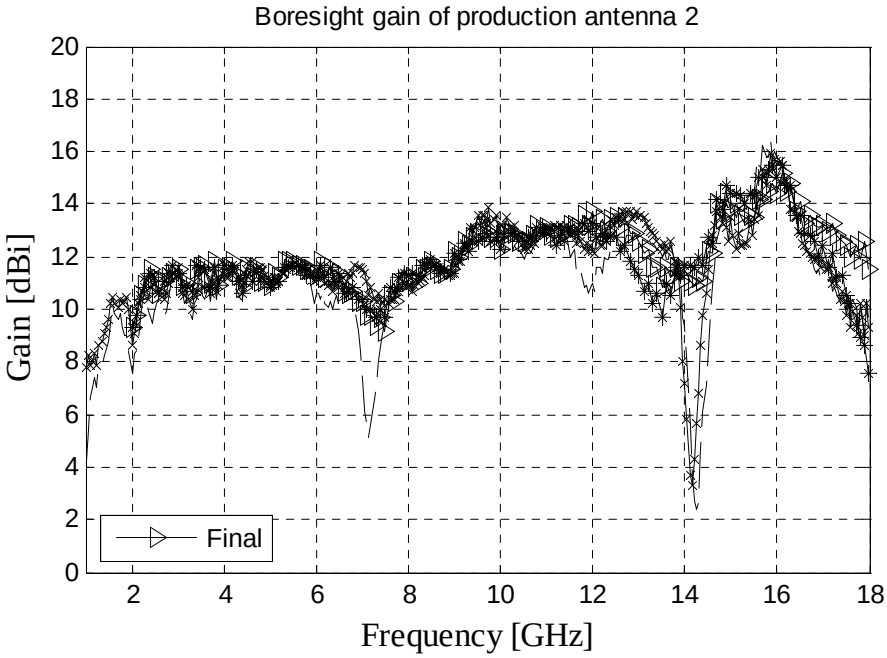

Figure 4.4. Typically measured gain results of production antenna 2.

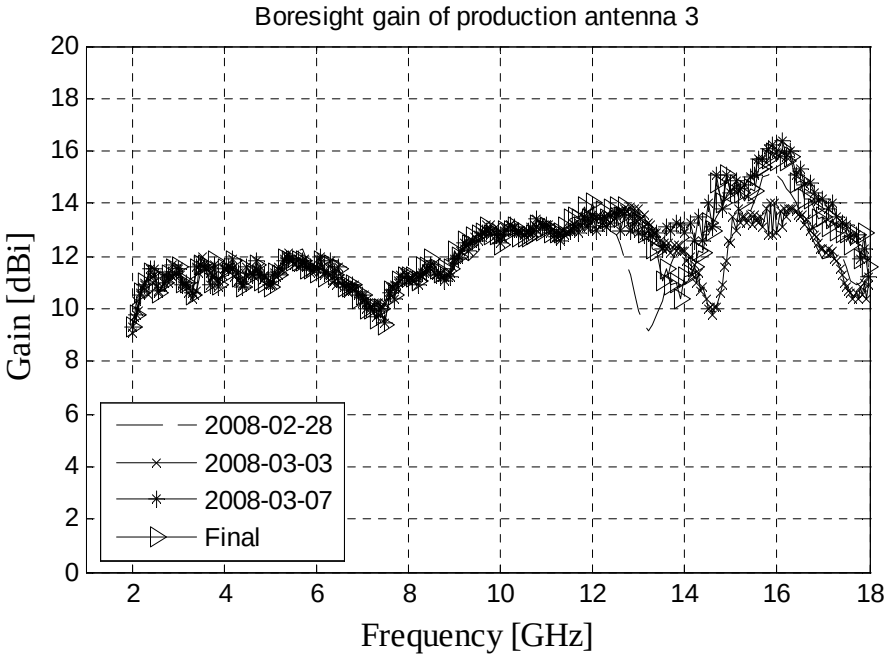

Figure 4.5. Typically measured gain results of production antenna 3.

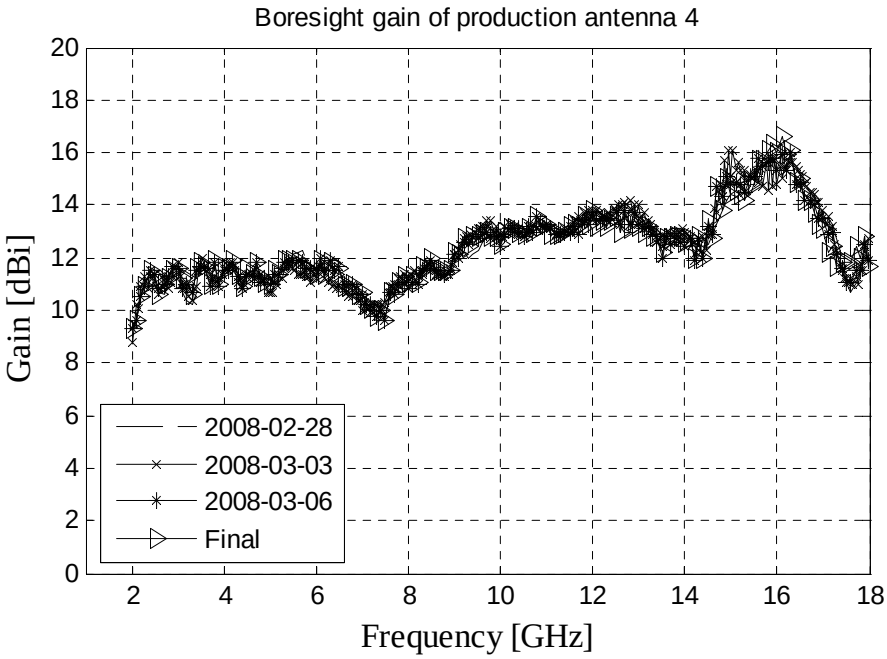

Figure 4.6. Typically measured gain results of production antenna 4.

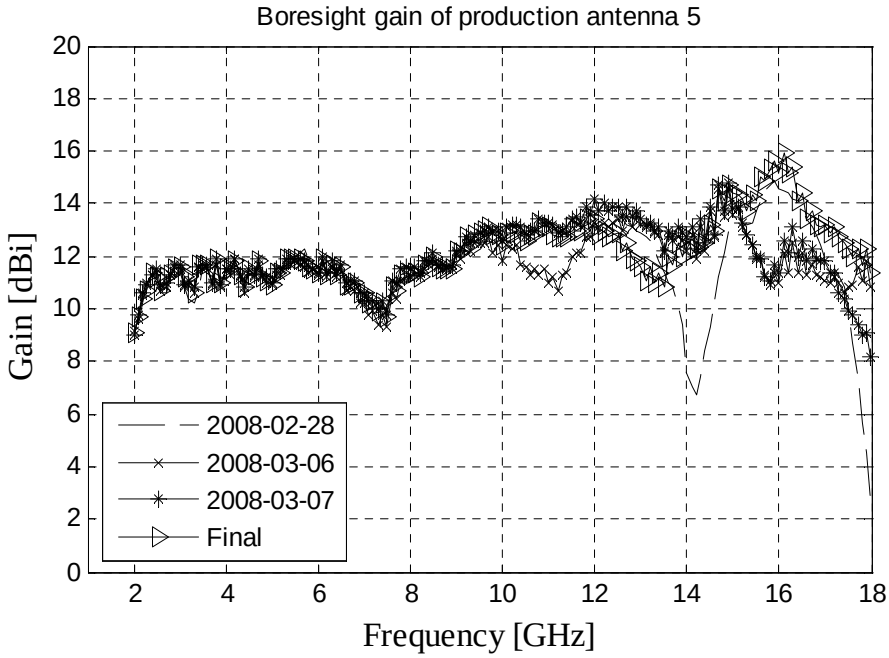

Figure 4.7. Typically measured gain results of production antenna 5.

With a lot of effort a number of antennas could be produced that had no deep resonances. The performance is, however, still far from desirable with a fair amount of gain variation between production antennas, especially in the vicinity of 14 GHz, see Figure 4.8.

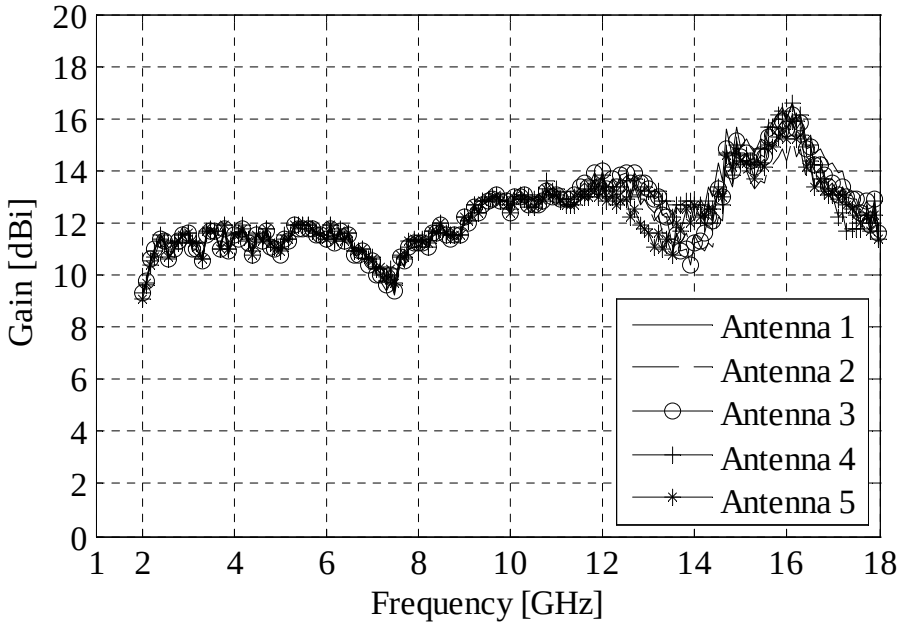

Figure 4.8. Typically measured gain variation of production antennas after significant tuning.

A single antenna from the first production batch that did not have any visible resonance effects when measured was chosen as the reference antenna. The boresight gain of this antenna is compared to the simulation model can be seen in Figure 3.23 and the VSWR in Figure 3.24 in the previous chapter.

4.4. Implementation of and simulated results for numerical model with gaps

4.4.1. Simulated results for reference model

Figure 3.23 shows the simulated co-polarised boresight gain results for the FEKO model of the 1-18 GHz DRGH antenna. Figure 3.24 shows the simulated VSWR. These two parameters were calculated at 86 equally spaced frequency steps between 1 and 18 GHz. Less simulation points would not give enough resolution to observe possible resonances. Mostly only the boresight gain was calculated in simulation as this parameter clearly shows the performance deterioration due to gaps. Calculation of the VSWR parameter in FEKO doubles the simulation time and therefore the effect on this parameter was only calculated for a small number of cases. As mentioned previously the various mechanical defects investigated were included in this model and therefore all the data in the next sections will be compared to these graphs.

4.4.2. Gaps in the flared waveguide section

4.4.2.1 Gap between H-plane flares of waveguide and waveguide launcher

A gap can form between the H-plane flare and waveguide launcher section if the mounting holes for the ridges and H-plane flares had been incorrectly machined or aligned. It can also form if the dimensions of the flare are incorrect and the flare is not aligned properly to the waveguide launcher (see Figure 4.9). This type of gap was simulated in FEKO with two flat plates for the faces of the gap as high as the thickness of the H-plane flare. It should be noted that this gap was only implemented between the top H-plane flare and the waveguide launcher. The gap was implemented right across the face of the waveguide.

The width of the gap is defined as the distance between the H-plane flare and the waveguide launcher. This width was adjusted to be 0.05 mm initially and then varied from

0.1 to 0.5 mm in 0.1 mm steps. Figure 4.10 shows the results from these simulations. When compared to Figure 3.23 it can be seen that there is no difference between the reference trace and all the other simulated results. It can be concluded that electrical contact is not needed between the H-plane flares and the waveguide launcher for proper operation of the antenna.

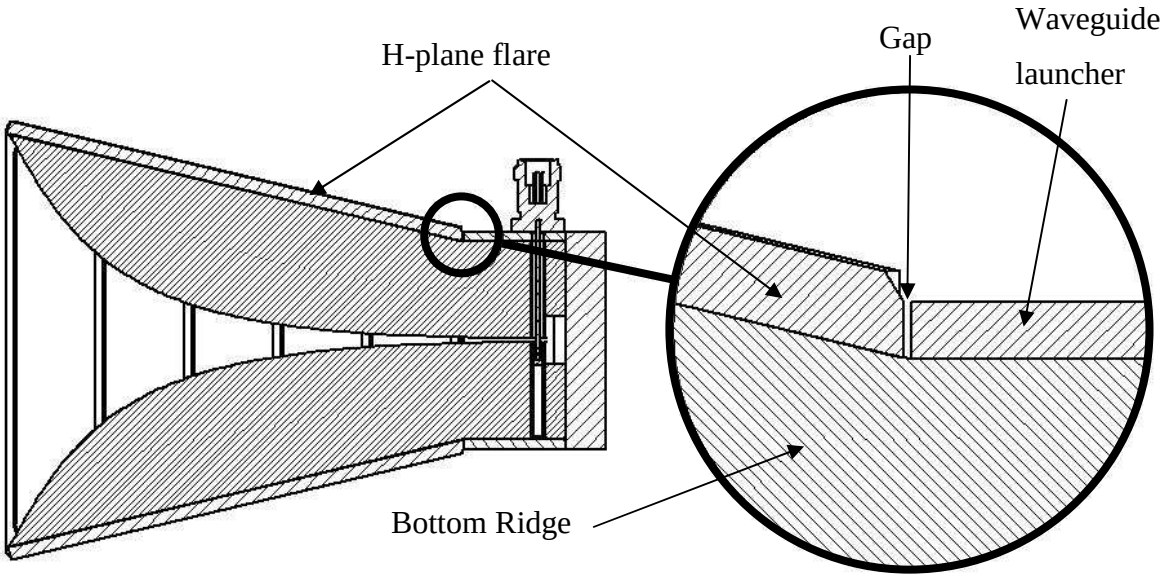

Figure 4.9. Gap between H-plane flare and waveguide launcher.

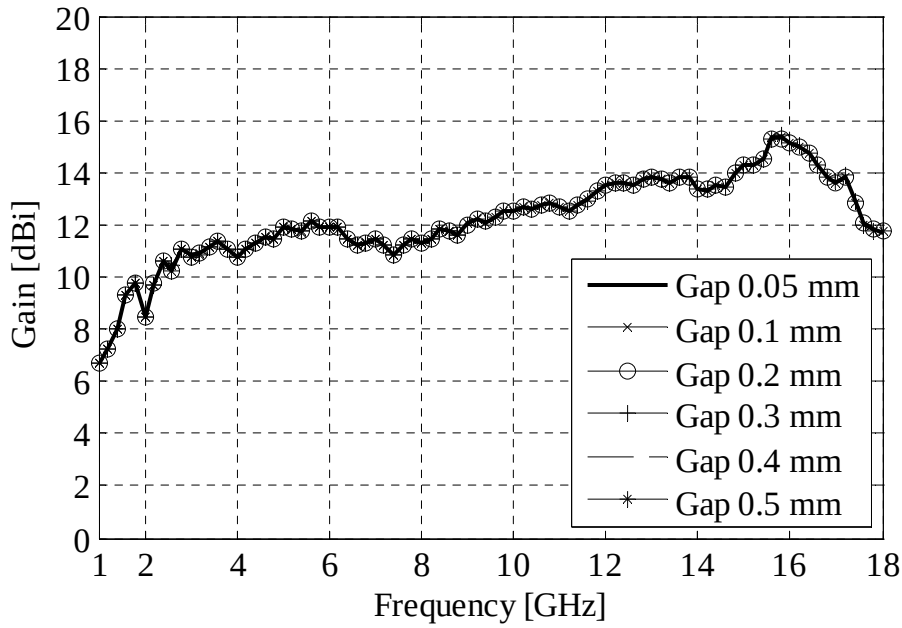

Figure 4.10. Boresight gain results for gaps between H-plane flare and waveguide launcher.

4.4.2.2 Gap between E-plane sidewalls of waveguide and waveguide launcher

If the E-plane sidewall is not properly aligned to make contact with the waveguide launcher, a gap forms between the sidewall and the front face of the waveguide launcher (see Figure 4.11). This might be due to incorrect dimensions on either parts or due to incorrect alignment in assembly. Incorrect alignment may result from human error or faults in machining of the mounting holes. This was simulated in FEKO by removing a small strip from the first grid of the sidewall. Gaps were implemented on both sides of the FEKO model since a magnetic symmetry plane was implemented for the antenna's E-plane to allow faster simulation. The width of the gap is defined as the distance between the sidewall first grid line and the waveguide launcher. This width was varied from 0.1 to 0.5 mm in 0.1 mm steps.

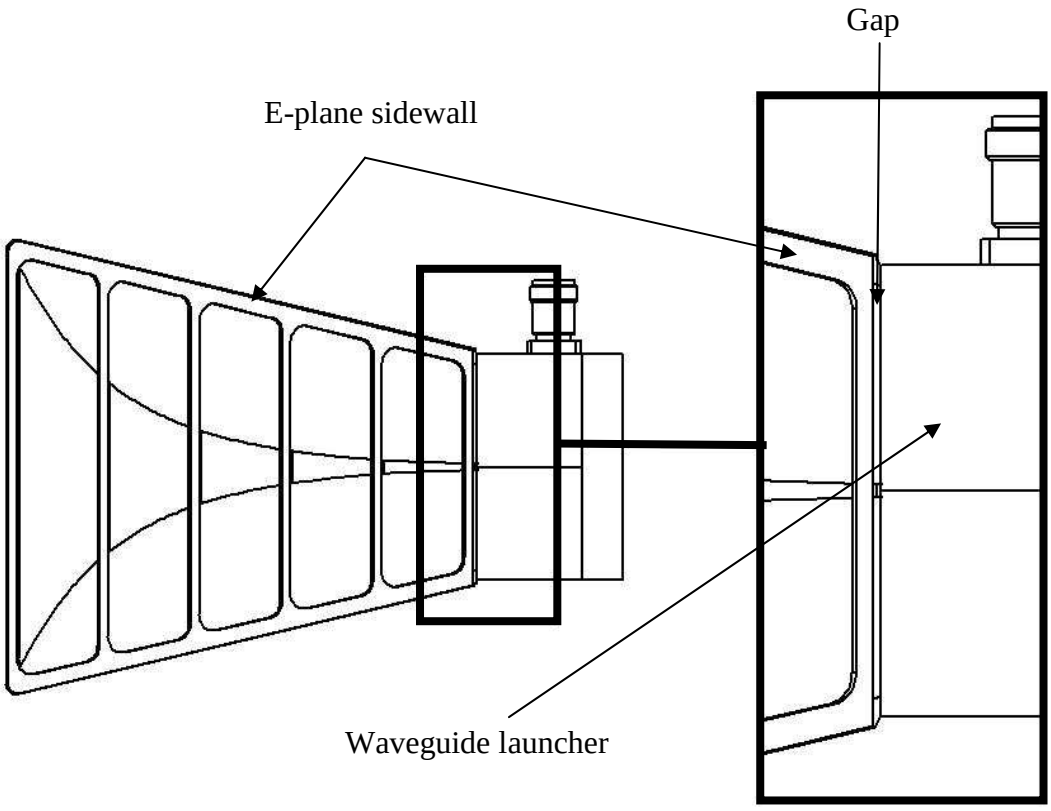

Figure 4.11. Gap between E-plane sidewalls and waveguide launcher.

Figure 4.12 shows the results from these simulations. When compared to Figure 3.23 it can be seen that there is no difference between the reference trace and all the other simulated results. It can be concluded that electrical contact is not needed between the E-plane metallic grid sidewalls and the waveguide launcher for proper operation of the antenna.

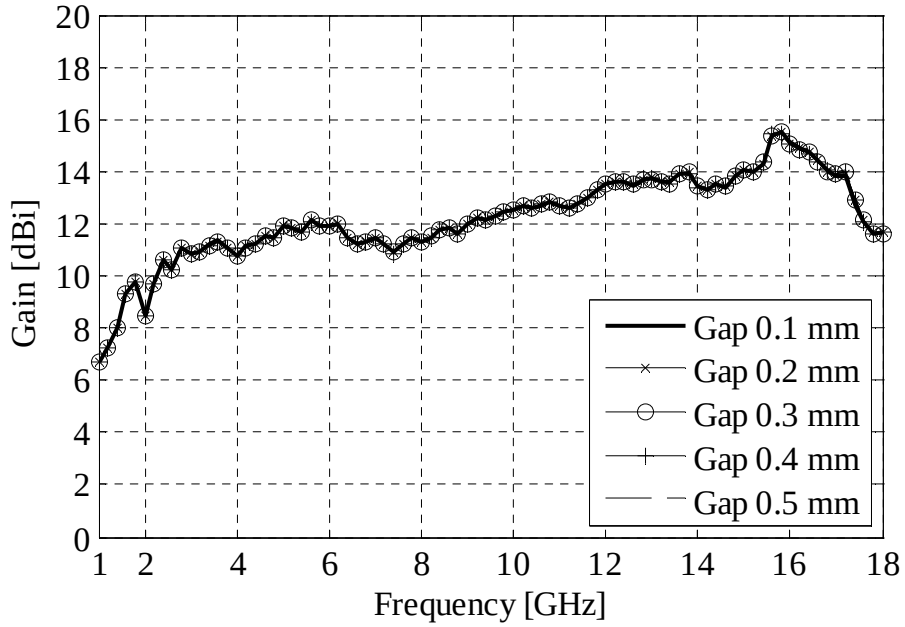

Figure 4.12. Boresight gain results for gaps between E-plane sidewalls and waveguide launcher.

4.4.2.3 Gap between E-plane sidewalls and H-plane flares

If the E-plane sidewall is not properly mounted to the H-plane flares small gaps can form between the faces (see Figure 4.13). This can also occur when the angles at which the sides of the H-plane flare was machined is incorrect. Most probably this type of gap would not be across the whole interface, there might be connectivity in some sections. The gap was implemented to be across the entire interface between the H-plane flare and the E-plane sidewall with faces the height of the H-plane flares' thickness for the sake of simplicity. Gaps were implemented on both sides of the magnetic symmetry plane. The width of the gap is defined as the distance between the E-plane sidewall grids and the H-plane flare interface on which the sidewall is mounted. This width was adjusted to be 0.05 mm initially and then varied from 0.1 to 0.5 mm in 0.1 mm steps.

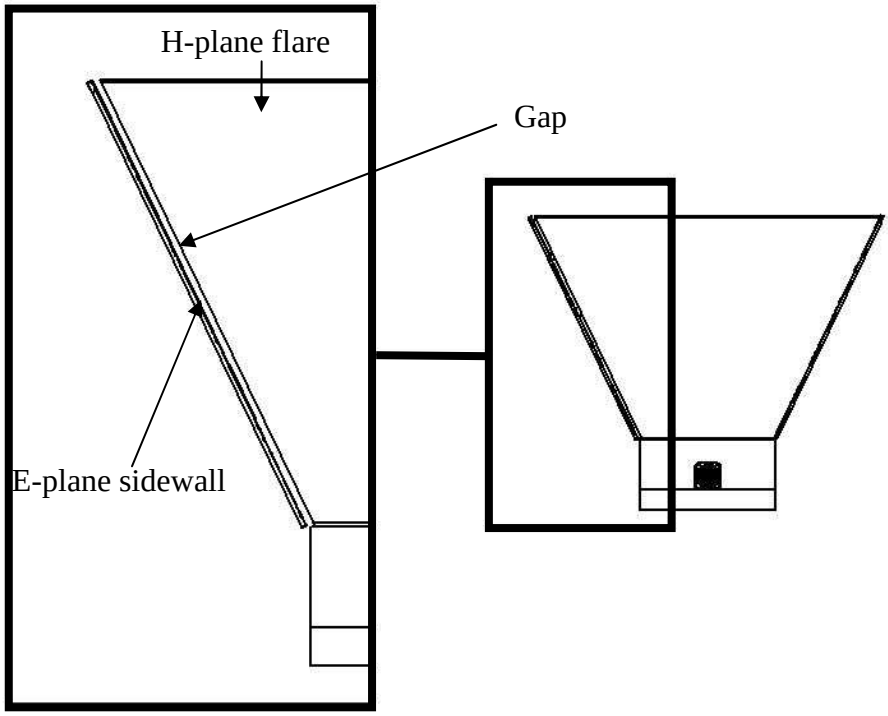

Figure 4.13. Gap between E-plane sidewalls and H-plane flares.

Figure 4.14 shows the results from these simulations. When compared to Figure 3.23 it can be seen that there is no difference between the reference trace and all the other simulated results. It can be concluded that electrical contact is not needed between the E-plane metallic grid sidewalls and the H-plane flares for proper operation of the antenna.

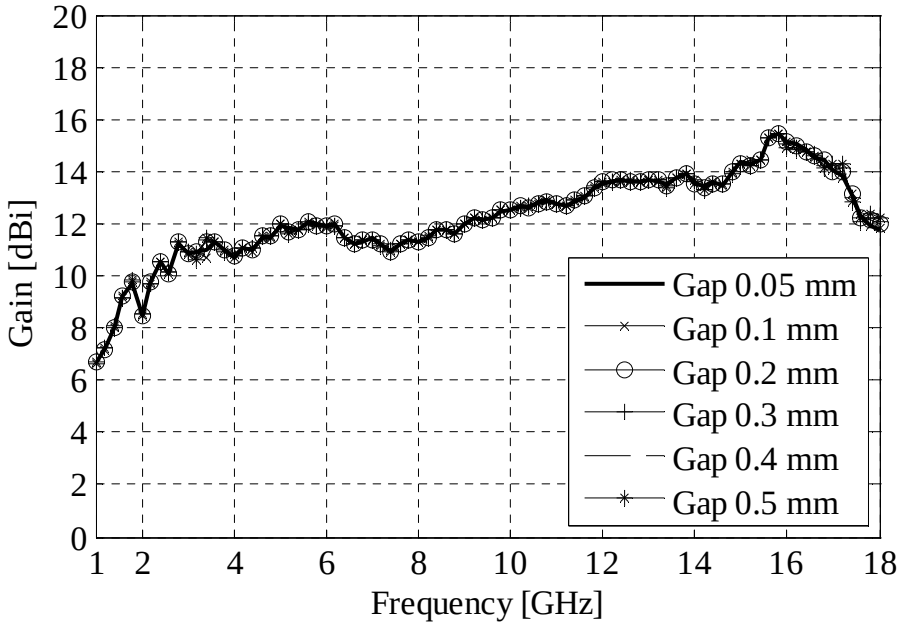

Figure 4.14. Boresight gain results for gaps between E-plane sidewalls and H-plane flares.

4.4.2.4 Gap between H-plane flares and ridges

If some of the dimensions of the ridges were incorrectly machined, a gap can form when assembling the ridge to the H-plane flare (see Figure 4.15). As with the previous gap this type of gap would probably not be across the whole interface, there might be connectivity in some sections. Again the gap was approximated by a gap across the entire interface between the ridges and H-plane flare for the sake of simplicity. It should be noted that this gap was only implemented between the top H-plane flare and the top ridge. The width of the gap is defined as the normal distance between the ridge interface onto which the H-plane flare is mounted and the H-plane interface that is mounted onto the ridge. This width was adjusted to be 0.05 mm initially and then varied from 0.1 to 0.5 mm in 0.1 mm steps.

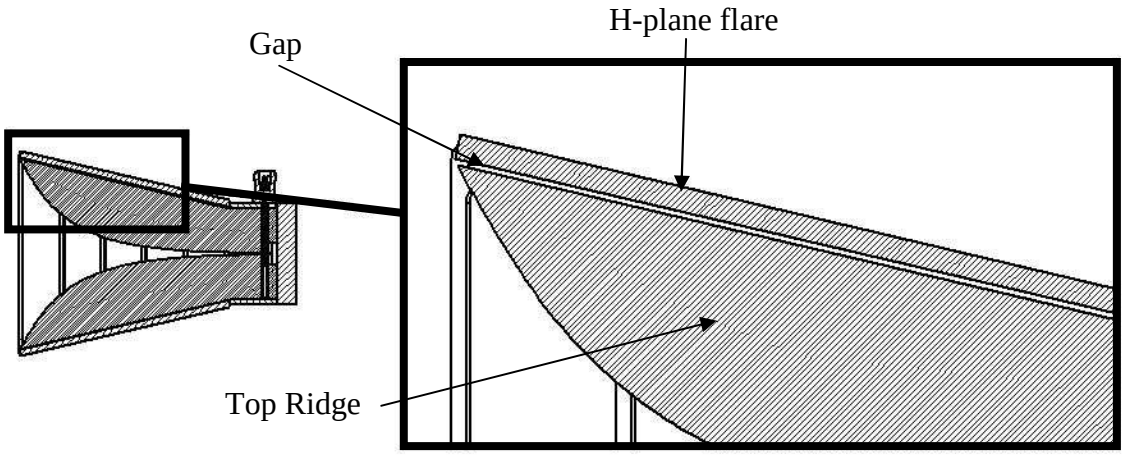

Figure 4.15. Gap between H-plane flares and ridges.

Figures 4.16 and 4.17 show the results from these simulations. When comparing Figure 4.16 to Figure 3.23 it can be seen that there is no difference between the reference trace and the other simulated results for smaller gaps. In the case of larger gaps as presented in Figure 4.17 the gain ripple at 11 GHz increases slightly in magnitude. The gaps in Figure 4.17 are quite large already and would be easily recognisable when inspecting the antenna. It can be concluded that a slight loss of electrical contact between the ridges and the H-plane flares would not be detrimental to the performance of the antenna.

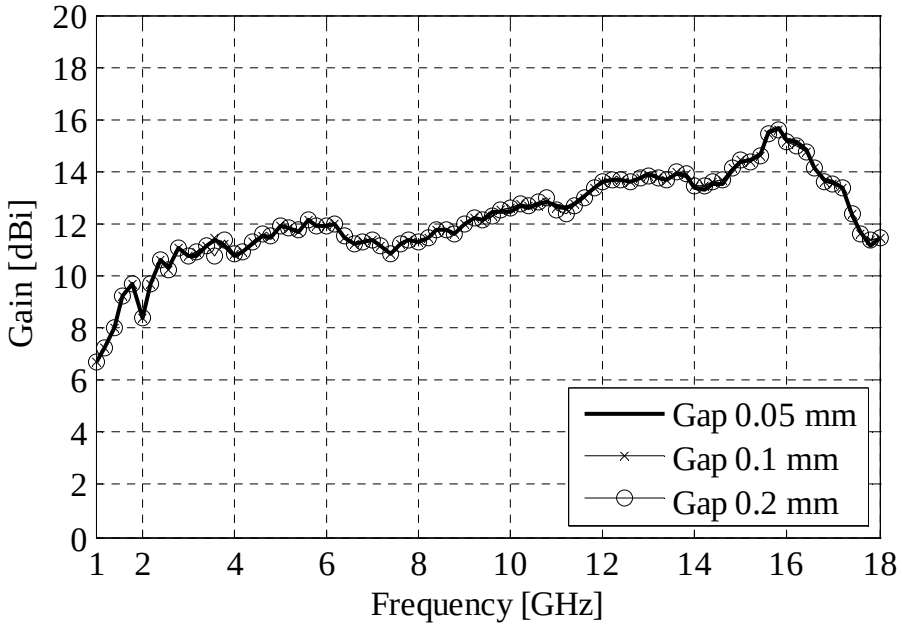

Figure 4.16. Boresight gain results for gaps between ridges and H-plane flares.

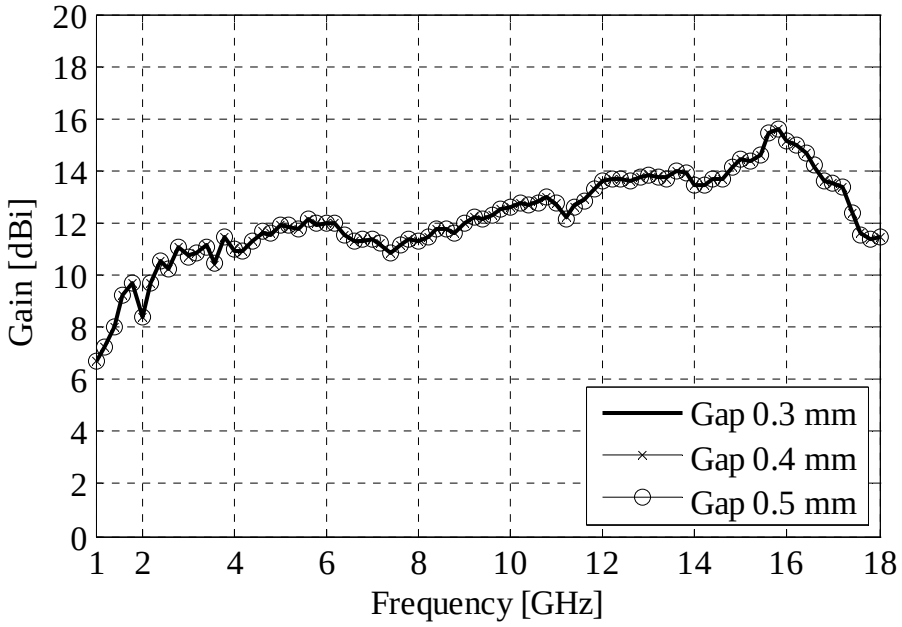

Figure 4.17. Boresight gain results for gaps between ridges and H-plane flares.

4.4.3. Gaps in the waveguide launcher section

4.4.3.1 Gap between wedges and flares

Gaps can form between the launcher wedges and the flares when the wedges are too small (in cross sectional width) or when the top and bottom flares do not make good contact with

one another and the gap between them is thus larger than usual. Figure 4.18 shows how gaps were implemented between the side faces of the wedge and the front faces of the launcher flares. These gaps were implemented on both sides of the magnetic symmetry plane (E-plane) as well as on both sides of the wedges. The width of the gap is defined as the distance between the wedge and the interface of the waveguide flare that connects with the wedge. This width was adjusted to be 0.05 mm initially and then varied from 0.1 to 0.5 mm in 0.1 mm steps.

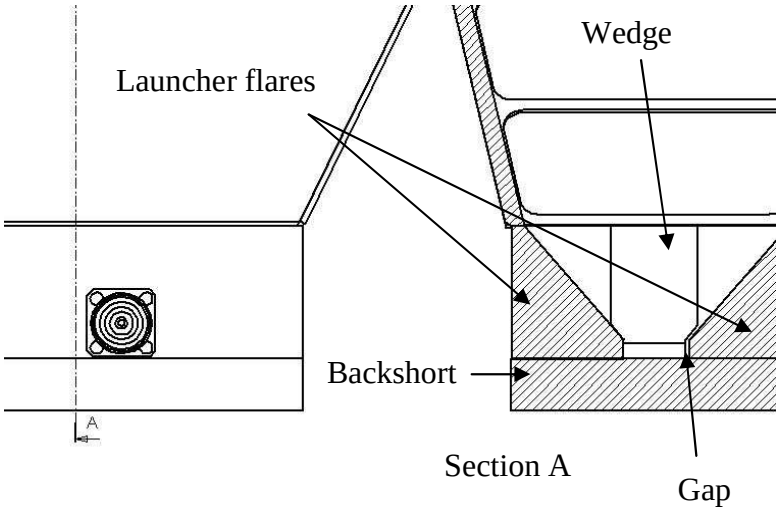

Figure 4.18. Gap between wedges and flares.

Figures 4.19 and 4.20 show the results from these simulations. With reference to Figure 3.23, these gaps cause small notches in the boresight gain to develop at approximately 10.5, 14 and 15 GHz with the notches deepening with an increase in gap size. At 14.5 and 18 GHz the gaps cause variations in gain with the gain increasing with an increase in the gap dimension. The gain in the lower frequency band remains largely unaffected. It is concluded that good electrical contact is necessary between the wedges and flares in the waveguide.

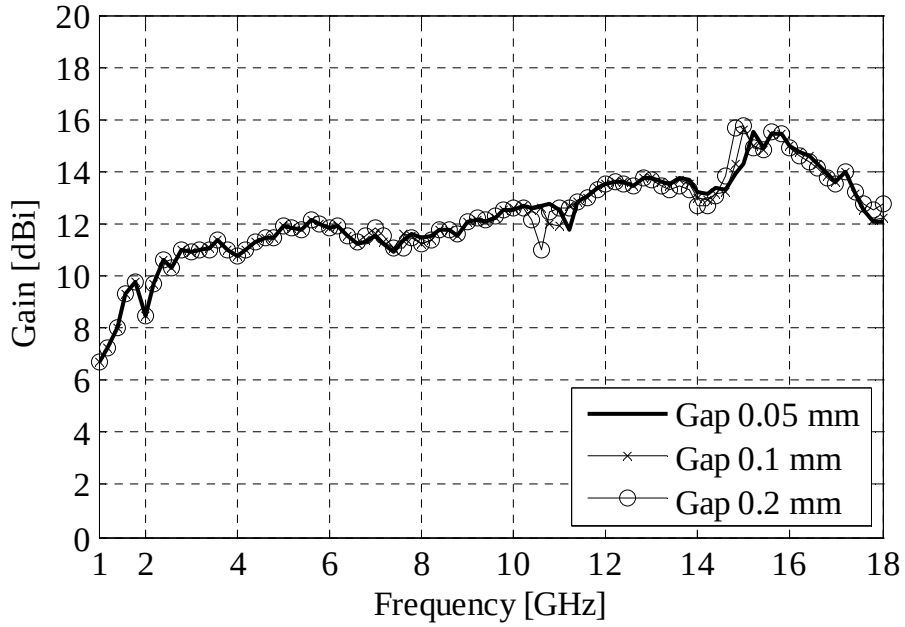

Figure 4.19. Boresight gain results for gaps between wedges and waveguide flares.

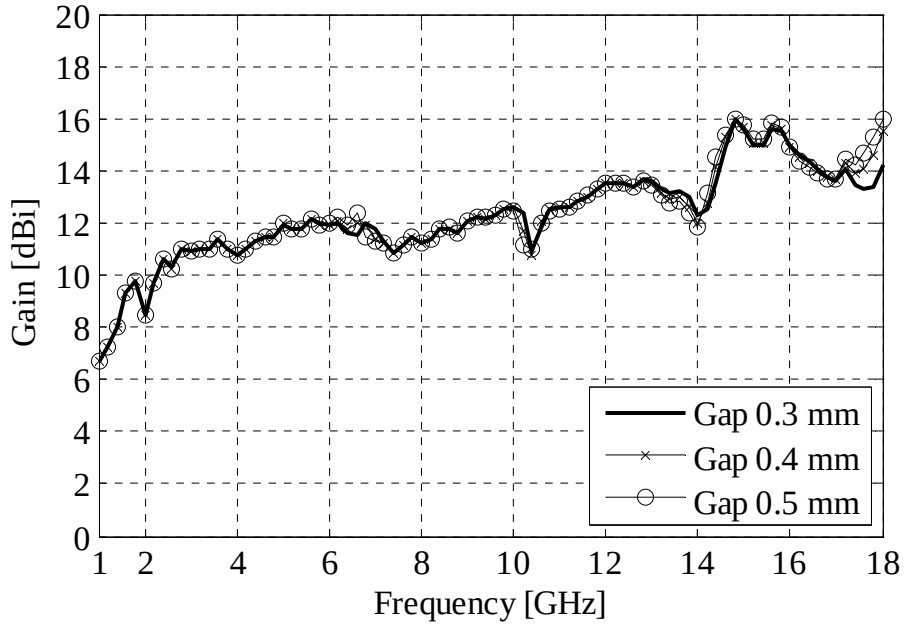

Figure 4.20. Boresight gain results for gaps between wedges and waveguide flares.

4.4.3.2 Gap between backshort and waveguide launcher

Typically gaps can be encountered in practice when the tolerances on the launcher wedges and flare parts are such that the interface with the front face of the backshort is irregular and not perfectly flat. Figure 4.21 shows how the gap is formed in the assembly. The gap is

thus formed between the front face of the backshort and the bottom faces of the launcher flares and wedges. This gap was implemented in FEKO with a parametric width that could be adjusted to be across the entire backshort face (only connected at the edges) or only a fraction of the backshort face. Two variations of this type of gap were implemented. In the initial simulations the gap was implemented across the entire backshort face with only the edges of the backshort connected to the bottom of the waveguide assembly. The other gap was applied across two thirds of backshort's smaller dimension and half of the backhort's larger dimension. Thus the gap forms approximately a rectangle of 20 by 40 mm which is symmetric with regards to the E-plane. The width of the gap is defined as the distance between the backshort and the mating interface of the waveguide launcher assembly onto which the backshort is mounted. This width was adjusted to be 0.05 mm initially and then varied from 0.1 to 0.5 mm in 0.1 mm steps.

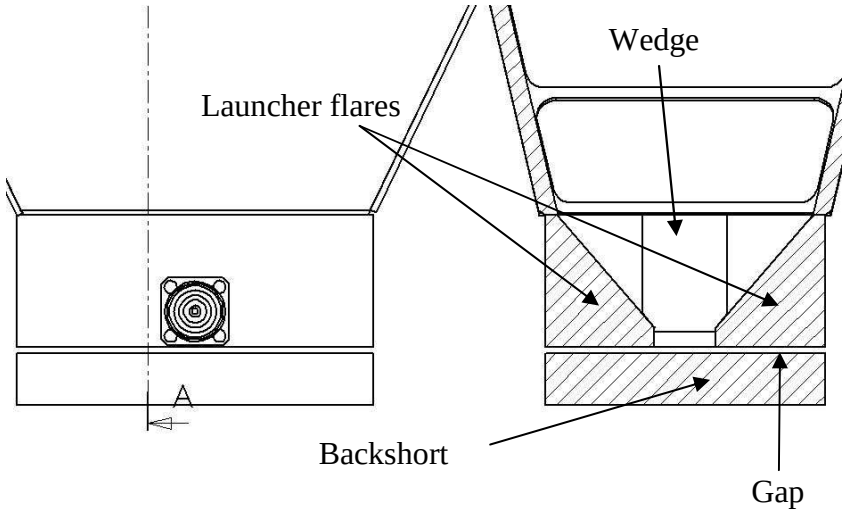

Figure 4.21. Gap between backshort and waveguide launcher.

Figures 4.22 and 4.23 show the results from the simulations in which the gap is across the entire backshort face. Figures 4.24 and 4.25 show the results from the simulations in which the gap is only across a part of the backshort face.

When comparing Figure 4.22 and Figure 4.23 with Figure 3.23, it can be seen that sharp notches in the boresight gain is formed at approximately 14, 14.5, 16, 17.5 and 18 GHz. A smaller notch forms around 9 GHz. The lower band remains largely unaffected.

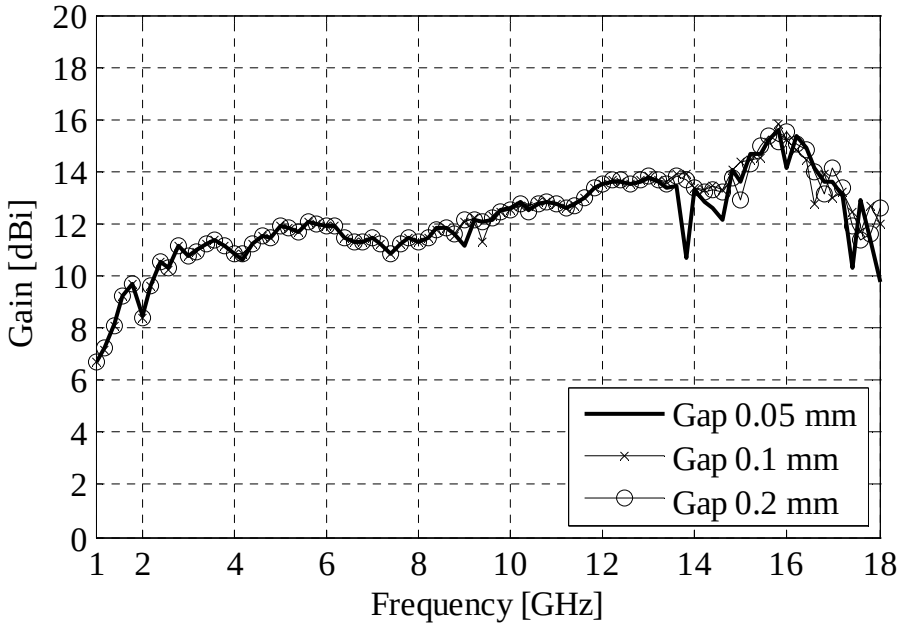

Figure 4.22. Boresight gain results for gaps between backshort and waveguide launcher (gap across whole interface).

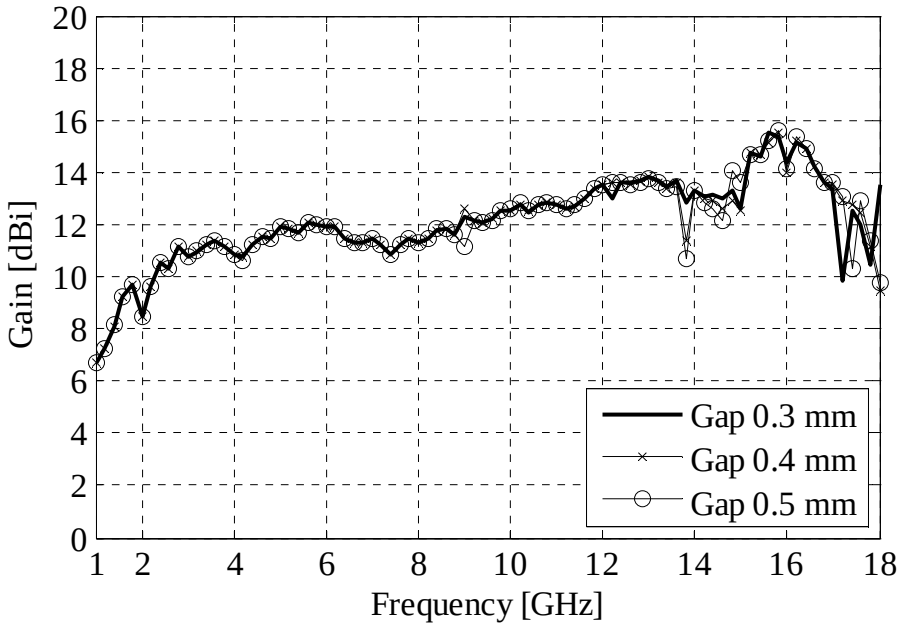

Figure 4.23. Boresight gain results for gaps between backshort and waveguide launcher (gap across whole interface).

For the gap only across a part of the interface (Figures 4.24 and 4.25) there is only one resonance that forms at 16 GHz as the gap size increases. Furthermore the gain drops at 14.5 GHz and increases at 18 GHz with an increase in gap size. It is concluded that good electrical contact is necessary between the backshort and waveguide launcher, however, if

the gap is small and only across a part of the interface the deterioration in performance is not that significant.

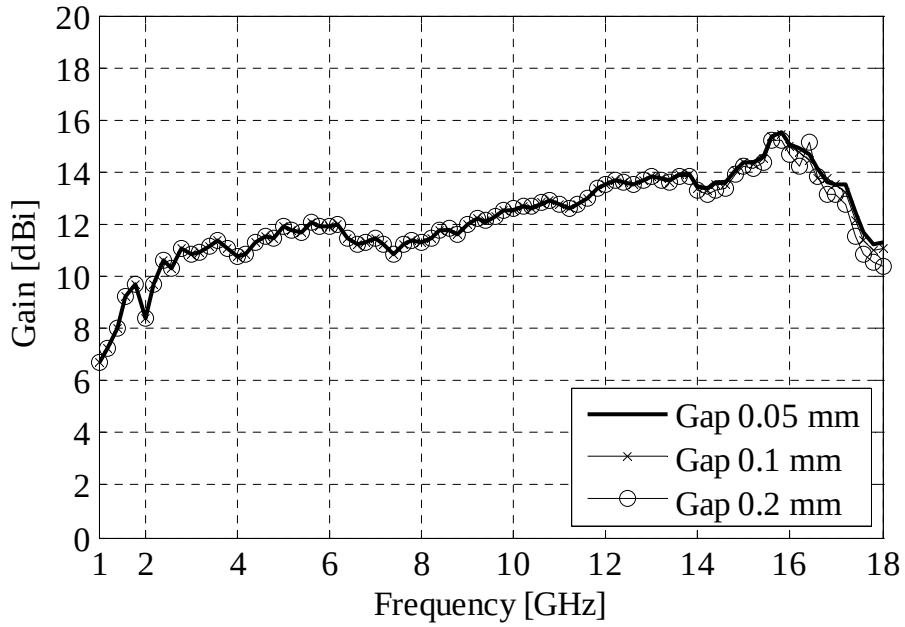

Figure 4.24. Boresight gain results for gaps between backshort and waveguide launcher (gap across part of interface).

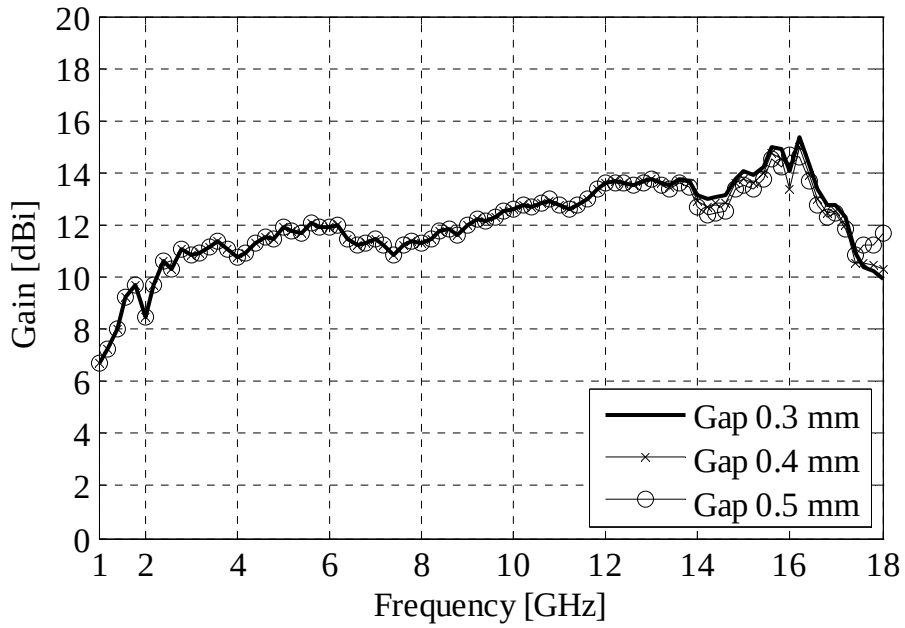

Figure 4.25. Boresight gain results for gaps between backshort and waveguide launcher (gap across part of interface).

4.4.3.3 Gap between backshort and wedges

Gaps can be formed when the launcher wedges do not seat properly on the bottom and top launcher flares (see Figure 4.26). This can happen when tolerances on the angle of the flare or the angle of the undercut that enables the wedge to seat on the flares, are not sufficiently tight. The result is a gap between the bottom face of the wedge and the top face of the backshort. Gaps were implemented on both sides of the magnetic symmetry plane. The width of the gap is defined as the distance between the mating interfaces of the wedge and backshort respectively. This width was adjusted to be 0.05 mm initially and then varied from 0.1 to 0.5 mm in 0.1 mm steps.

Figures 4.27 and 4.28 show the results from these simulations. This type of gap had very little effect on the boresight gain. Only the gain at 18 GHz was influenced for gaps between 0.05 and 0.5 mm. It seems that the performance of the antenna is not as sensitive to good electrical contact between the wedges and the backshort interface as compared to gaps in other areas.

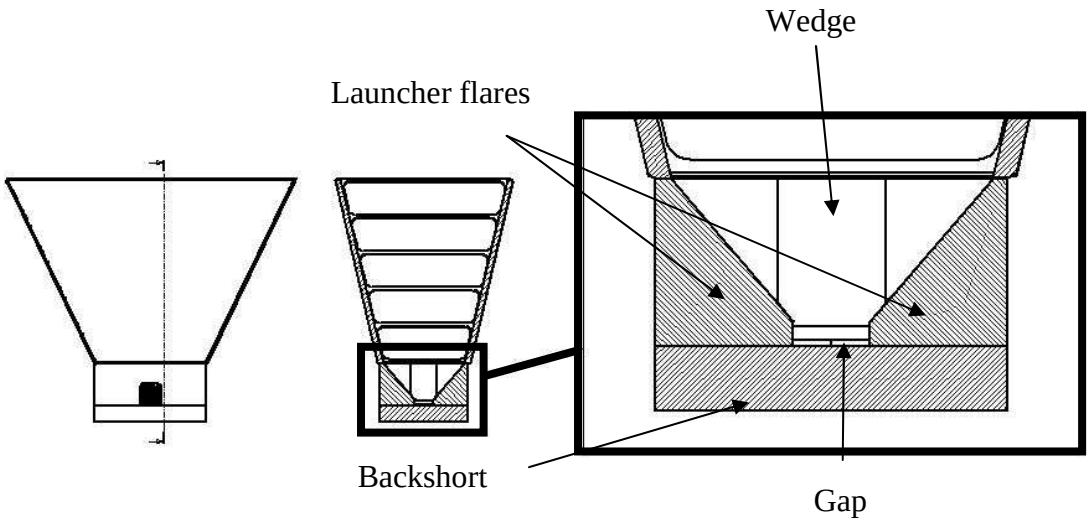

Figure 4.26. Gap between wedge and backshort.

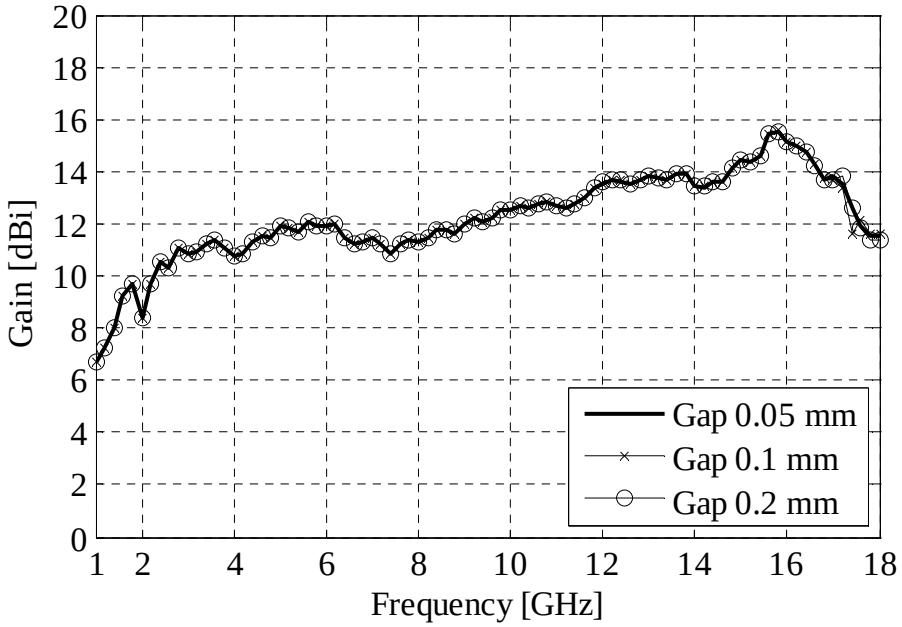

Figure 4.27. Boresight gain results for gaps between backshort and wedge.

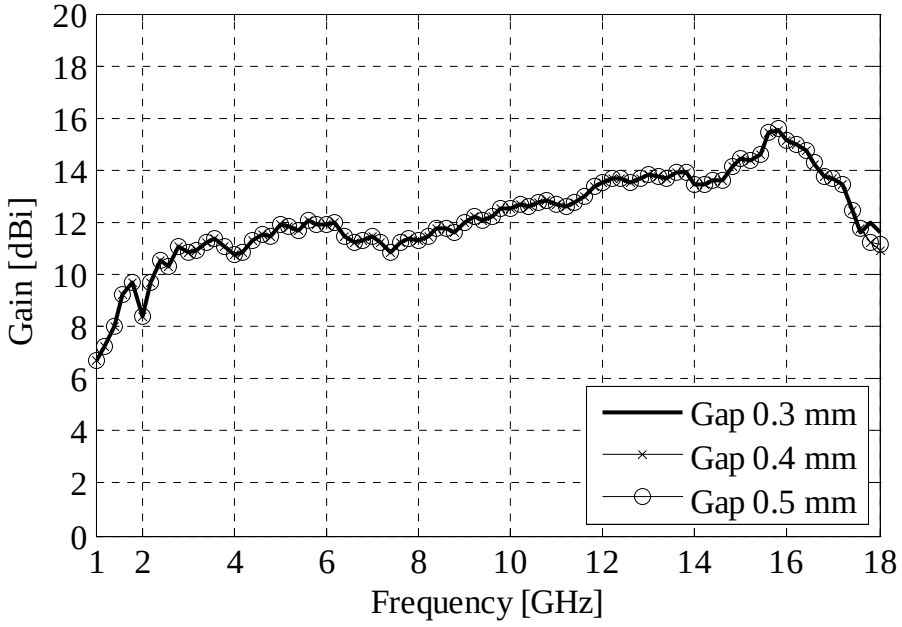

Figure 4.28. Boresight gain results for gaps between backshort and wedge.

4.4.3.4 Gap between ridges and feeding section

Figure 4.29 shows how the gaps in the feeding section were implemented. These gaps can form between the interfaces of the bushes and the ridges due to a number of reasons.

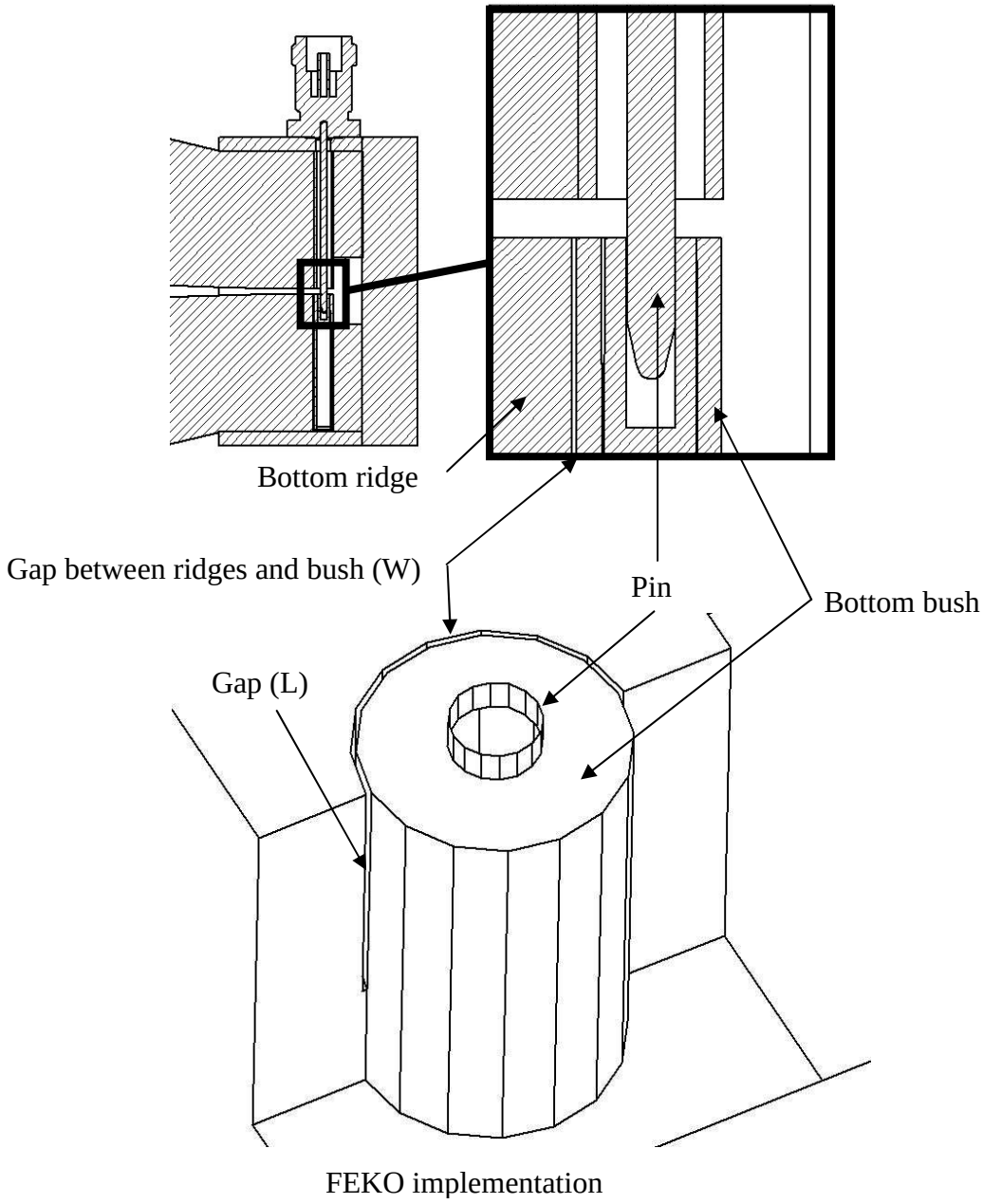

Figure 4.29. Gap between ridges and feeding section.

Firstly tolerances in the machining process can lead to gaps. The way in which the shaft (into which the bushes fit) in the ridges was machined can lead to gaps. If the shaft was drilled after the ridge was machined, the drill will tend to bend away when it passes the point where half of the drill is in the air and the other half in the ridge. The use of grub screws to keep the bushes in place inside the shaft can lead to bending of the bushes which in turn can lead to gaps. Individual gaps were implemented in the top and bottom ridges of the model, respectively. The gaps were implemented to be symmetric in the E-plane. The

width of the gap is defined as the distance between the mating interfaces of the ridge and the bush respectively. The length of the gap is defined as the length along the bush that the gap is applied to. Gaps were implemented in the top, bottom and both ridges respectively.

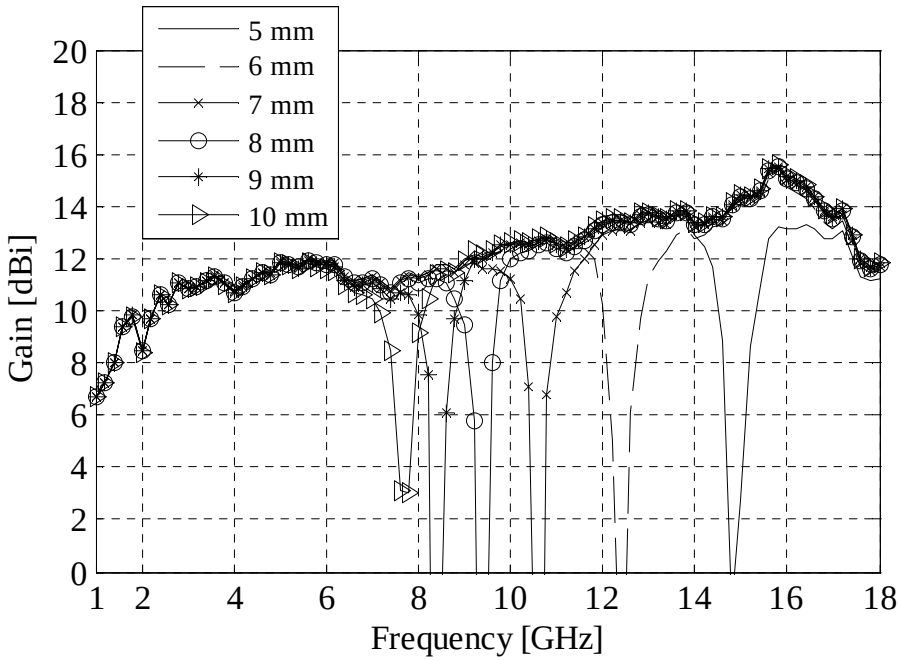

Figure 4.30. Ridge bush gap only in top ridge. Gap is 0.1 mm.

Figures 4.30 to 4.32 show the results for gaps of 0.1, 0.05 and 0.02 mm implemented in the top ridge. The length of the gap was varied between 5 – 10 mm in 1 mm steps. This type of gap causes narrow deep resonances in the boresight gain at different frequencies depending on the length of the gap. As the gap length is increased the resonance frequency decreases. Also it seems that as the gap width decreases the resonance becomes smaller.

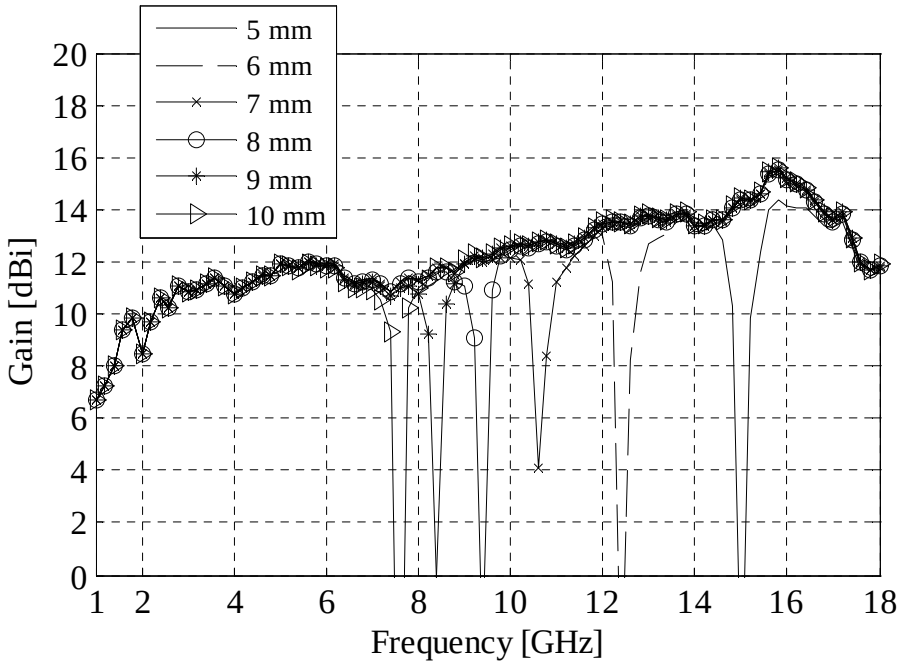

Figure 4.31. Ridge bush gap only in top ridge. Gap is 0.05 mm.

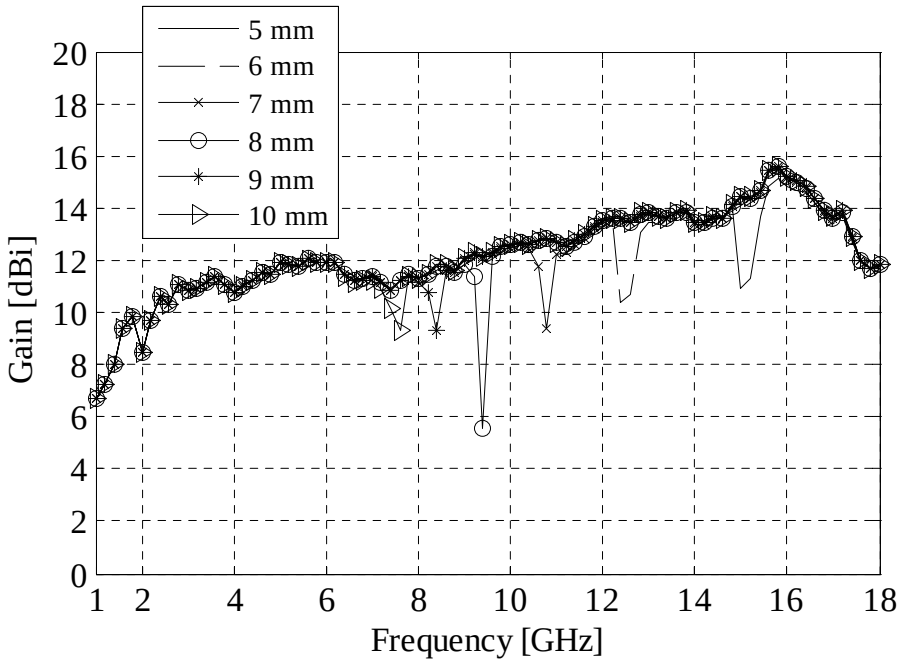

Figure 4.32. Ridge bush gap only in top ridge. Gap is 0.02 mm.

Figures 4.33 to 4.35 show the results for gaps of 0.1, 0.05 and 0.02 mm implemented in the bottom ridge. The length of the gap was varied between 5 – 10 mm in 1 mm steps. This type of gap also causes narrow deep resonances in the boresight gain at different frequencies depending on the length of the gap. As the gap length is increased the

resonance frequency decreases. As was the case with the top ridge it seems that decreasing the gap width reduces the resonance size.

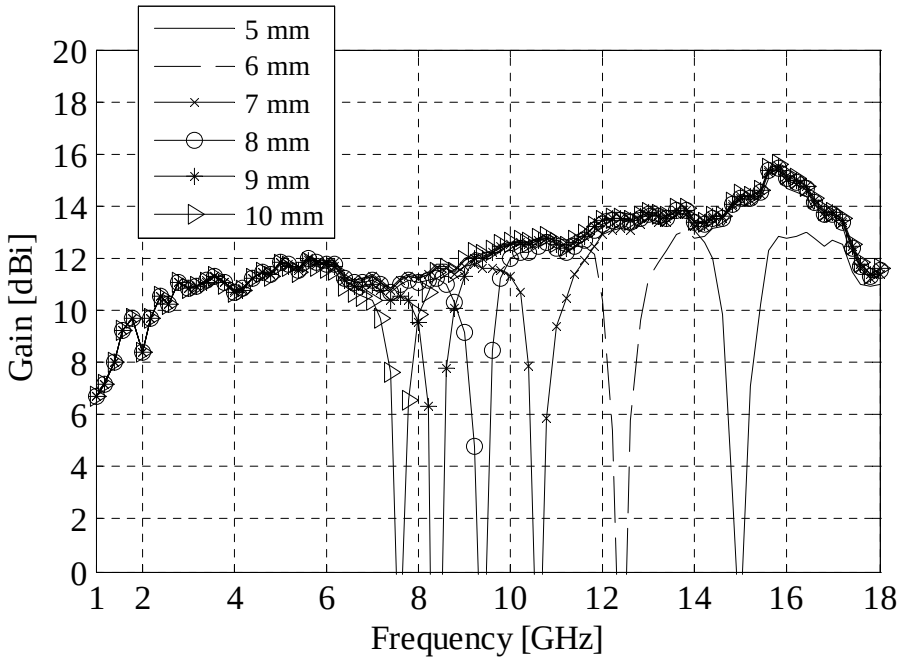

Figure 4.33. Ridge bush gap only in bottom ridge. Gap is 0.1 mm.

When comparing these figures to the results for the gap in the top ridge it can be seen that the results are very similar and both types of gaps produce resonances at nearly the same frequency depending on the length of the gap.

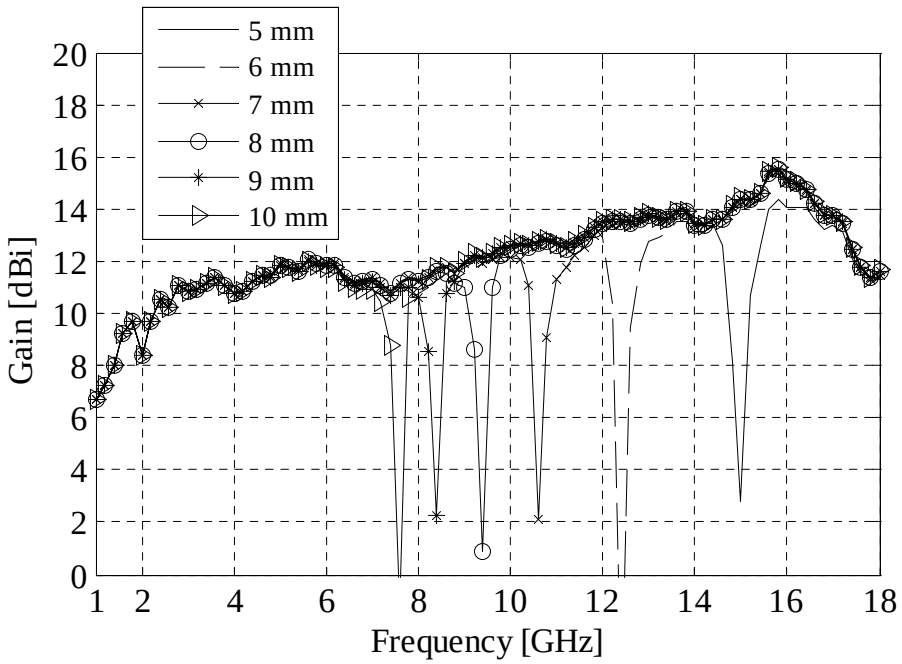

Figure 4.34. Ridge bush gap only in bottom ridge. Gap is 0.05 mm.

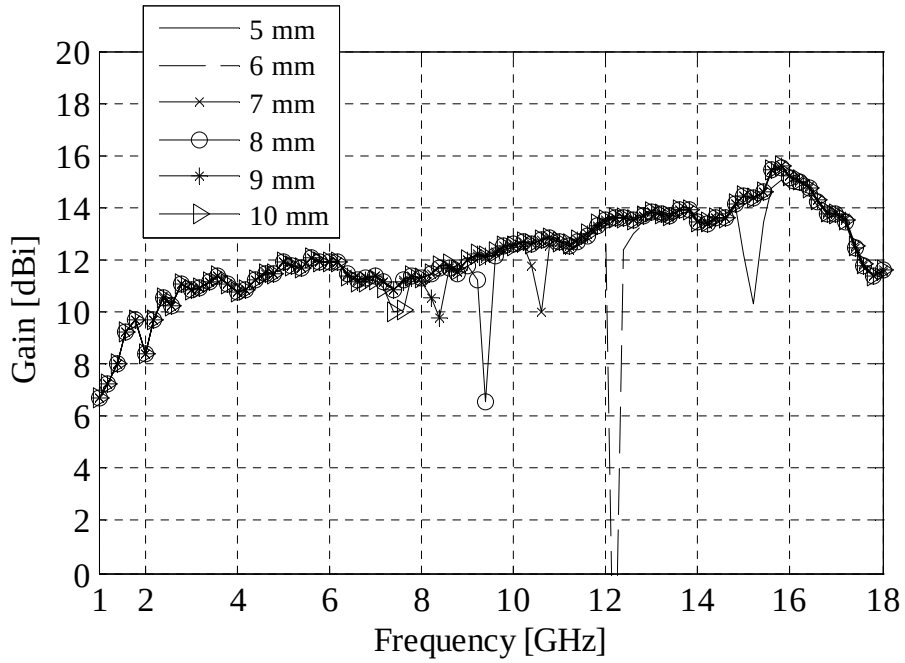

Figure 4.35. Ridge bush gap only in bottom ridge. Gap is 0.02 mm.

Figures 4.36 to 4.38 show the results for gaps of 0.1, 0.05 and 0.02 mm implemented in both the ridges respectively. The length of the top gap was held constant at 5 mm. The length of the bottom gap was varied between 6 – 10 mm in 1 mm steps.

The double gap causes two narrow deep resonances in the boresight gain at different frequencies depending on the length of the gap (compare this result with the measured results of Figure 4.1). One of the resonances is constant at about 14.5 GHz. Since the length of the top gap was held constant it is believed that this resonance is due to the top gap. It is interesting to note that for the simulation of the single top gap, the resonance is at approximately 15 GHz. Thus it seems that the presence of the bottom gap has shifted the resonance of the top gap slightly lower in frequency. On the other hand when comparing Figure 4.36 with Figure 4.33 it seems as if the bottom gap is unaffected by the presence of the top gap since the resonance is at approximately the same frequencies.

Again as the gap length is increased the resonance associated with the bottom gap shifts lower in frequency, and as the gap width decreases the resonances become smaller. In fact the resonance, due to the top gap, has shifted to 13 GHz for the 0.02 mm gap width case and is nearly nonexistent. Thus it seems that the effect of the bottom gap dominates the top gap’s resonance for small gap widths.

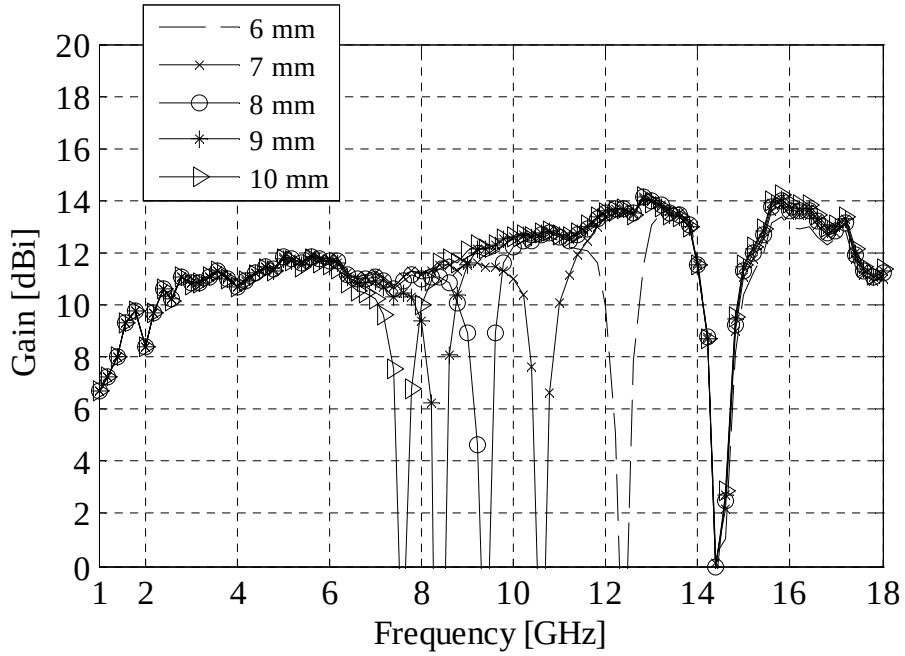

Figure 4.36. Ridge bush gap in both ridges. Gap width is 0.1 mm. Top gap length held constant at 5 mm. Length varied in bottom ridge.

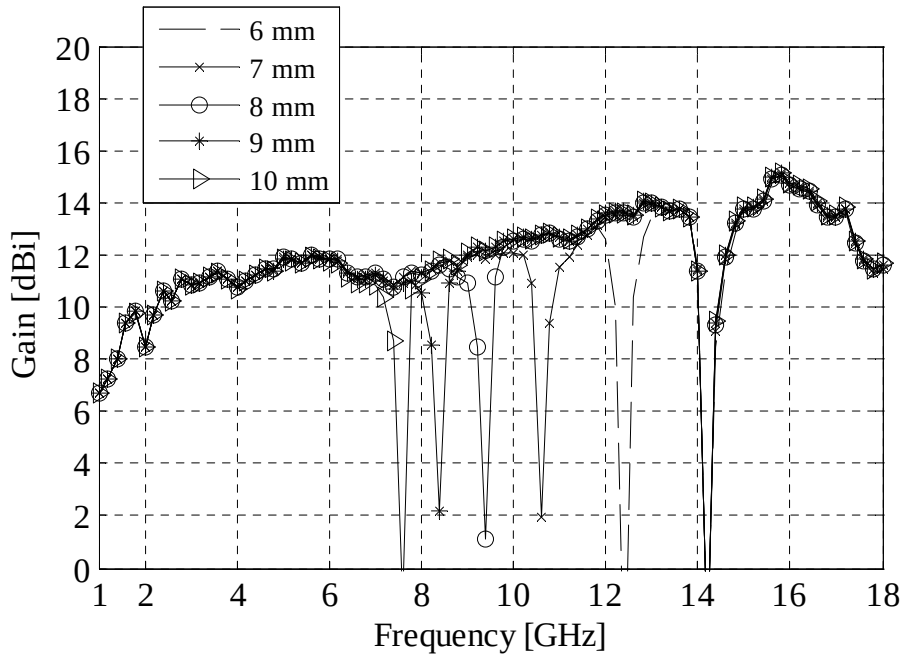

Figure 4.37. Ridge bush gap in both ridges. Gap width is 0.05 mm. Top gap length held constant at 5 mm. Length varied in bottom ridge.

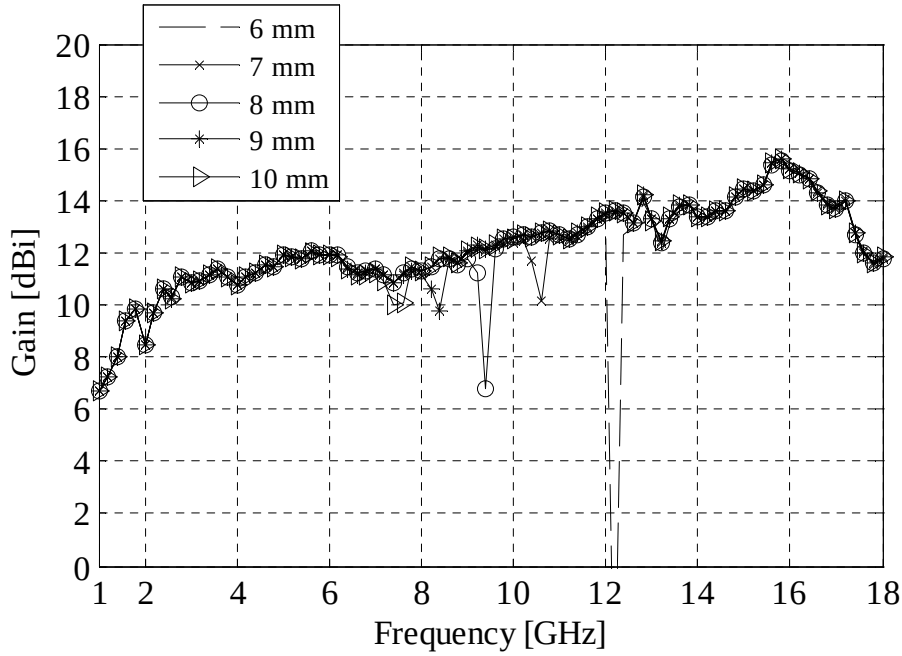

Figure 4.38. Ridge bush gap in both ridges. Gap width is 0.02 mm. Top gap length held constant at 5 mm. Length varied in bottom ridge.

Figure 4.39 shows a comparison of a typical measured boresight gain result with a typical simulated result for a ridge bush gap. This specific ridge bush gap was implemented in the bottom ridge with a width of 0.05 mm and length of 5.25 mm. The results compare well and differences might be as a result of the presence of other types of gaps or tolerances in the manufactured antenna.

Figure 4.40 shows a comparison of a typical measured VSWR result with a typical simulated result for a ridge bush gap. This specific ridge bush gap was implemented in the bottom ridge with a width of 0.05 mm and length of 5.75 mm. The resonances are not at exactly the right frequency which means that the simulation would have to be rerun with a gap length somewhere between 5.25 and 5.75 mm. This figure shows that the same effect that is observed in the boresight gain can be observed in the VSWR as well.

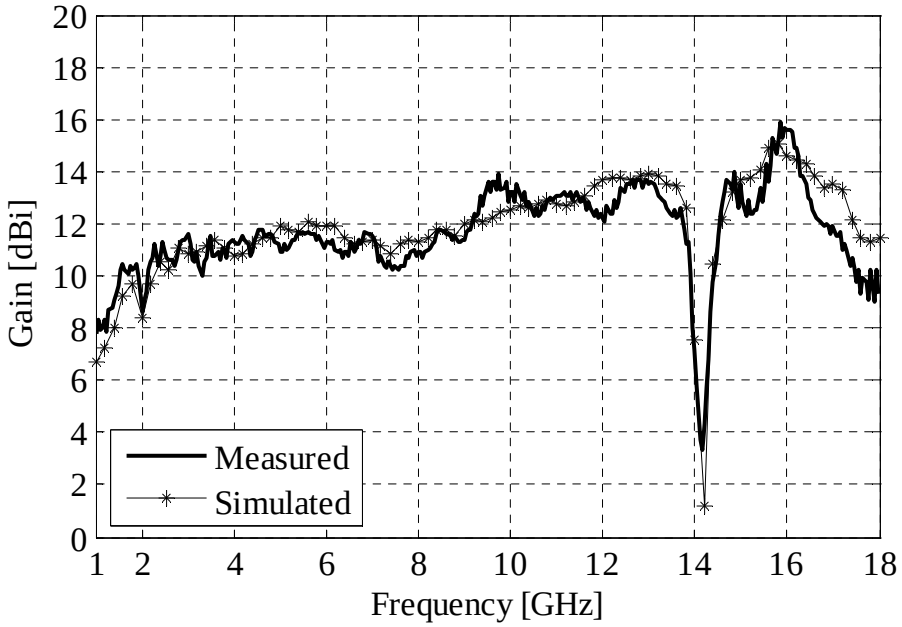

Figure 4.39. Boresight gain comparison between typical measured and simulated gain for antenna with ridge bush gap in bottom ridge 0.05 mm wide and 5.25 mm long.

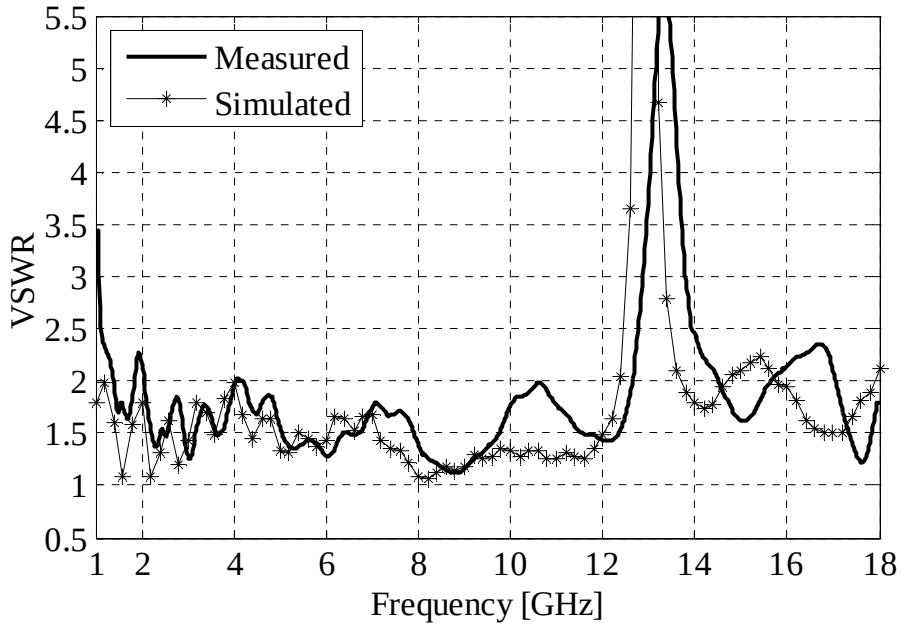

Figure 4.40. VSWR comparison between typical measured trace and simulated VSWR for antenna with ridge bush gap in bottom ridge 0.05 mm wide and 5.75 mm long.

In FEKO the current data is readily available, while the near field data have to be calculated since MoM calculates currents unlike FDTD, which calculates E and H fields on a grid.

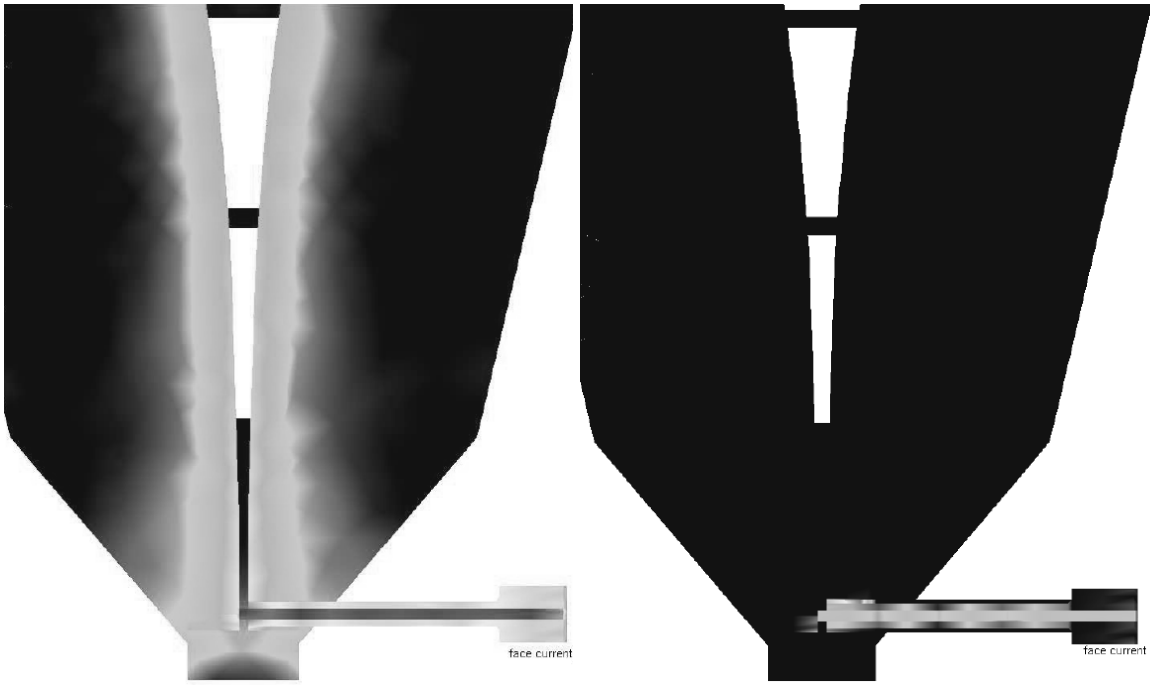

Figure 4.41. Current distribution at 15 GHz for the basic model (left) and model with a gap that resonate at 15 GHz (right).

The currents for a gap in the top bush-ridge interface were compared to the basic model without gap (see Figure 4.41). The gap is implemented in the top-ridge bush interface and causes a resonance at 15 GHz. It was found that at frequencies far from the gap a significant quantity of current is transported along the inner coax and flows onto the ridges thus causing fields between the ridges and allowing radiation. Near the gap (starting at approximately 14 GHz and ending at 17 GHz) the currents starts to get trapped inside the gap and at 15 GHz no current flows along the ridges and a standing wave is developed on the feed coax which explains the lack of radiation and large VSWR resonance.

4.5. Summary

At the beginning of this chapter representative measured results for 1-18 GHz DRGH antennas with extreme performance deviations (resonance effect) were presented.Various gaps were implemented in the FEKO model of the 1-18 GHz DRGH antenna developed in Chapter 3. The antenna was divided into two main sections, namely the flared waveguide section and the waveguide launcher section for the purpose of the parametric study on the

effect of manufacturing and assembly tolerances on the performance of a DRGH antenna. Typical gaps in the flared waveguide section included gaps at the interfaces between the waveguide flares and sidewalls with the waveguide launcher section and ridges. It was shown in this chapter that these gaps produced no significant effect on the VSWR and gain performance of the 1-18 GHz DRGH antenna. Typical gaps in the waveguide launcher section included gaps between the wedges, launcher flares, backshort and ridge-bush interface. These gaps were found to have the most pronounced effect on the performance of the antenna.

The observations made for the simulation results in this chapter can be summarised as follows:

- Gaps in the flared waveguide part of the DRGH antenna do not contribute significantly to deterioration in performance. Gaps in the waveguide launcher section, however, can cause significant deterioration in performance.
- Gaps between the ridge-bush interfaces are the main causal agent for sharp deep boresight gain resonances. These resonances can also be observed in the VSWR.
- The length and width of the ridge-bush gaps controls the magnitude and location (in frequency) of the resonances. Multiple resonances can be caused if there are gaps in both the ridges. These gaps interact with each other.
- The typical resonance effects observed in measurement could be recreated accurately in simulation.

In conclusion, the hypothesis that the main source of performance deviations, most notably resonances in gain and VSWR, is the coaxial feeding section and the interface of this section with the ridges was confirmed by the results in this chapter.

CHAPTER 5 IMPROVEMENTS IN DESIGN TO REDUCE THE EFFECT OF MANUFACTURING TOLERANCES

5.1. Introduction

The main conclusion from the parametric study in the previous chapter is that the ridge-bush gaps in the feeding section are the dominant parameter affecting the performance of Double Ridge Guide Horn (DRGH) antennas. The ridge-bush gaps cause sharp, deep resonances in boresight gain and VSWR. Performance deterioration is also experienced by the presence of other gaps in the launcher section, though not as significantly as with the ridge-bush gap. The elimination of gaps in the waveguide launcher and especially the coaxial feeding section is thus critical for the repeatable manufacturing of high performance DRGH antennas.

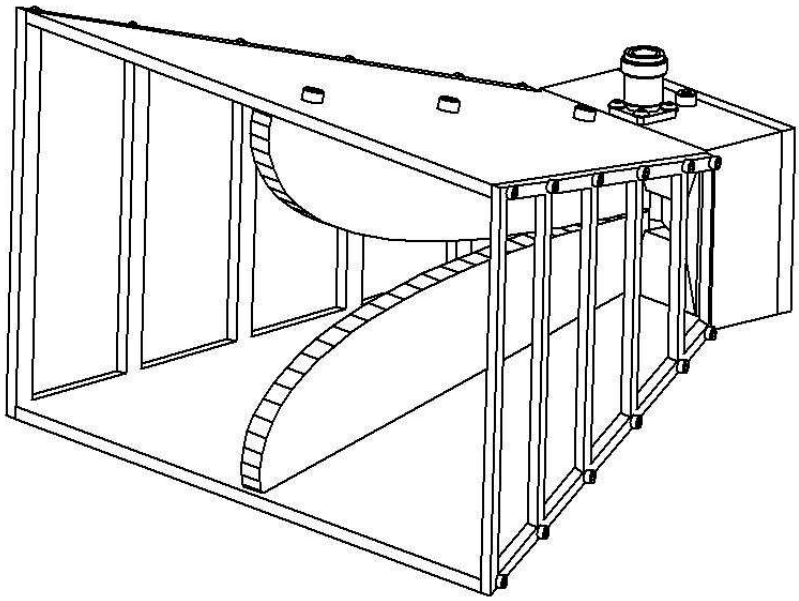

Figure 5.1. New improved 1-18 GHz DRGH antenna design.

Section 5.2 shows how an antenna with extreme resonance effects can be repaired using the knowledge from the previous chapter. In Section 5.3 a new improved 1-18 GHz DRGH antenna, shown in Figure 5.1, was designed using the numerical model of Chapter 3 and the results from Chapter 4 with regard to the tolerance sensitive areas of the traditional 1-18 GHz DRGH antenna. This design has fewer parts and some of the parts were redesigned to reduce the possibility of gaps. The performance of the antenna has also been improved compared to current state of the art designs. The simulated and measured results for this

design are presented in Sections 5.4 and 5.5 respectively. Section 5.6 presents a short summary of this chapter.

5.2. Method of repairing antennas with extreme resonance effects

With the results of the previous chapter in mind, one of the pre-production prototypes that had a sharp deep resonance in the boresight gain was re-measured. After this re-measurement the backshort was removed from this antenna and conductive, silver loaded epoxy applied to the ridge-bush interface without disassembling the antenna. The backshort was replaced and the antenna was then re-measured in the same setup. The results for this experiment can be seen below in Figure 5.2.

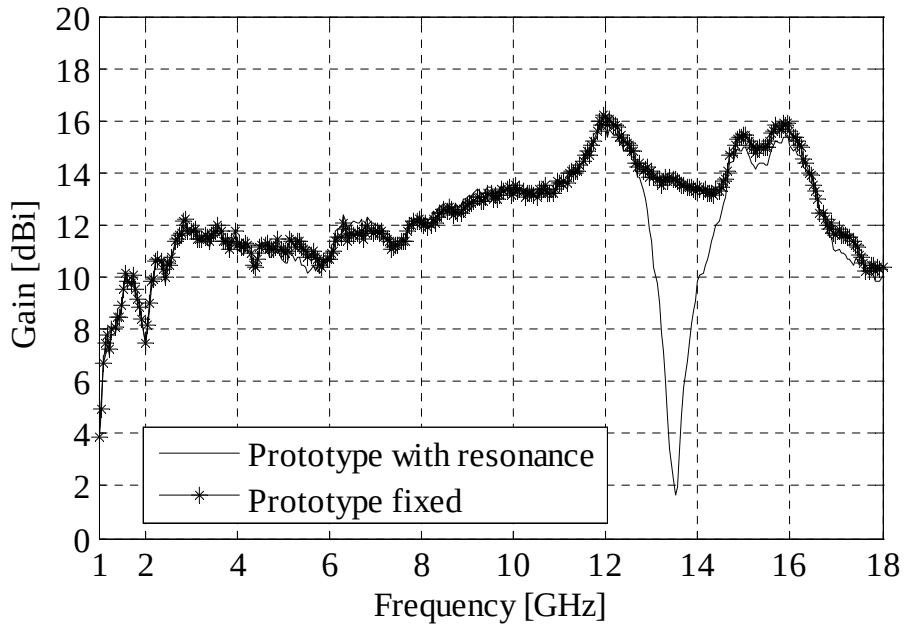

Figure 5.2. Boresight gain comparison between prototype with resonance effect and same prototype with conductive epoxy applied to ridge-bush interface.

From this figure it is clear that the sharp deep resonance in boresight gain at approximately 13.5 GHz has been removed by the application of the conductive epoxy. Therefore the hypothesis that gaps between the ridge-bush interface causes sharp deep boresight gain drops was confirmed with numerical simulation as well as a measured experiment. This also shows that antennas with extreme resonance effects in the boresight gain and or VSWR can be repaired by application of conductive epoxy to the sensitive areas as identified in the previous chapter.

5.3. New design with reduced sensitivity towards manufacturing tolerances

The coaxial feeding section was improved by incorporating the bushes that form the outer conductor and termination of the inner conductor into the top and bottom ridges, respectively (see Figure 5.3). This integration of coaxial line with the top and bottom ridges would eliminate the use of bushes and the resulting gaps in the feeding section of the DRGH antenna. The main disadvantage of this approach is that top and bottom ridge will no longer be identical. Although the ridge profile can remain unaltered, different parts are required for the top and bottom ridges.

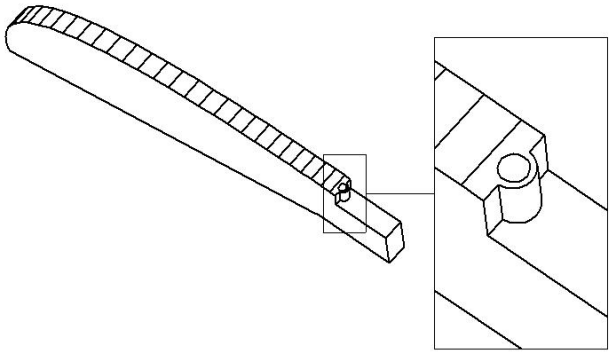

Figure 5.3. Redesigned top ridge with incorporated bush.

The hole in the top ridge has a size corresponding to a 50 Ω coaxial airline in relation to the inner conductor. The bottom ridge is machined in such a way that custom made spring fingers can be inserted into the ridge in order to capture the inner conductor with good electrical contact. The application of conductive epoxy to the critical areas identified in the parametric study further significantly reduce any effects on antenna performance caused by manufacturing and assembly tolerances.

Then the waveguide feeding launcher was redesigned with two purposes in mind. The first was to reduce the number of subsections in this assembly to the minimum thereby eliminating possible sources of gaps. The second was to redesign the waveguide launcher in such a way as to eliminate the pattern deterioration at the higher frequencies typically experienced by the traditional design. It was clear from previous studies and the new designs suggested in [18 - 20] that the waveguide launcher section is the main source of modes that cause pattern deterioration. A parametric study was performed to find the

optimised dimensions for this new feeding section. The new waveguide launcher section consists of only one section that can be machined with a 5 axis Numerically Controlled (NC) machine. Figure 5.4 below shows the geometry of the new waveguide launcher section.

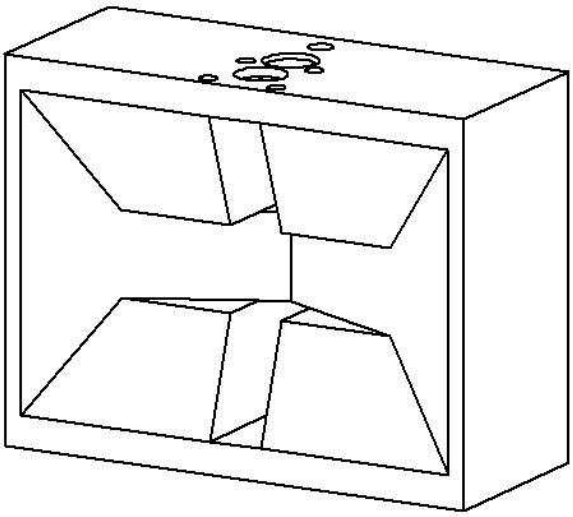

Figure 5.4. New waveguide launcher section.

The new waveguide launcher section design changed the impedance of the waveguide launcher and therefore the ridge profile had to be adjusted to ensure a good match at the aperture of the horn antenna. It is important to note that the antenna dimensions were not made smaller as in the design presented in [18]. Especially the aperture was kept the same as the traditional antenna to still conform to the MIL standard specification. Furthermore the metallic grid type sidewalls were retained to ensure better gain at the low end of the band. The waveguide launcher section was able to suppress all higher order modes even without scaling the antenna smaller and removing the sidewalls.

It was decided to make the coaxial feed length a function of the new waveguide launcher design. Therefore the coaxial feed length was determined by the ridge gap, waveguide launcher height and thickness of the waveguide launcher walls. This also makes for an easier design. Increasing or decreasing the length of the coaxial feed would either lead to extra machining steps or using a larger billet of material to machine the waveguide launcher (see Figure 5.5).

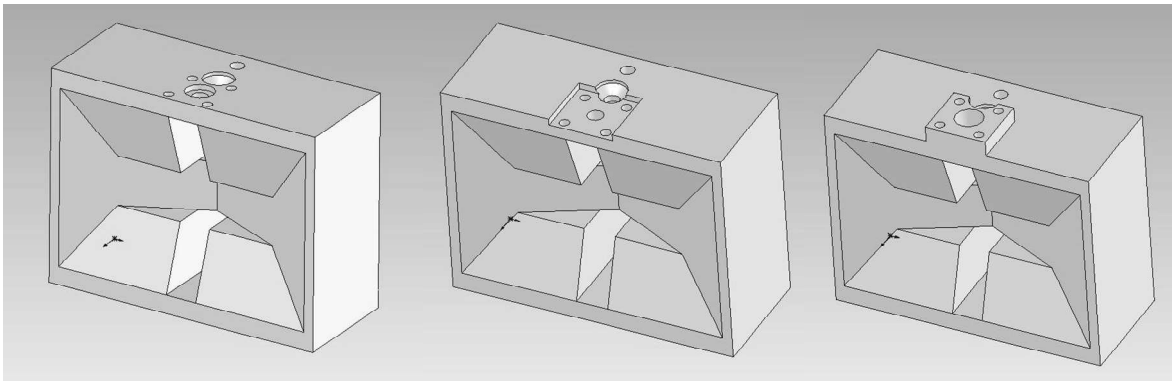

Figure 5.5. Launcher section (left), with a shorter feed (centre), with a longer feed (right).

Two simulations were run to test the effect of varying the feed length. The results show that variation of the coaxial feed length does not influence the boresight gain as is expected (Figure 5.6). The VSWR is influenced (see Figure 5.7). For the shorter and longer feed lengths the VSWR ripple increases in magnitude, especially at 18 GHz.

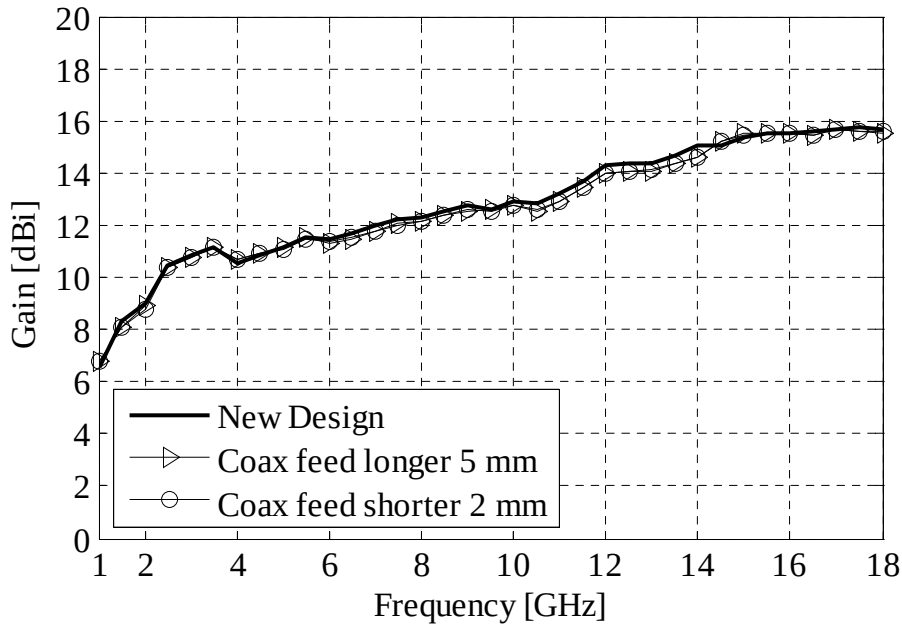

Figure 5.6. Boresight gain of new design with variation in coaxial feed lengths.

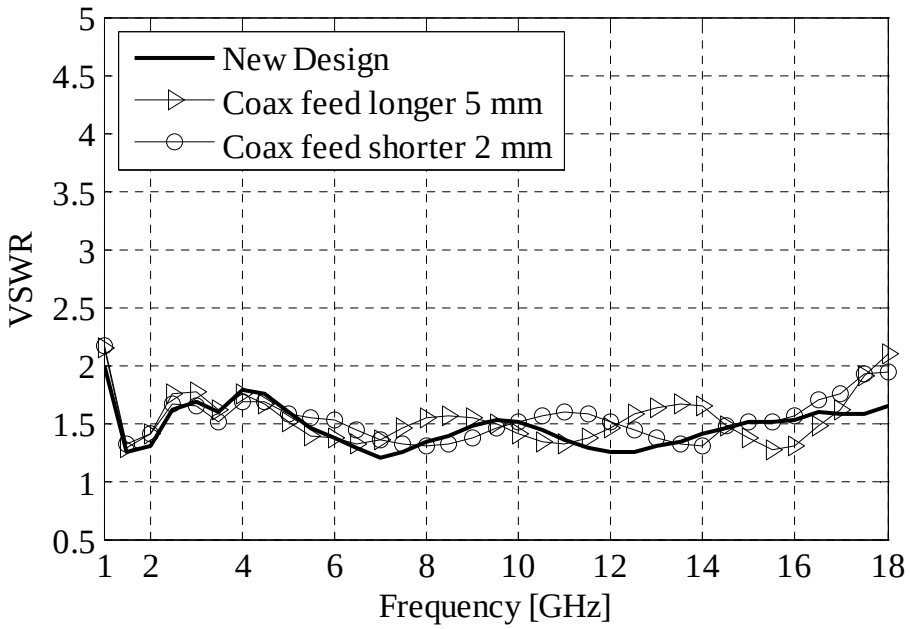

Figure 5.7. VSWR of new design with variation in coaxial feed lengths.

5.4. Simulated and measured results for the new improved design

This section presents the simulated and measured results for the new design. Figure 5.8 shows the meshed FEKO model of the antenna

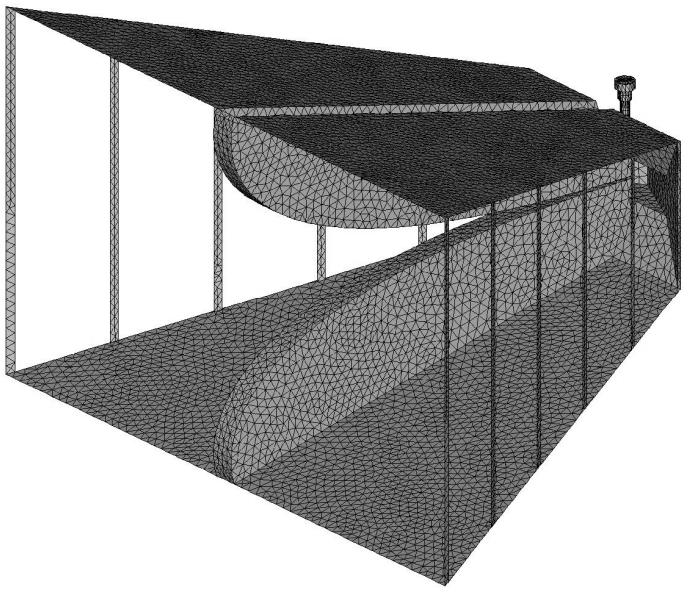

Figure 5.8. Meshed FEKO model of the new improved 1-18 GHz DRGH antenna.

The simulated three dimensional radiation pattern at 18 GHz of the new design can be seen in Figure 5.9. The four off-axis sidelobes are just starting to form, the main beam is still, however, well defined and directed on axis.

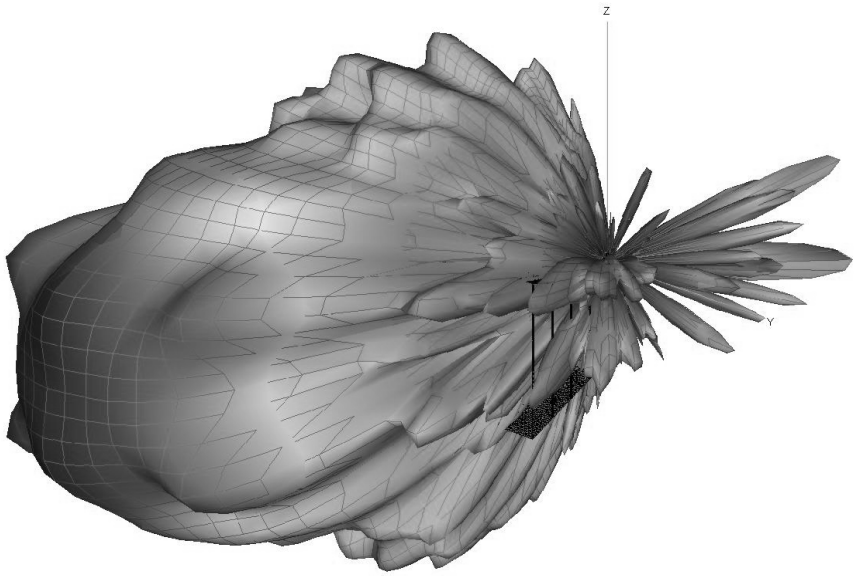

Figure 5.9. The simulated three dimensional radiation pattern at 18 GHz of the new design.

Two prototypes of the new improved design were fabricated. Figure 5.10 shows one of the prototypes.

Figure 5.10. New improved 1-18 GHz DRGH antenna.

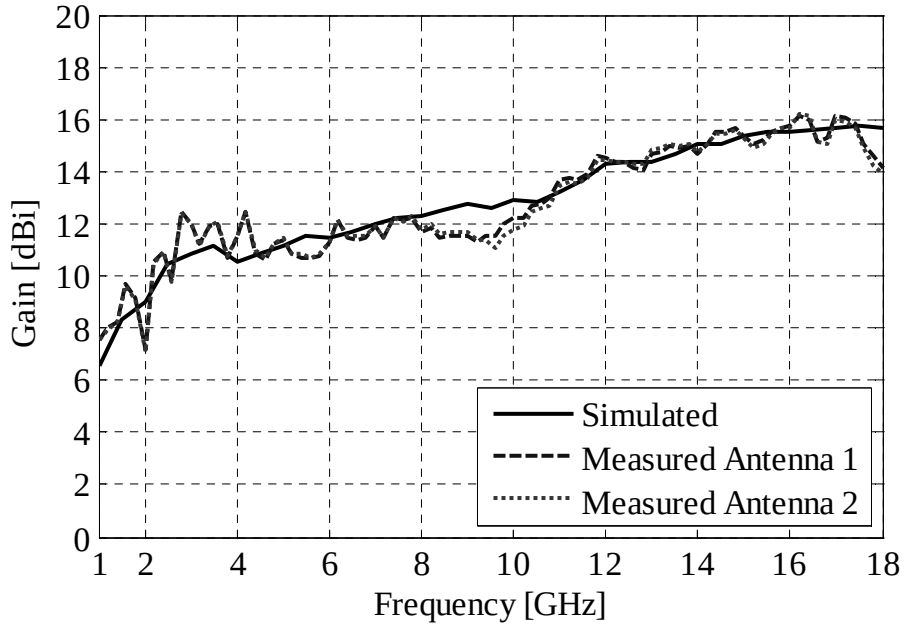

Figure 5.11. Boresight gain comparison between simulated and measured results.

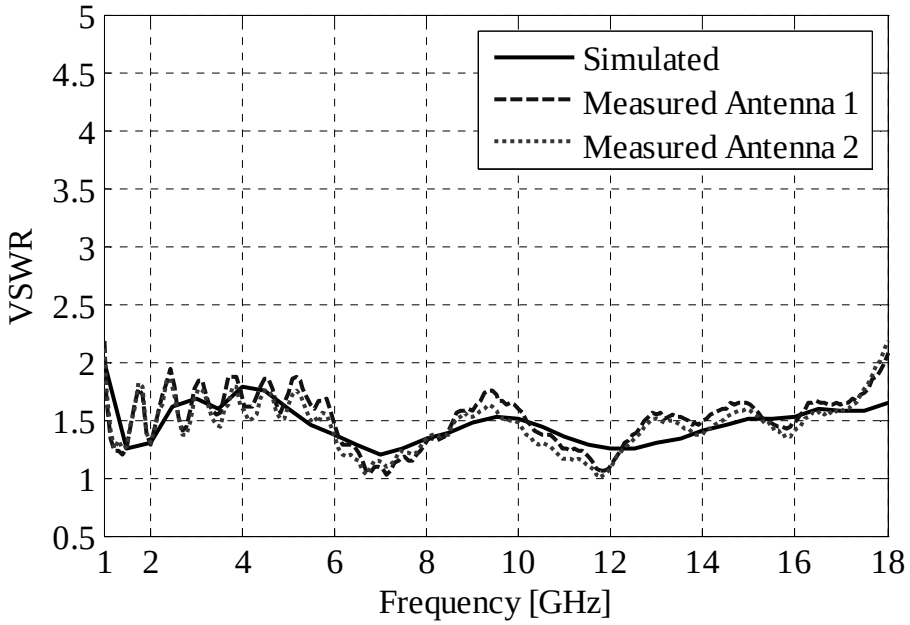

Figure 5.12. VSWR comparison between simulated and measured results.

Figure 5.11 shows the measured boresight gain of the two prototypes compared to the simulated results. The simulated and measured gain compares well. The only variations are a 1 and 1.5 dB gain drop for the measured antennas between 8-10 GHz and at 18 GHz respectively. The gain is typically 6.5 to 16 dBi, similar to the traditional design. The gain for the new antenna increases approximately linearly over most of the band and does not have the sharp gain peak near 16 GHz which is typical of traditional 1-18 GHz DRGH

antennas with pattern deterioration. With the old design there were large variations in performance in the same production batch (see Figure 4.3). The measured results for the two prototypes are nearly exactly the same. This gives confidence that the new design can be manufactured repeatedly with the same performance results.

Figure 5.12 shows the measured VSWR of the two prototypes compared to simulated results. As with the gain the VSWR of the two prototypes track each other extremely well. The simulated and measured VSWR is also in excellent agreement. The measured results have slightly more ripple than the simulated results. The VSWR of the measured antennas is below 2:1 over most of the band with a slight increase at 18 GHz to a max of 2.1:1.

Figures 5.13 and 5.14 show the comparison between the measured and simulated azimuth and elevation patterns at 1 GHz. At angles between 90° and 270° there is excellent correlation between the measured and simulated results. In [1] the difference between the measured and simulated results at the outer angles is attributed to the difference between the space surrounding the antenna in simulation and measurement. In the simulations this is numeric infinite space compared to the finite anechoic chamber volume with weak scatterers for the measured results [1]. Therefore this can be the same effect observed here. It is observed that as the frequency increases the comparison at the outer angles improves somewhat.

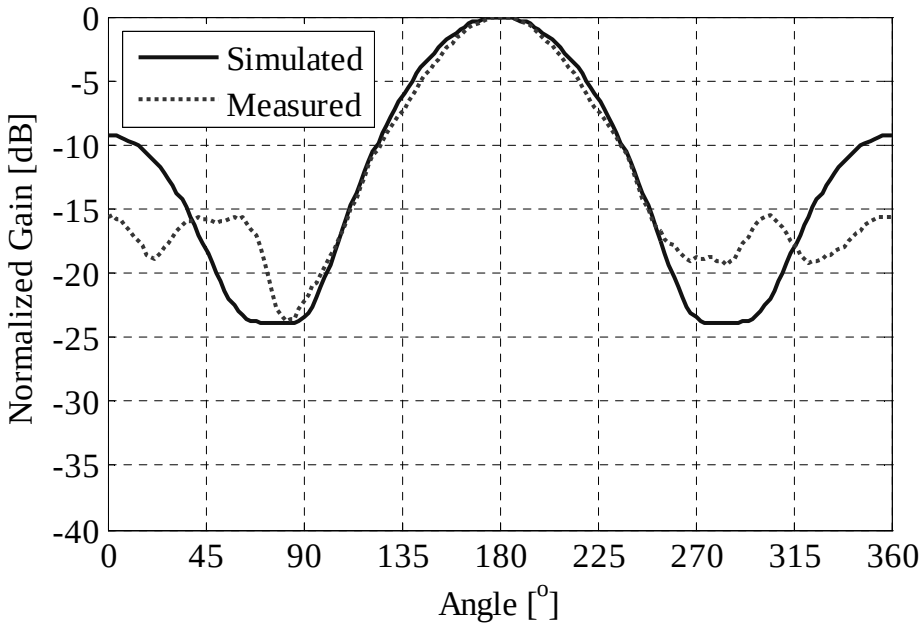

Figure 5.13. Comparison between measured and simulated azimuth patterns (1 GHz).

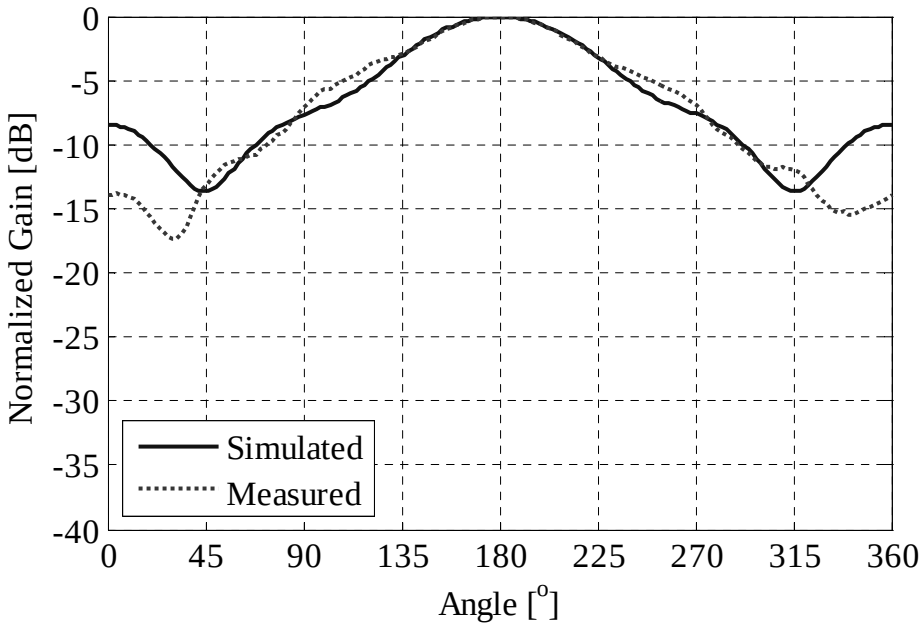

Figure 5.14. Comparison between measured and simulated elevation patterns (1 GHz).

A comparison between the measured and simulated azimuth and elevation patterns at 6 GHz is shown in Figures 5.15 and 5.16. Figures 5.17 and 5.18 show the comparison between the measured and simulated azimuth and elevation patterns at 12 GHz and Figures 5.19 and 5.20 shows the comparison at 18 GHz. Overall excellent agreement between measured and simulated results is observed.

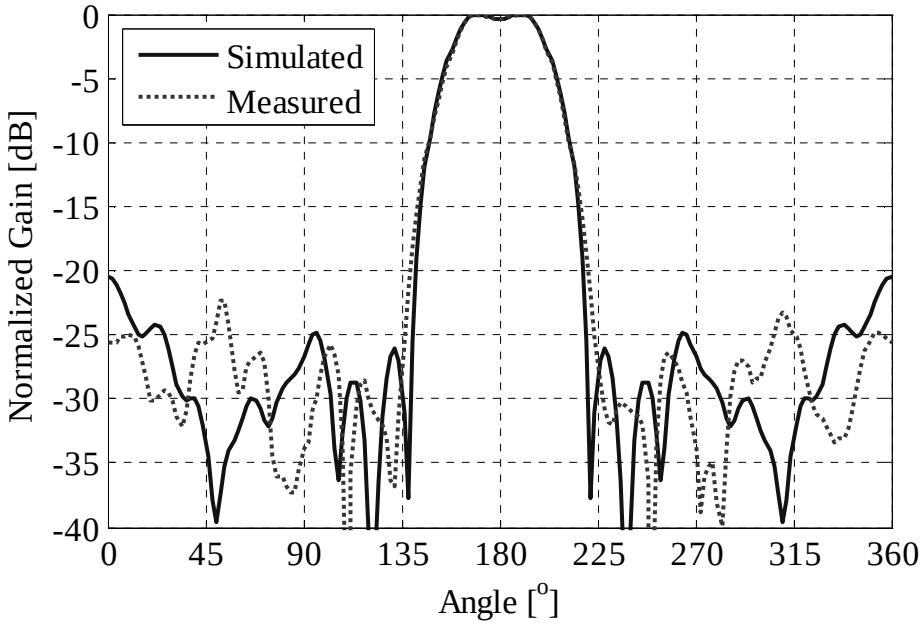

Figure 5.15. Comparison between measured and simulated azimuth patterns (6 GHz).

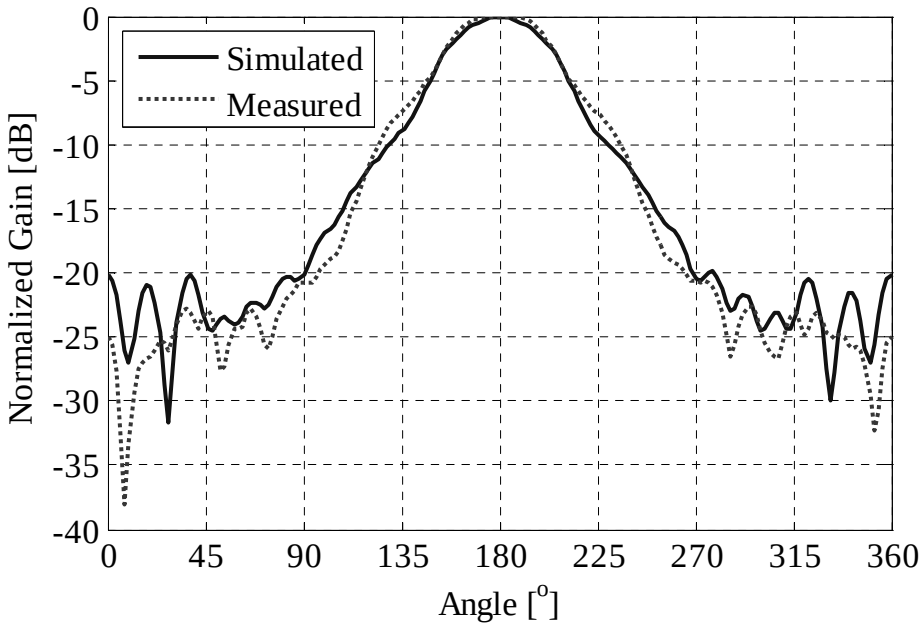

Figure 5.16. Comparison between measured and simulated elevation patterns (6 GHz).

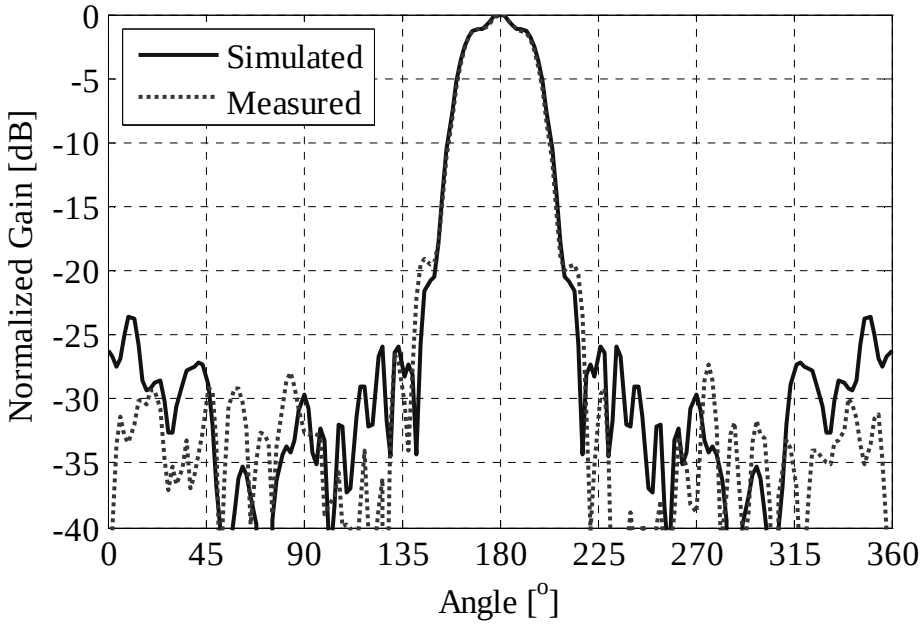

Figure 5.17. Comparison between measured and simulated azimuth patterns (12 GHz).

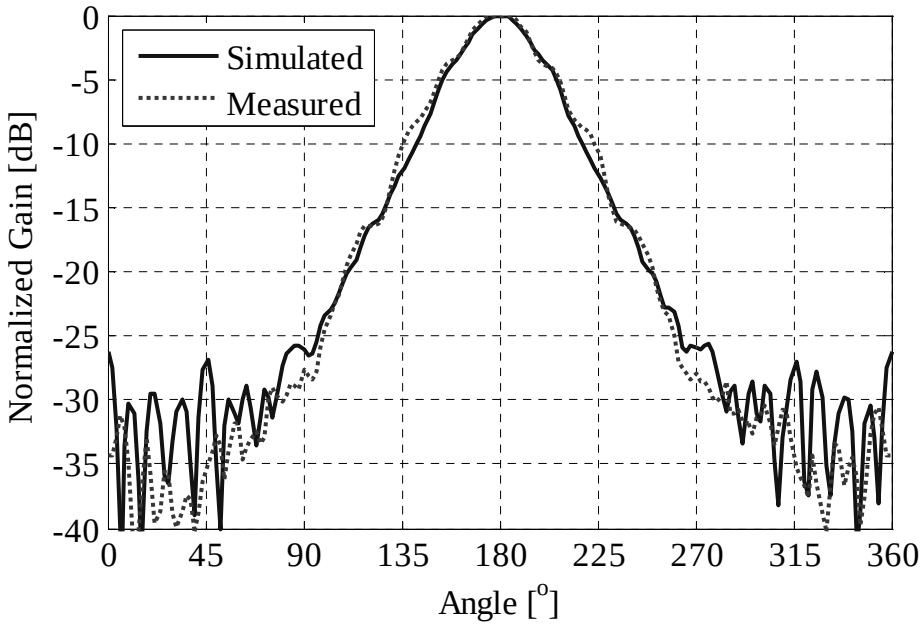

Figure 5.18. Comparison between measured and simulated elevation patterns (12 GHz).

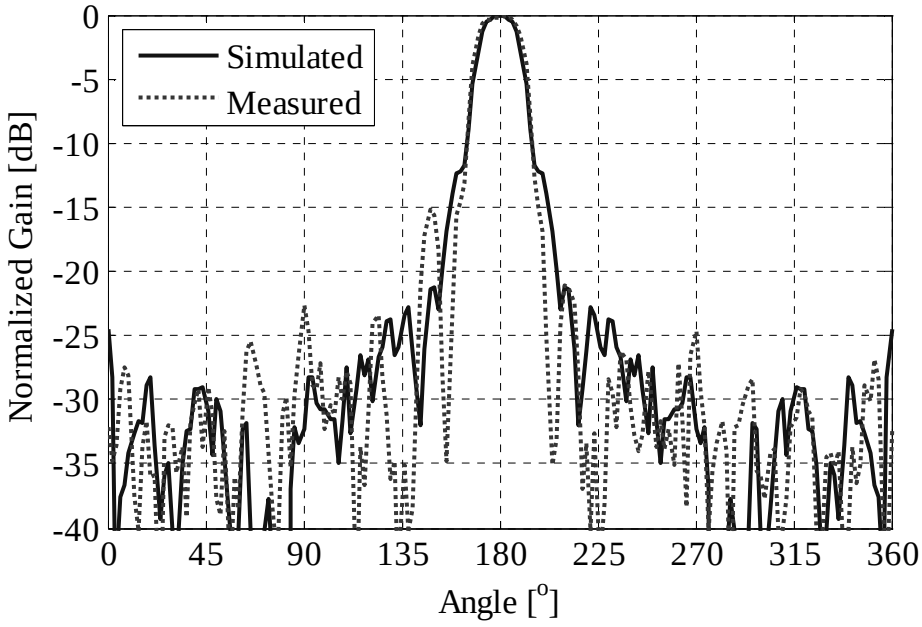

Figure 5.19. Comparison between measured and simulated azimuth patterns (18 GHz).

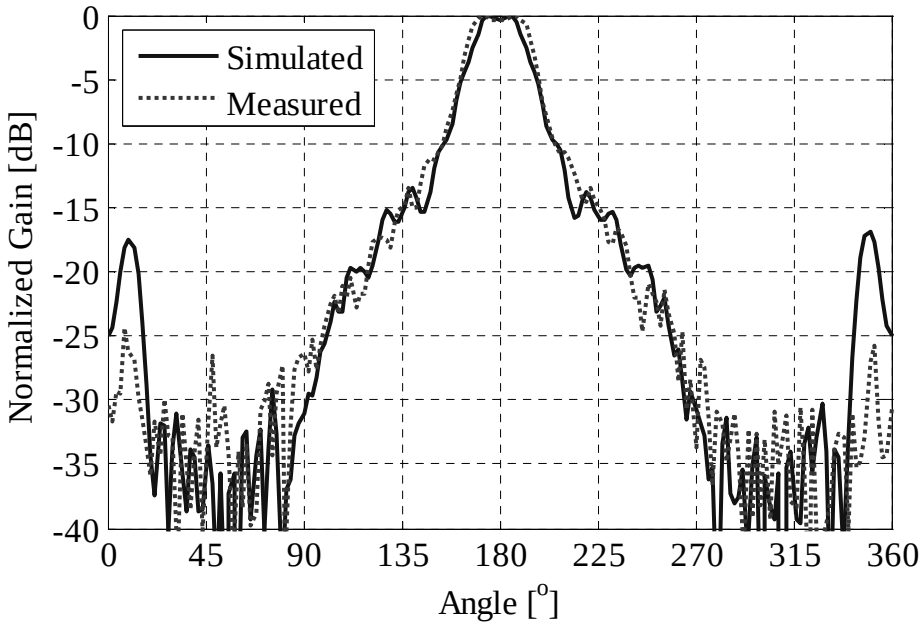

Figure 5.20. Comparison between measured and simulated elevation patterns (18 GHz).

Figure 5.21 shows the co-polarised measurement of the 45° plane of one of the prototype antennas. This figure clearly shows that sidelobes are just starting to form, but the main beam is still directed on boresight. It is therefore clear that this antenna does not have pattern break-up in the high band as observed in the traditional 1-18 GHz antenna. The antenna also has more gain and better VSWR when compared to the current state of the art 1-18 GHz DRGH antenna that does not have pattern break-up [18].

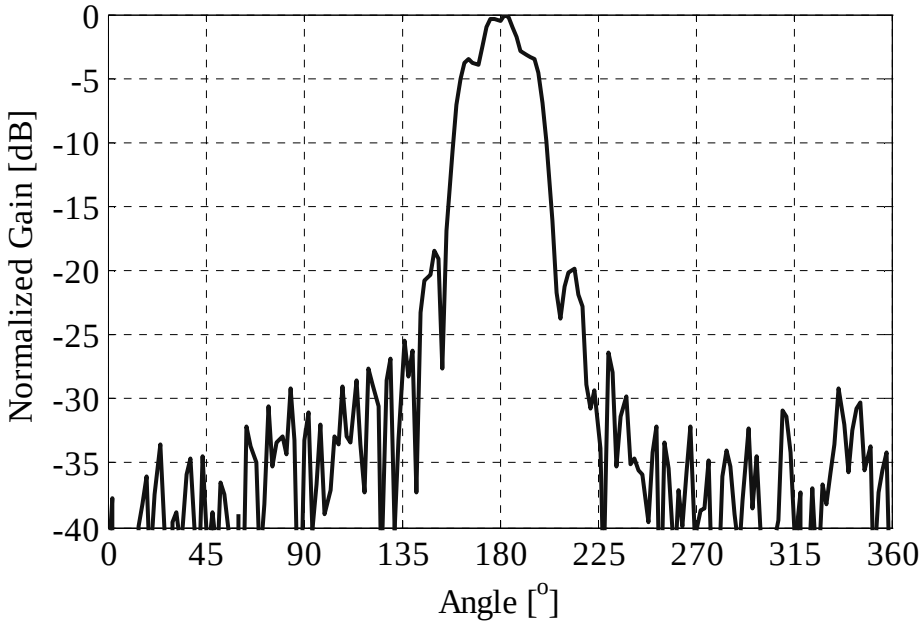

Figure 5.21. Measured co-polarised pattern in 45° plane (18 GHz).

5.5. Summary

In this chapter it was shown how a 1-18 GHz DRGH antenna with extreme resonance effects in the boresight gain and or VSWR can be repaired by application of conductive epoxy to the sensitive areas as identified in Chapter 4. The new improved 1-18 GHz design presented has significantly fewer parts especially in the waveguide launcher section. This reduces the possibility of gaps substantially. The measured results from two prototype antennas manufactured using the new improved design compares well to simulated results. Previously with the old design there were large variations in performance in the same production batch. The measured results for the two prototypes are nearly exactly the same. This gives confidence that the new design can be manufactured repeatedly with the same performance results. The antenna also has improved performance compared to the current state of the art designs.

CHAPTER 6 CONCLUSION

The main objective of this dissertation was to investigate and characterise the effect that gaps between parts of the 1-18 GHz Double Ridge Guide Horn (DRGH) antenna has on performance of the antenna. Knowledge of which areas are most sensitive was required in order to suggest improvements that will assist in the mass production of the 1-18 GHz DRGH antenna.

The literature study conducted in Chapter 2 revealed that although a number of studies have been done on the sensitivity problems of wideband DRGH antennas, no study could be found that investigated the effects of small gaps between the various parts of the antenna and methods to effectively address such effects.

A numerical model of the 1-18 GHz DRGH antenna was developed in FEKO and was presented in Chapter 3. This model was validated using measured data of a carefully constructed DRGH antenna. The antenna measured was assembled with care to reduce any effects from manufacturing or assembly tolerances. Comparisons between measured and numerical boresight gain and VSWR for this DRGH antenna showed excellent agreement between measurement and simulation.

The various types of gaps implemented in the FEKO model of the 1-18 GHz DRGH antenna as well as the simulation results were presented in Chapter 4. Based on the results of this parametric study, a redesigned coaxial feeding section was proposed in Chapter 5 to reduce/eliminate the effects of the manufacturing and assembling tolerances on the performance of a typical DRGH antenna. The waveguide launcher section as well as the ridges were also redesigned to reduce the possibility of gaps, reduce the number of parts as well as improve the performance of the antenna.

In conclusion, the hypothesis that the main source of performance deviations, most notably resonances in gain and VSWR, is the coaxial feeding section and this section’s interface with the ridges, was confirmed by the results in Chapter 4.

6.1. Contribution to the improvement of DRGH antennas

A short summary of the contributions made by this study is given below:

- An improved numerical model with dielectric materials for the N-type connector was developed.
- A comprehensive investigation of manufacturing tolerances with specific emphasis on the effect of gaps was presented.
- The causal relationship between gaps and resonance effects was established.
- Methods to repair antennas with performance deviations were presented.
- A new improved design less sensitive to manufacturing tolerances and with improved performance was developed.

6.2. Future work

While conducting this study the following future research needs with regard to DRGH antennas were identified:

Constant beamwidths: There is a pressing need in a variety of applications for wideband antennas that has nearly constant (frequency independent) beamwidths. Therefore research can be done to develop a wideband DRGH antenna with more constant beamwidths over such a wide band. Such an antenna would be well suited for use as a feed in wideband reflector antennas and Direction Finding (DF) systems.

Increased bandwidth DRGH antennas: The trend in modern Electronic Warfare (EW) systems is for ever increasing wideband coverage. Typically previous EW bands were 2-18 GHz which has now increased to 0.5 -18 GHz systems. There is also a need for solutions that cover these bands in a single antenna. For measurement purposes this means that there is a need for source and calibration antennas that can operate over a very wide band. A wideband source drastically reduces measurement time and therefore costs. Future work would therefore be to increase the bandwidth of the new improved DRGH antenna design at least to 0.75 -18 GHz.

REFERENCES

1 C. Bruns, P. Leuchtmann and R. Vahldieck. “Analysis and Simulation of a 1-18-GHz broadband double-ridged horn antenna.”*IEEE Trans. Electromagn. Compat.*, vol. 45, no. 1, pp. 55–60, 2003.

2 ——, “Comprehensive analysis and simulation of a 1-18 GHz broadband parabolic reflector horn antenna system.” *IEEE Trans. Antennas Propagat.*, vol. 51, no. 6, pp.1418–1422, 2003.

3 M. Abbas-Azimi, F. Arazm, J. Rashed-Mohassel and R. Faraji-Dana. “Design and optimization of a new 1-18 GHz double ridged guide horn antenna.” *J. of Electromagn. Waves and Appl.*, vol 21, no. 4, pp. 501–516, 2007.

4 K. L. Walton and V. C. Sundberg. “Broadband ridged horn design.” *Microwave J.*, pp. 96–101, 1964.

5 S. B. Cohn. "Properties of Ridge Wave Guide." *Proceedings of the IRE,* vol. 35, no. 8, pp. 783-788, Aug. 1947.

6 S. Hopfer, “The Design of Ridged Waveguides.” *IRE Trans. Microwave Theory and Techniques*, vol 3, no. 5, pp. 20-29, 1955.

7 J. Helszajn. “Ridge waveguides and passive microwave components.” *IEE Electromagnetic Wave Series*, vol 49, 2000.

8 R. Bunger, R. Beyer and F. Arndt. “Rigorous combined mode-matching integral equation analysis of horn antennas with arbitrary cross section.” *IEEE Trans. Antennas Propagat.*, Vol. 47, No. 11, pp. 1641–1648, 1999.

9 T. Wriedt, K. Wolff, F. Arndt and U. Tucholke. “Rigorous Hybrid Field Theoretic Design of Stepped Rectangular Waveguide Mode Converters Including the Horn Transitions into Half-space.” *IEEE Trans. Antennas Propagat.*, vol. 37, no. 6, pp. 780–790, June 1989.

10 D.M. Pozar. *Microwave Engineering.* : John Wiley and Sons Inc., Third Edition, 2005.

11 F. F. Dubrovka, G. A. Yena, P. Y. Stepanenko and V. M. Tereschenko. “Ultra Wideband Double Ridged Horns With Rectangular Aperture,”in *International Conf. on Antenna Theory and Techniques,* 2003, pp. 590-593.

12 J. L. Kerr. “Short axial length broad-band horns.” *IEEE Trans. Antennas Propagat.*, vol. 21, no. 5, pp. 710–714, 1973.

13 M. Abbas-Azimi, F. Arazm and J. Rashed-Mohassel. “Design of a New Broadband EMC Double Ridge Guide Horn Antenna.”, *European Conf. on Antennas and Propagat.*,2006.

14 MIL-STD-461-F. “Requirements for the Control of Electromagnetic Interference Characteristics of Subsystems and Equipment.” *Department of Defense*, December 2007.

15 C. Bruns, P. Leuchtmann and R. Vahldieck. “Full wave analysis and experimental verification of a broad band ridged horn antenna system with parabolic reflector.” *IEEE Antennas and Propagat. Soc. Int. Symp. 2001*, 2001,.

16 M. Abbas-Azimi, F. Arazm and J. Rashed-Mohassel. “Sensitivity analysis of a 1 to 18 GHz broadband DRGH antenna.” *IEEE Antennas and Propagat. Soc. Int. Symp*, 2006,pp. 3129–3132.

17 M. Botello-Perez, H. Jardon-Aguilar and I. G. Ruiz. “Design and Simulation of a 1 to 14 GHz Broadband Electromagnetic Compatibility DRGH Antenna.” *2nd Int. Conf. Electrical and Electronics Engineering*, 2005, pp. 118–121.

18 V. Rodriguez. “New broadband EMC double-ridged guide horn antenna.” *RF Design*, pp. 44–47, 2004.

19 V. Rodriguez. “The Dual-Ridged Horn Antenna.” *EE – Evaluation Engineering*, October, 2006.

20 V. Rodriguez. “Recent Improvements to Dual Ridge Waveguide Horn Antennas: The 200MHz to 2000MHz and 18GHz to 40GHz models.” *IEEE Int. Symp. on Electromagnetic Compatibility*, 2009.

21 Dehdasht-Heydari, H. R. Hassani and A. R. Mallahzadeh. “Quad Ridged Horn Antenna for UWB Applications.” *Progress In Electromagnetics Research*, PIER 79, 23–38, 2008.

22 R. Dehdasht-Heydari, H. R. Hassani and A. R. Mallahzadeh. “A new 2-18GHz Quad-Ridged Horn Antenna.” *Progress In Electromagnetics Research*, PIER 81, 183–195, 2008.

23 W. D. Burnside and C. W. Chuang. “An Aperture-Matched Horn Design.” *IEEE Trans. Antennas Propagat.*, vol. AP-30, no. 4, July 1982.

24 L. Botha and D. A. McNamara. “Examination of antenna patterns of profiled horns using the method of moments.” *Antennas and Propagation Soc. Int. Symp.*, vol. 23, 1985.

25 N. Marcuvitz. *Waveguide Handbook*, New York: McGraw-Hill, 1951.

26 J. R. Whinnery and H. W. Jamieson. “Equivalent Circuits for Discontinuities in Transmission Lines.” *Proc. of the IRE*, vol. 32, no. 2, pp. 98-114, Feb. 1944.

27 D. Baker and C. Van Der Neut, “A compact, broadband, balanced transmission line antenna derived from double-ridged waveguide.” *Antennas and Propagation Soc. Int. Symp.*, vol. 20, 1982.

28 A. Vasylchenko, Y. Schols, W. De Raedt and G.A.E. Vanderbosch. “Quality Assessment of Computational Techniques and Software for Planar-Antenna Analysis.” *IEEE Antennas and Propagation Magazine*, vol. 51, no. 1, February 2009.

29 D.B. Davidson, *Computational Electromagnetic for RF and Microwave Engineering. Cambridge University Press*, 2005.

30 EM Software & Systems, FEKO User’s Manual, Suite 5.4, July 2008.

31 K. S. Yee, “Numerical solution of initial boundary value problems involving Maxwell’s equations in isotropic media.” *IEEE Trans. Antennas Propagat.*, vol. AP-14, pp. 302-307, May 1966.

32 S. Dey and R. Mittra. “A Locally Conformal Finite-Difference Time-Domain (FDTD) Algorithm for Modeling Three-Dimensional Perfectly Conducting Objects.” *IEEE Microwave and Guided Wave Letters*, vol. 7, no. 9, September 2007.

33 S. Benkler, N. Chavannes and N Kuster. “A New 3-D Conformal PEC FDTD Scheme With User-Defined Geometric Precision and Derived Stability Criterion.” *IEEE Trans. Antennas Propagat.*, vol. 54, no. 6, June 2006.

34 C. A. Balanis. *Antenna Theory.* John Wiley and Sons Int., 1997.

35 W. L. Stutzman and G. A. Thiele. *Antenna Theory and Design***.** John Wiley and Sons Int., Second Edition, 1998.

36 V. Rodriguez. “Dual Ridge Horn Antenna.”, United States. Patent 6,995,728 B2, 7 February 2006.